ABSTRACT

Title of Document: DEVELOPING A DISPLAY SCREEN CORRELATION METRIC FOR THERMAL IMAGING CAMERAS

Joshua Benjamin Dinaburg, Master's of Science, 2007

Directed By: Dr. Gregory Jackson, Associate Professor of Mechanical Engineering

Thermal imaging cameras detect infrared radiation to semi-quantitatively determine the thermal profile of the surroundings. Previously, no standard performance measurements have been established for thermal imaging cameras in applications such as search and rescue and firefighting. The spatial contrast resolution in realistic atmospheric conditions was assessed for several TIC through full scale fires of methanol, toluene, and common household materials. Absorbing gas-phase combustion products greatly affected the ability of the TIC to measure local contrast in temperatures as a function of spatial frequency. The cost, labor, and repeatability of full scale fire testing make it difficult to include such tests as a standard metric and relatable bench scale options are explored. In this regard, performance metrics have been based on a voltage output signal to determine image quality. A test was developed using a thermal gradient target to relate the output signal to the luminance projected by the LCD screen seen by the user. The target produces a voltage ramp in

the output signal which is recorded in 8 bit digital tape format and is compared to the luminance profile measured by a 16 bit CCD camera array with an IR filter. The relationships between the signals were nonlinear and unique to each imager tested. Measurements of the output signal only do not describe the final performance and a complete standard performance evaluation must measure the display luminance. A standardized test for determining the relationship between output and display luminance including gradient target design, luminance measurement system, and optical components has been proposed for the National Fire Protection Association.

DEVELOPING PERFORMANCE METRICS FOR THERMAL IMAGING CAMERAS

By

Joshua Benjamin Dinaburg

Thesis submitted to the Faculty of the Graduate School of the
University of Maryland, College Park, in partial fulfillment
of the requirements for the degree of
Master's of Science
2007

Advisory Committee:
Professor Gregory Jackson, Chair
Dr. Jungho Kim
Dr. Bao Yang
Dr. Anthony Hamins

Acknowledgements

There are many people who deserve recognition and gratitude for the production of this document. First I would like to thank my advisor Dr. Greg Jackson, for assisting me through the University of Maryland and helping me obtain my masters degree. I would like to thank Dr. Francine Amon from National Institute of Standards (NIST) and Technology for welcoming me onto her metrology project. She has shared her office, her lab, her time, and her thought willing and graciously. She constantly made herself available to help me with any questions I had, or to discuss any issues that came up, technical or personal, or even to fill out my time card if I forgot. Her assistance has been invaluable during my graduate career. I am also grateful to Dr. Jungho Kim for originally getting me involved with the TIC metrology project at NIST. I would like to thank Dr. Anthony Hamins and Nelson Bryner, my group leaders at NIST for their constant support academic, technical and financial. I am grateful to the secretarial staff at NIST Yalasha Redd, Barbie Huff, and Sharon Rinehart, who always kept my paperwork in working order despite my best efforts to make it difficult. I would also like to thank the crew at NIST who run the large scale fire facility and who help design and build anything needed in a lab, Alexander Maranghides, Ed Hnetkovsky, Laurean DeLauter, Jay McElroy, Roy McLane, and the memory of Jack Lee, who taught me to weld my first thermocouple. I would also like to thank Aykut Yilmaz and Justin Rowe, fellow students at NIST who would discuss any issue or just get some lunch. Finally I would like to thank all the members of my advisory committee, Dr. Greg Jackson, Dr. Jungho Kim, Dr. Bao Yang, and Dr. Anthony Hamins for their support in the completion of my degree.

Table of Contents

List of Tables

List of Figures

Acronyms and Abbreviations

BNC - Bayonet Neill Concelman, a standard connection type for coaxial cable

CCD – charge coupled device, a type of ROIC

CMOS – complementary metal-oxide semiconductor, a type of ROIC

CRT – cathode ray tube

CTF – contrast transfer function

DUT – device under test

EI – electronic iris, for controlling thermal sensitivity of TIC

EOTF – electro-optical transfer function, also known as a gamma function

ESF – edge spread function

FDM – frequency division multiplexed, a data transfer method

FFT – fast fourier transform

FOV – field of view

FPA – focal plane array

fps – frames per second

HRR – heat release rate

IEEE 1394 – a standard data transfer connection type

IR – infrared

LCD – liquid crystal display

LSF – line spread function

MRTD – minimum resolvable temperature difference

MTF – modulation transfer function

NETD – noise equivalent temperature difference

NFPA – National Fire Protection Association

NIST – National Institute of Standards and Technology

NPT – National Pipe Thread, a standard plumbing connection type

NTSC – National Television Systems Committee, a defined standard for video transmission in the USA

PSD – power spectrum density

PSF – point spread function

RMS – root mean square

ROIC – readout integration circuit

SBIG – Santa Barbara Instrument Group

SITF – system intensity transfer function

TCR – temperature coefficient of resistance

TIC – thermal imaging camera, both singular and plural tenses

VESA – Video Electronics Standards Association

Symbols

a_L –an empirical constant used to define LCD display screen luminance as a function of input signal,

a_D - the diameter of a particulate in the atmosphere

a_s - the dispersion exponent for soot absorption

A – area of a detector element

B – rotational constant

C – heat capacity

C_s – an empirical constant for soot absorption

c_0 – speed of light in a vacuum

c_1 – planck's first constant

c_2 – planck's second constant

$C_{Michelson}$ – Michelson contrast

C_N – coefficient for determining heat transfer over a cylinder

D – the distance from a target to a detector

d – the width of one cycle of a contrast target

dq/dt – the change in pyroelectric charge due to temperature per unit area

E – energy, subcripts (elec – electronic,rot –rotational, trans – translational, vib vibrational)

G – total thermal conductivity from a detector pixel

Gr_D – Grosshof number

f_v – the volume fraction of a particulate

h - Planck's constant equal to 6.626×10^{-34} J·s

H – heat capacity

i – a single iteration in a process

I – spectrally integrated radiative intensity

I_b – bias current in a microbolometer pixel

$I_{b\lambda}$- blackbody radiative intensity

I_λ – spectral radiative intensity

$I_{\lambda 0}$ – incident radiative intensity on a surface

j – the square root of negative one; rotational quantum number

k_d - TIC detector constant

k - absorption index

L – luminance

L_b – luminance projected by an LCD pixel with zero input signal

m - mass

M – Total radiative flux

$M(\lambda,T)$ – spectral radiative flux

n – refractive index

$\bar{n}$ - complex optical constant

N – The total number of iterations in a process

Nu – Nusselt number

Nu_D – Nusselt number for natural convection

O – the deviation between an ideal thermal gradient and a real one

O_λ- optical thickness

p – pyroelectric coefficient

p_s - size parameter for Rayleigh scattering

Pr – Prandtl number

r – statistical correlation coefficient for data sets

r_e – distance between two atoms

R – resistance of a microbolometer pixel, rotational moment of inertia (2-11)

$R_D(\lambda)$ – TIC detector spectral responsivity

s – optical path length through a transmitting medium

S_i – output signal from a single detector pixel i

S_{MAX} – maximum detector output signal, used to calculate contrast

S_{MIN} - minimum detector output signal, used to calculate contrast

T – temperature

t - time

T_0 – average temperature of a microbolometer detector

T_b - Background temperature in a thermal scene

T_{base} – temperature of the connecting substrate to a detector pixel

$T_{chopper}$ – the temperature of a pyroelectric chopper

T_H – The temperature of hot liquid flow for a thermal gradient target

$T_{i,m}$ – The temperature of an ideal linear thermal gradient target at postion m

T_L - The temperature of cold liquid flow for a thermal gradient target

T_m – the temperature of an actual thermal gradient target at position m

T_{target} – the temperature of a thermal target

u – exponent for Reynold's number for determining heat transfer over a cylinder

v – exponent for Prandtl number for determining heat transfer over a cylinder

V – The input signal to an LCD pixel

V_{pixel} – voltage signal from a microbolometer detector

x – measured CCD camera output values at known luminances

x_m – a single cell m in the axial direction for modeling heat transfer in a thermal gradient target

y – line fit CCD camera output values as a function of luminance

Z_{out} – the output from a CCD camera as a function of luminance

$\alpha(\nu)$ – absorption coefficient of spectral radiation

γ – a logarithmic coefficient used to define LCD display screen luminance as a function of input

ΔQ – The differential charge created by pyroelectric detectors

ΔS – differential signal output as a function of ΔT

ΔT – Temperature difference between the background and a target

$\Delta V_{detector}$ – Differential voltage output of a microbolometer detector

α – absorptivity, labels (‘ – directional, λ – spectral)

ε – emissivity, labels (‘ – directional, λ – spectral)

κ – temperature coefficient of resistance

κ_λ – linear absorption coefficient for optical media

λ – wavelength

ν – frequency

ξ – spatial frequency in cycles per milliradian

π – the constant pi

σ – Boltzman’s constant equal to 5.67×10^{-8} W/m^2-K^4

$\Phi_f(t)$ – radiant flux as a function of time

υ – vibrational quantum number

τ – transmissivity, labels (‘ – directional, λ – spectral)

ρ – reflectivity, labels (‘ – directional, λ – spectral)

$\sigma_{s\lambda}$ – scattering coefficient

$\vec{\mathbf{s}}_i$ - direction of radiative transfer

$\vec{\mathbf{s}}$ - direction of radiative transfer

Ω- solid angle

θ – angle from perpendicular in spherical coordinates

φ – azimuthal angle in spherical coordinates

w – distance between particulates in the atmosphere

1 TIC Technology overview

1.1 Thermal Imaging Camera Applications

Thermal imaging cameras (TIC)[1] are non-contact temperature measurement devices. They rely upon infrared radiation emitted by substances to determine the apparent temperature of an emitting gas or a surface. A thermal imager uses an array of radiation detectors to measure the thermal properties of an entire scene. The array produces a thermal image that couples information about both the temperature and radiative properties of a scene.

Thermal imaging is extremely valuable when contact temperature measurements are not possible or cannot provide adequate information. Thermal imaging is used to locate leaks, electronic defects, moving objects, or access the safety of a situation. Many fire departments currently employ TIC for firefighting applications. Imagers are used for locating victims and other firefighters, determining safe paths through a burning building, and finding possible reignition points after a fire has been extinguished. The spectral responsivity of the detectors used in commercial uncooled TIC make them very valuable for use in fire conditions due to the limited interference of atmospheric gases and particulates (Holst 2000) .

The performance of the TIC in firefighting applications is often integral to the protection of both lives and property. To aid in first responder operations, TIC are designed to operate in very harsh conditions, provide users with a wide field of view,

[1] In this paper, TIC is used as an acronym for both the singular and plural forms of thermal imaging camera(s), whichever form is applicable to the context of the sentence.

and are capable of adjusting signal output to more clearly portray the thermal scene with minimal input from the user. The performance needs of the user are designated by the intended use. For example, a TIC used to determine a fire source in a building may not require the same resolution or sensitivity as a TIC used to locate unconscious victims in a smoky environment. In general, the harsh and varied environments in which TIC are used for emergency response imparts challenges not present in other more traditional applications of thermal imaging. Thermal imagers are relatively expensive when compared with other personal protective equipment and users may be interested in well-characterized performance criteria to ensure that the equipment meets requirements for use. In addition, manufacturers of TIC should be able to objectively evaluate the performance of their product against the other options in the market. The goal of the current study is to develop test methodology that objectively describes aspects of the performance of TIC under realistic use conditions for fire imaging applications.

1.2 Imager Function and Technology

1.2.1 Basic Function of TIC

TIC detect thermal radiation emitted from objects in a scene. Thermal radiation is transmitted in the form of electromagnetic waves, and these waves oscillate at specific frequencies. The intensity of radiation, characterized by the number of wavepackets or photons, at each frequency is a function of the temperature and the surface properties of the emitting material. The frequency of peak intensity or emission is usually determined by the temperature of an object. Objects at extremely high temperatures, such as the sun (5780 K), emit peak intensity in the visible part of

the electromagnetic spectrum (wavelengths from ~400 nm-700 nm). Objects at about 300 K will emit a distribution of radiation shifted to much longer wavelengths (700 nm-1000 μm) which are not visible to the human eye. TIC capable of detecting radiation at these longer wavelengths are extremely valuable when visible light is not available.

The maximum possible spectral radiative intensity emitted by an object is governed by the Planck Function, Eq. (1-1),

$$I_{b\lambda}(\lambda,T) = \varepsilon \frac{c_1/\pi}{\lambda^5\left(1/e^{(c_2/\lambda T)}-1\right)} \qquad 1\text{-}1$$

where ε is the emissivity and c_1 and c_2 are constants equal to $3.7411\text{x}10^8$ W-μm/m^2, and $1.4388\text{x}10^4$ μm-K, respectively.

A blackbody is an ideal emitter whose emissivity, ε, equals 1.0 in all directions and at all frequencies. A blackbody signifies perfect emission. The emissive properties of real materials will be dependent upon the material, the emission angle, the wavelength of emission, and the temperature of the object. The Stephan-Boltzman Law, Eq. (1-2),

$$I = \varepsilon\sigma T^4 \qquad 1\text{-}2$$

is obtained when Planck's function is integrated over a hemisphere to determine the flux and summed over all wavelengths, and σ is the Boltzman constant equal to $5.67\text{x}10^{-8}$ W/m^2-K^4.

The apparent radiation of a thermal scene is not only affected by emission from the target, but also from absorption, emission, and scattering of gases and particulates over the path length from the target to the TIC. The optics of the TIC may also influence spectral intensity of the image. Firefighters will often encounter environments containing smoke, dust, water mist, carbon dioxide, and carbon monoxide. These environments have transmissivity of visible light of less than 1%, making it extremely difficult to see in fire conditions (Grosshandler 1993). TIC are tailored to function within specific spectral frequency ranges to best comply with the atmospheric conditions and applications. TIC for firefighter applications are designed to work in the 8-14 μm range because burning condition atmospheres do not absorb or emit radiation intensely at these wavelengths. The wavelength of this radiation is about 15 times that of visible light, making it less prone to scattering from water vapor or particulates in the atmosphere (Kruse 1997). In addition to effectively transmitting the wavelengths of interest, burning atmospheres do not contribute high intensity radiation from emission. Atmospheric emission would obscure the actual thermal target and reduce the image quality. The effect of burning atmospheres on radiative transmission is discussed in chapter 2.

1.2.2 Target Detection

TIC can be used to identify targets within a scene via their thermal signatures.are important tools because they view a complete thermal scene. Thermal signatures are the spectral radiative intensity of a target relative to the intensity of the background. Foreknowledge about a target's characteristic thermal signature can be critical for its identification.

Detected thermal signature can be greatly affected by the surrounding environment. Temperature, emissivity, absorptance, heat capacity of the material, time of day, and ambient conditions can all influence the target signature. If the target has very similar heat capacity to the background, they will both heat or cool at the same rate and no temperature difference is visible. But if one heats (cools) much more slowly than the other, a temperature difference can be seen even though both are gaining (losing) the same amount of heat. Also, if the target is very reflective or absorptive compared to the background a large thermal effect can be seen due to the surrounding radiation. This can make the surrounding conditions and viewing direction very significant because thermal radiation or the lack thereof, i.e. from flames, sunlight, or the night sky, may make the target appear hotter or colder than the environment depending on the conditions. Also, the presence of moisture or other materials may reduce/increase the thermal capacity of objects and therefore change the thermal signature with respect to the background. For example, in an ambient room a person will appear warmer than the surroundings, but in a burning environment the person may appear cooler than the surroundings (Holst 2000).

The ability of a TIC to distinguish between a target and a background is based on several factors of the sensor. The differential output of a detector for a target on a background when the temperature difference is not great is described by Eq. (1-3),

$$\Delta V_{\text{detector}} = k_D R_D(\lambda) \Delta I_\lambda \approx k_D R_D(\nu) \sigma T_b^3 \Delta T \qquad 1\text{-}3$$

where k_D is a detector constant, $R_D(\lambda)$ is the spectral responsivity, T_b is the background temperature, and ΔT is the temperature difference between the target and the background.

A TIC sensor should be designed based upon the desired temperature differences of target and background and the intended environmental conditions for use. Both k_d and $R_D(\lambda)$ can be designed to optimize the temperature and spectral performance of TIC sensors for specific applications.

1.2.3 Technology and Design

A TIC is a complex system of assembled components. Each component serves a purpose in the goal of changing invisible, infrared radiation into an informative image that can be viewed by a human. A basic schematic of the components of a TIC system are shown in Fig. (1-1). Thermal sources and atmospheric radiative transfer include radiative intensity at various wavelengths, I_λ, and the variation of that intensity over an optical distance, $dI_\lambda(s)$. This will be described in more detail in chapter 2. The following sections will focus upon the design, function, and operation of the components of the imaging system. This discussion will include: the transmissive properties of the optics (1-1-2); the electrical response, V_{pixel}, of the sensor array (1-1-3) to incident radiative flux, Φ_f; the internal amplification, multiplexing, interpolation, and filtering devices (1-1-4); and the conversion of the data into useful output signals (1-1-5) through image recording and LCD screen luminance, L.

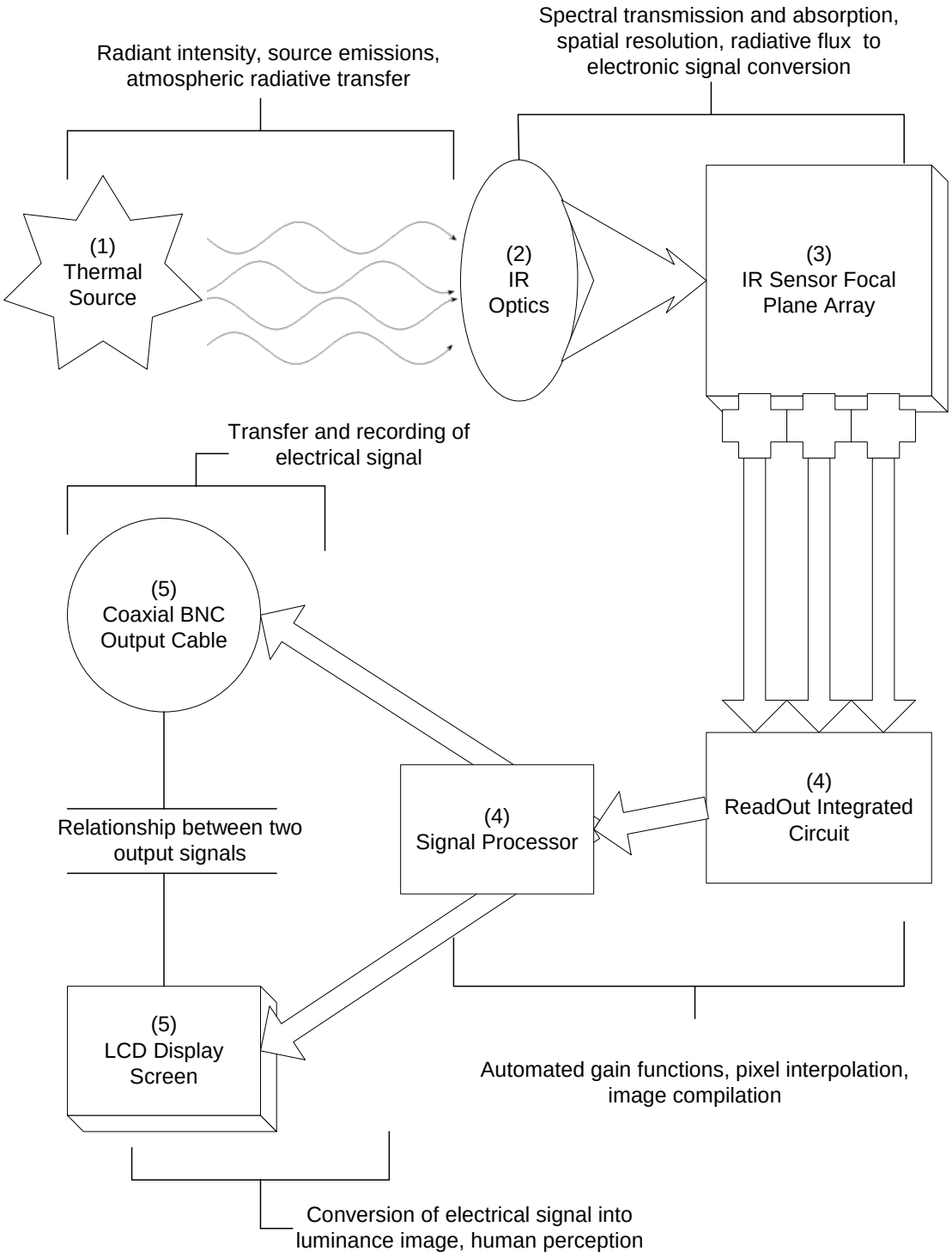

Figure 1-1 - Basic schematic of conversion of IR radiation into useful data and images through a TIC including transfer processes and technical considerations of system components

1.2.3.1 Optics

Infrared (IR) optics are designed to focus the image of the thermal scene onto the detector array. They are simple lenses similar to those found in any optical device. The distinctions for IR optics are the materials used. Regular transparent lens materials that transmit visible light are extremely reflective in the infrared region of the spectrum, and are thus unacceptable for use in thermal imaging applications.

Germanium (Ge) and Zinc Selenide (ZnSe) are the two most common materials used to construct optics for TIC because they transmit radiative energy well in the 8-14 μm range. Fig. (1-2) displays the radiative transmission of Ge and ZnSe as a function of wavelength and highlights the 8-14 μm range.

The lens design is important for reducing aberrations and internal reflections. The lens is also designed to provide a wide field of view (FOV) to provide first responders with a broad scope of the thermal scene. TIC designed for first responders often have a FOV from 40 to 60 degrees. The wide FOV and minimum focusing distance of one meter create challenges in designing performance tests for TIC because thermal targets may be extremely large, additional optics must be used, or the target will fill only a small portion of the detector array.

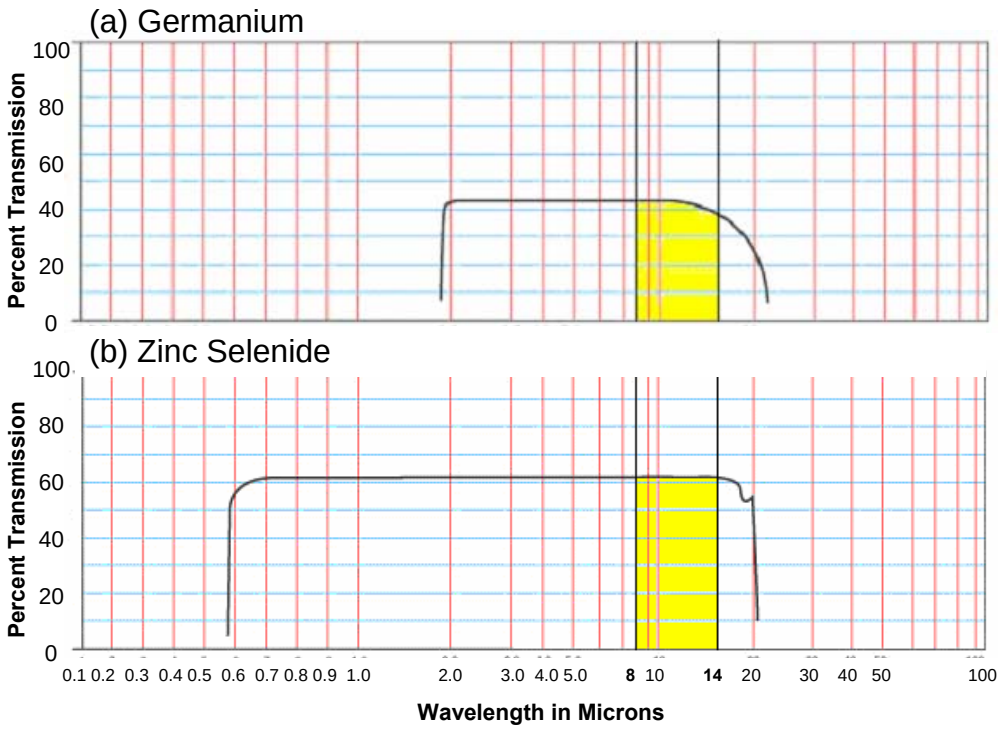

Figure 1-2 – Optical transmission of (a) germanium and (b) zinc selenide as a function of wavelength in micron (Infrared Crystal Laboratory 2006)

1.2.3.2 Detector Technology

The oldest and most traditional method of detecting thermal radiation is a cryogenically cooled quantum energy detection device. In recent years, a great deal of research has moved away from quantum devices and focused upon thermal detectors.

Thermal detectors are constructed of a material with an electrical property that changes dramatically with temperature. This electrical property can then be measured to determine the amount of irradiation incident upon the detector from changes in the material temperature. Most handheld TIC use thermal detectors because they do not

require advanced cooling systems or large power requirements like quantum detection devices. This makes them ideal for the handheld, battery-operated units used by firefighters. The detector used in these cameras is specifically designed to have the greatest responsivity in the desired spectral region. The material should have high absorption coefficients in this range or be coupled with another material that does. Pyroelectric and microbolometer sensors are the primary types of thermal detectors used for handheld TIC (Holst 2000).

Pyroelectric detectors measure radiation by a change in material temperature due to incoming radiation. The detector is constructed of a polar, dielectric material containing a surface charge that is proportional to changing temperature. The detector material directly generates an electric signal by acting as a capacitor whose charge is described by Eq. (1-4)

$$\Delta Q = Ap\Delta T \qquad 1\text{-}4$$

where A is the area of the capacitor and p is the pyroelectric coefficient of the material. This can also be assumed to be dq/dT, the change in charge per unit area due to temperature. Pyroelectric detectors can be constructed of ferroelectric metals, polymers, or pyroelectric crystals (Muralt 2001).

The faces of pyroelectric materials take on opposite electric charges. When the temperature is steady, these charges are kept balanced by internal charges. When the temperature is changing, however, the magnitude of this polarization also changes and a change in the surface charge can be detected during the transient temperature

condition. This effect can also be enhanced in ferroelectric materials by applying an additional, external electric field. This field acts to change the dielectric permittivity of the material and thus increase the apparent pyroelectric coefficient and is known as the field-enhanced pyroelectric effect. TIC sensors constructed from barium strontium titanate (BST) take advantage of this effect and are common for handheld imaging devices. The actual physics and mathematics of this phenomenon are extremely complex and not necessary for the scope of this text. Further information on this topic can be found in references (Hanson 1997); (Polla and Choi 1997).

Because pyroelectric detectors measure transient changes in temperature they require the use of a rotating chopper to continuously reference the temperature of each pixel to ambient and keep the temperature dynamic. For this reason these detectors are very low in thermal mass so that the temperature can change very rapidly (Tsai and Young 2003). An example of a pyroelectric straight blade chopper and the resulting temperature of a pixel are shown in Fig. (1-3). The detected signal of the pyroelectric detector will be proportional to both the absolute temperature and the slope of temperature with respect to time.

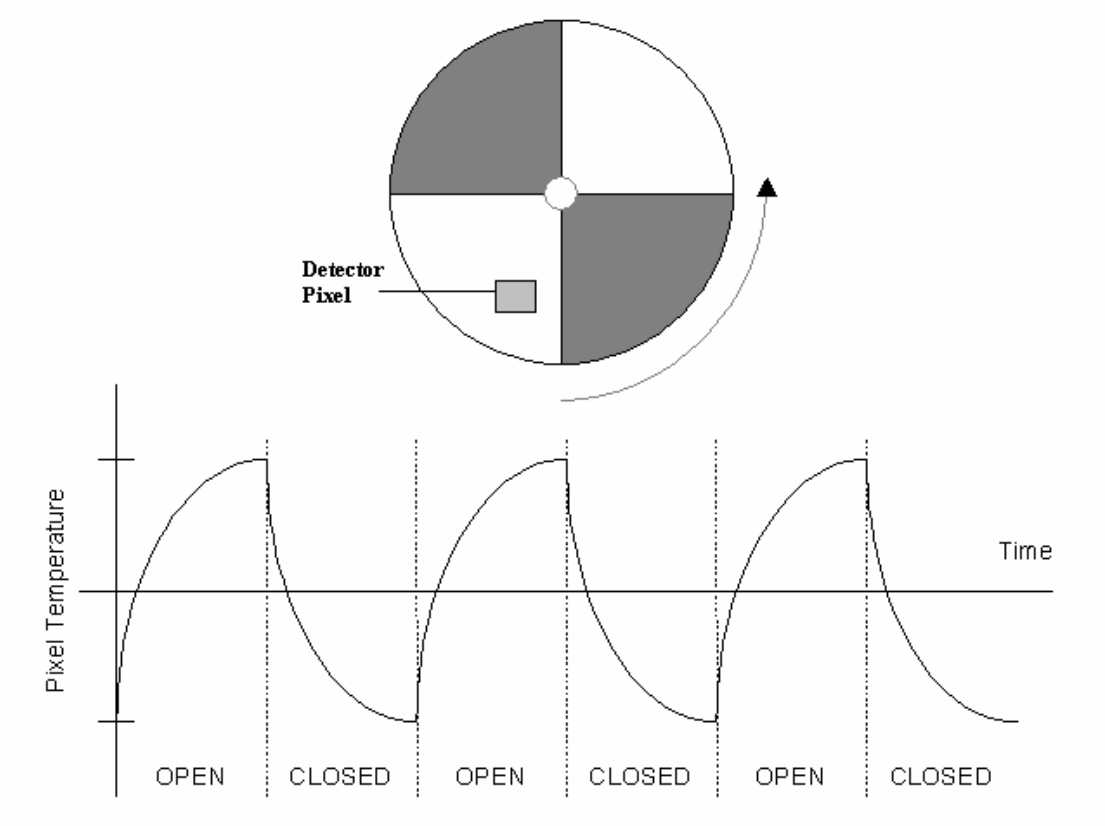

Figure 1-3 – Pyroelectric chopper with straight blades and the temperature of a pixel as a function of time when the chopper is open and closed (Based upon figures introduced by Hanson)

A microbolometer functions by changing electric resistance with changes in temperature. A bias voltage is applied to the detector and the temperature is determined from the amount of current passing through the circuit (Holst 2000). Microbolometers can be made from vanadium oxide (VO_x) or amorphous silicon (aSi). These materials are chosen for their strong resistive response to temperature and the ability to construct them into detector arrays. A typical value of the temperature coefficient of resistance (TCR) for these materials is about -0.003 K^{-1} and they are capable of producing resistances in micro arrays of about 10 kΩ. The voltage response of a pixel is then proportional to Eq. (1-5),

$$V_{pixel} \propto \kappa R I_b [T(t) - T_0] \quad \text{1-5}$$

where κ is the TCR, R is the resistance, I_b is the bias current, T_0 is the average temperature, and $T(t)$ is the temperature as a function of time (Muralt 2001).

Each detector pixel contains a small layer of thermally resistive material coupled with an IR-absorbing material. The detector is supported over the circuitry by two small legs in order to reduce the thermal conductivity while still maintaining electric contact. The detector itself contains VO_x bonded to another layer, in this case silicon nitride. The other layer acts to increase the absorption of the thermal radiation in the spectral band of interest. An example of a microbolometer pixel is shown in Fig. (1-4). The individual pixels are constructed as part of a large array, often 320 x 240 or 160 x 120 for commercial TIC. The pixel array is stored in a near vacuum to eliminate convection of heat between pixels and thermally isolate each detector. The pixel can only lose heat by radiating back into the environment or conduction through the electrical contacts. This makes the detector respond quickly to changes in the temperature of the scene. The temperature of each pixel element is nearly directly controlled by the net intensity of thermal radiation received and lost by the pixel. One advantage of bolometers over pyroelectric devices is that they do not require the use of a chopper for temperature reference; instead they measure the absolute temperature of the pixel, rather than a variation in that temperature (Kruse 1997).

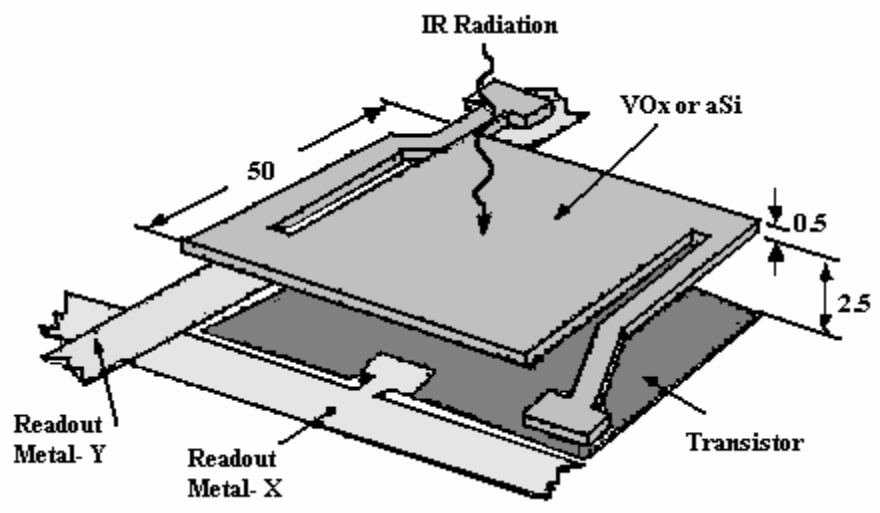

Figure 1-4- Basic microbolometer pixel design with typical sizes given in μm (Based upon figures introduced by Kruse)

The detection limit of thermal sensors is described by the noise equivalent temperature difference (NETD). This is essentially the temperature difference detected by the sensor that creates a differential signal equivalent to the amount of variation caused by noise. There are two basic methods of decreasing this measurable temperature difference. The effect of the noise can be reduced by decreasing the total heat capacity (mC_p) of the detector element where m is mass and C_p is the thermal capacity. This will increase the temperature change from incoming radiation and thus increases the signal from an equivalent input. In addition, the intensity of noise can be reduced by decreasing the total heat conduction from the detector element (G) (Muralt 2001). The temperature of the sensing element will be defined by Eq. (1-6),

$$mC_p \frac{dT}{dt} + G(T - T_{base}) = \alpha(T)\Phi_f(t) \qquad 1\text{-}6$$

where mC_p is the thermal heat capacity of the detector, α is the absorption coefficient for spectral radiation, T_{base} is the temperature of the connecting substrate, and $\Phi_f(t)$ is

the incident radiant flux as a function of time. For microbolometer detectors, the measured electric resistance will be a function of *T*, the temperature of the detector pixel. For field-enhanced pyroelectric devices, the measured polarization will be a function of both *dT/dt* and *T*, and the incoming radiation $\Phi_f(t)$ will be a waveform controlled by the chopper device (Hanson 1997).

1.2.3.3 Readout and Signal Processing

The signal from a microbolometer is detected by measuring the voltage response of the pixel as described by equation (1-5). The charge signal on a pyroelectric detector can be measured in two ways. The voltage or the current can be measured and both should be roughly proportional to $\{T_{T\arg et}^4 - T_{Chopper}^4\}$.

Once a signal has been generated by the thermal detector it must be delivered into a circuit and processed into a coherent video image. Each detector pixel is connected to an electronic readout system. There are two options for integrating a readout circuit to the detector pixels, monolithic or hybrid design.

The monolithic design incorporates the readout integration circuit (ROIC) on the same layer as the detector itself. While this allows for simpler and cheaper manufacturing, it also reduces the amount of detecting area on each pixel, or the fill factor. The increased space taken up by the output electronics reduces the sensitivity of the detectors to small temperature difference or low input temperatures. In

general, the monolithic design sacrifices image quality for reduced manufacturing cost.

The hybrid design separates the detector elements and the signal transmission network onto two separate layers in electrical contact. While this process is more complex and expensive to manufacture, the fill factor can be raised from about 55% for monolithic arrays to around 90% for hybrid designs. In addition to improving thermal sensitivity, the hybrid design also improves cooling efficiency, which leads to increased battery life and reliability. The decision to design a focal plane array with monolithic or hybrid design should be based upon the need for image quality vs. cost.

After each pixel has been connected electrically, the signals must be compiled and formatted for signal processing in a multiplexer. The array signals can be multiplexed by a charge-coupled device (CCD) or by a complementary metal-oxide semiconductor (CMOS) device.

A CCD device transfers electrons from each detector down the entire row of detectors to a readout device at the end of each row. This design allows for a less complex pixel design with a high fill factor and uniformity but a relatively slow readout speed. This process can be subject to errors through charge loss along rows or by charge overflow between adjacent pixels, known as blooming.

A CMOS device directly outputs a voltage signal from each pixel into the readout device. This requires the use of transistors on the pixel, reducing the uniformity and fill factor, but increasing the readout speed allowing for high speed imaging.

Once a ROIC has been implemented, the compiled signal is then electronically adjusted to produce a crisper, coherent, and contrasted image. This includes amplification and gain based on dynamic range control, interpolation to smooth the image from pixel to pixel, and various other complex algorithms designed to improve image quality. Because processing algorithms are unique to each imager and the intellectual property of each manufacturer, individual functions will not be the focus of this work. Instead it is the goal of this project to measure the performance of TIC as complete systems from lens to display screen, not to reverse engineer processing algorithms.

In addition to filtering the signal and adjusting the gain to produce a meaningful image, most TIC have an automatic mode shift operation. When a certain trigger is reached, the thermal sensitivity of the imager is reduced so that a larger temperature range can be surveyed. The trigger to this function is different for each imager. Some imagers shift when radiation from a specific transition temperature is detected. Others shift when a certain percentage of the pixels detect the transition temperature. Still other imagers contain several gradual mode shifts inherent in the gain electronics. There is no standard governing the function of the electronic iris (EI) mode, making it very difficult to quantify or account for in system performance testing.

1.2.3.4 Output Signals

Each thermal imaging camera outputs its video signal through an electronic port. The output signal transmits the video data to a recording device or to a central location. Firefighters sometimes often use radio transmitters to relay the signal to a central controller where the data from all thermal imagers can be observed to define a unified strategy for firefighting or rescue.

In the United States, the output signal is a National Television System Committee (NTSC) analog video signal composed of three signals called Y, U, and V. The Y signal contains luminance data and a frame synchronization pulse. The U and V signals contain the color data for each image. The NTSC standard contains 29.97 frames per second (fps) and interlaces even and odd lines at a refresh rate of 59.94 Hz with 486 total lines. The three signals are then frequency-division multiplexed (FDM) and output through a Bayonet Neill Concelman (BNC) coaxial connection (National Television Systems Committee 2006).

In addition to being output as a television signal, the image is also further modified and digitized for transmission to a display screen where the pixel intensities are converted into a projected luminance visible to the human eye. The screen is the final transmission of the thermal information to the user of the camera. Although any display technology can be implemented in the imager, this work will focus on imagers employing liquid crystal displays (LCD).

An LCD is an array of liquid crystal chambers acting as controllable light filters. Small chambers are filled with long thin liquid crystal molecules that flow easily like fluid but bend light waves like solid crystals. The crystals are sandwiched between two plates with small parallel grooves etched into them. The grooves act to orient the long crystals and the two plates are set at 90° from one another. In the no voltage state, this orients the liquid crystals as shown in Fig. (1-5a). As light passes through the chamber, light waves are twisted along this 90° rotation. Polarizing filters are placed on either side of the plates at 90° so that only parallel oriented polarized light can enter the chamber, and it is then rotated 90° by the crystals, and all the light is allowed to exit the chamber through the second polarizer.

The amount of light passing through can be controlled by applying an electric field to the chamber. The crystals have weak intermolecular forces and are able to be moved by an electric field. When a strong field is applied, the crystals all shift into the direction of the field as shown in Fig. (1-5b), and no longer cause light to twist in the chamber. This results in no light passing through the chamber because the two polarizers are aligned 90° apart, cutting off all transmission. The amount of light passing through the chamber is controlled by the strength of the electric field, thus adjusting how much light is twisted and allowed to pass through the polarizers.

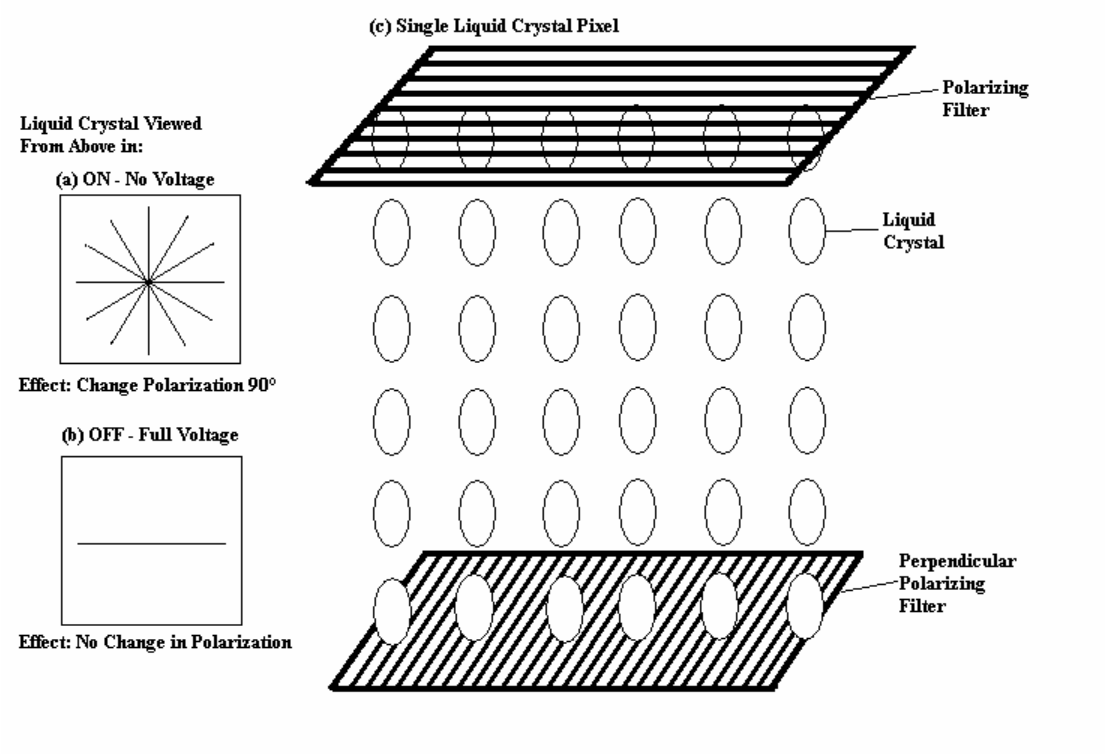

Figure 1-5 – A single LCD pixel with perpendicular polarizing filters (c), and the liquid crystal viewed from above in the the ON, (a), and OFF, (b), positions

An LCD display uses a backlight behind the array of chambers and the amount of light allowed to pass through each chamber is digitally controlled by a voltage applied to small transparent electrodes placed on the plates of each chamber. The basic LCD design incorporates only gray levels for each pixel, but it can be designed with three separate chambers at each pixel location filtering/transmitting amounts of red, blue, and green light to create a full color image. Although some TIC utilize color options for their display screens, this paper will only focus upon measuring the quality of monochrome LCDs.

1.3 Existing Performance Metrics

The objective of the current study is to develop a test methodology that objectively describes aspects of the performance of TIC under realistic use conditions. There are currently a number of tests defining camera performance, image quality, and LCD performance. These tests have been designed to test individual aspects of the imaging system, but a single standard test has not been developed to measure the performance of a complete thermal imaging system. The existing standard tests also are not focused on testing the performance of an imager under realistic first responder conditions such as environments containing flames or smoke. It is important to design objective tests so that imagers can be compared and selected by the user based on their specific needs and applications. There is a great deal of value, however, in the existing performance metrics and they will be discussed here.

1.3.1 Standard Imaging System Quality Metrics and Methods

There are several standard methods for measuring the quality of an imaging system. These tests are designed to measure the performance of an imager with respect to noise, temperature resolution, and spatial resolution.

The standard test for detector noise in a TIC is the noise equivalent temperature difference (NETD). This is used to measure the temperature difference that gives a signal to noise ratio of exactly one (ASTM E1543-00 2006). This measurement is made by viewing a temperature controlled target over a uniform temperature blackbody background. The target for measuring NETD is shown in Fig. (1-6a). The temperature of the target, T2, is varied around the range of the blackbody

temperature, T1, and the signal is the difference in output from the blackbody and the target. A typical signal obtained from scanning one horizontal line is shown in Fig. (1-6b). This series of measurements provides the system intensity transfer function (SITF) which is a graph of differential signal output, ΔS, as a function of temperature difference, ΔT , shown in Fig. (1-6c).

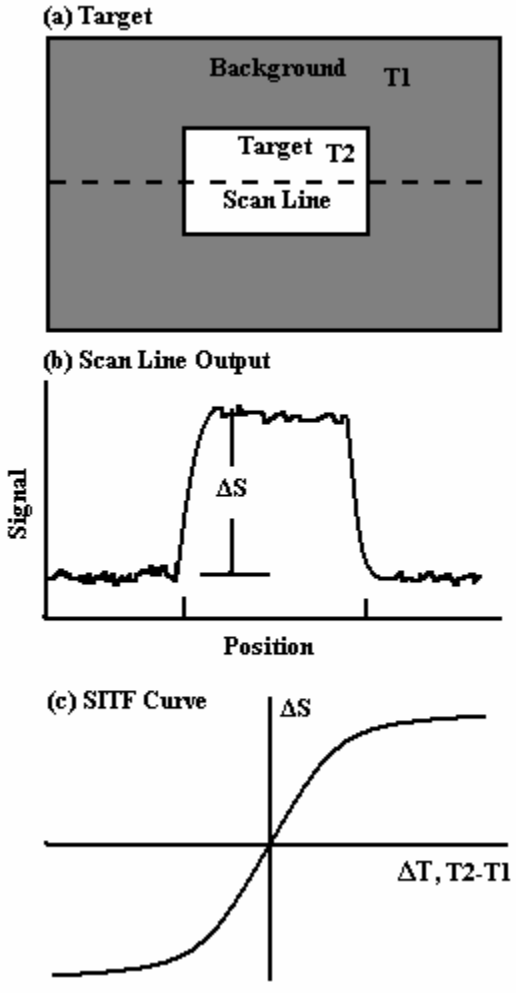

Figure 1-6– NETD target (a), generalized scanline output (b), and generalized SITF curve (c) obtained from many temperature differences (Based upon figures introduced by Driggers, et al)

The noise is the root mean square (RMS) of the signal, S_i, obtained from the uniform blackbody N times. The NETD is then calculated by Eq. (1-7)

$$NETD = \frac{\frac{1}{N}\sum_{i=1}^{N} S_{i,T=T1}}{\frac{d(\Delta S)}{d(\Delta T)}_{\Delta T=0^{+}_{-}}} \qquad 1\text{-}7$$

where the numerator is the RMS of the noise and the denominator is the slope of the SITF at small temperature differences (Driggers et al. 1999).

The signal and noise measurements must be made by measuring direct voltage from the sensor array, measuring the analog video output signal from the imager, or by digitizing the analog video output into gray levels.

The system resolution is determined by the modulation transfer function (MTF). Modulation is the ratio of the amplitude of a sine wave to the average of the wave. The MTF is a measure of the ability of an optical system to transfer the modulation of a target to the image produced. The MTF will have a value for each spatial frequency of sine wave, thus describing the resolution of the system.

There are numerous ways to measure the MTF of a thermal imaging system. The MTF can be measured directly by viewing sinusoidal targets of various spatial frequencies and determining the modulation of each image. It would be extremely difficult and expensive to construct sinusoidal thermal targets for direct MTF measurements, however, so the application of Fourier analysis can simplify the

measurements mathematically. MTF can be measured by determining a point spread function (PSF) or an edge spread function (ESF) as shown in Fig. (1-7).

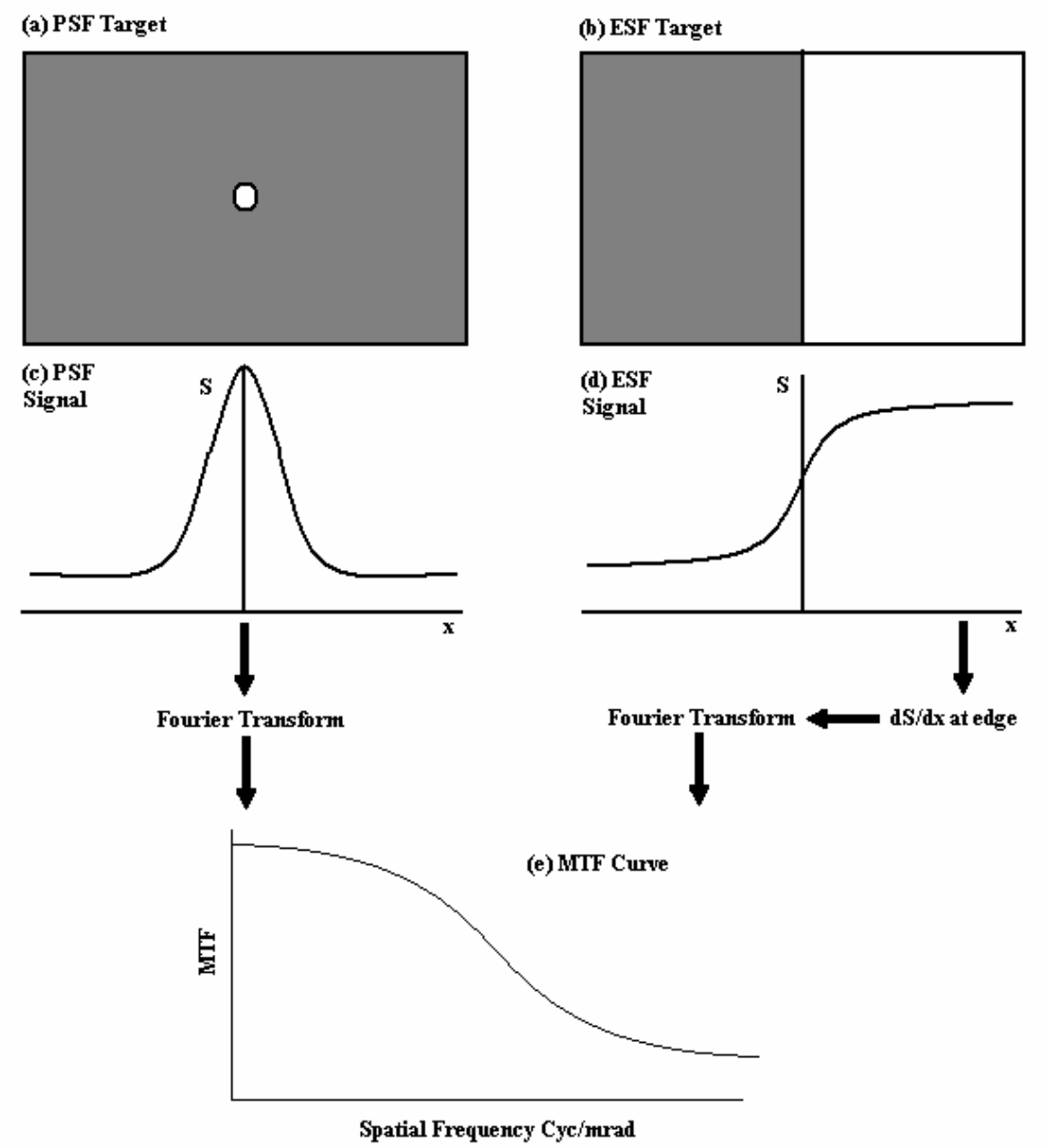

Figure 1-7 – Determining MTF with point source and edge source targets (a) and (b), generalized scan line output signals (c) and (d), and a generalized MTF curve (e) (Based upon figures introduced by Driggers, et al)

The PSF is the impulse response of the optical system to a point source input shown in Fig. (1-7a). A single point source will result in a finite sized blur in the sensor output as shown in Fig. (1-7c). The size of this blur can be used to determine the MTF of the system through a 2-D Fourier transform. The ESF is the response of the optical system to a sharp contrast edge shown in Fig. (1-7b). The MTF can be derived from the ESF by differentiating intensity with respect to the x-direction to get the line spread function (LSF) and taking a 1-D Fourier transform. The Fourier transform is valuable because it separates an image into the sum of its sine wave components at various frequencies. This allows for the MTF to be determined at all spatial frequencies simultaneously with one target. A sample MTF curve is shown in Fig.(1-7e) (Driggers et al. 1999).

The LSF can also be measured directly without differentiating the ESF to determine MTF. A target containing an impulse in the horizontal direction and a constant line in the vertical direction will provide the LSF and its value can be directly transformed to yield the MTF. The ESF and LSF both provide the MTF in only one dimension, although the additional differentiation required by measuring the ESF contributes noise to the measurement. While the PSF provides the MTF in two dimensions with just one measurement, the amount of radiance from the point may not be sufficient to provide accurate results. In general, these mathematical tests for MTF are subject to errors, but can greatly simplify test setups (Boreman 2001).

A drawback of MTF measurements requiring Fourier analysis is that the system must be linear shift invariant. Staring imagers are constructed of a finite number of pixels with limited fill factor and a thus a limited spatial resolution. Slight vertical or horizontal adjustments of the imager with respect to the target may vary the image quality. Because TIC for commercial applications are not perfectly linear shift invariant, the application of Fourier analysis to their output signals is not reliable.

The problem of spatial invariance can be overcome by measuring MTF with a random pattern target. The target for this test is a random white noise filter over a uniform source, such as a flat panel blackbody. The target filter is generated by applying a white noise power spectrum across a range of spatial frequencies from zero to the Nyquist frequency of the imager. A white noise power spectrum density (PSD) means that the intensity of the signal is nearly uniform for all spatial frequencies, see Eq. (1-8),

$$PSD = \left| \frac{\sum_{i=1}^{N} FFT(S_i)}{N} \right|^2 \qquad 1\text{-}8$$

where the PSD is determined by the signal intensities along row i, N is the number of rows, and FFT implies taking a Fast Fourier Transform. The Fourier transform yields complex numbers defining amplitude and phase of frequency components which are averaged for all the rows and the PSD is the square of the absolute value of the averaged frequency terms. The PSD is a vector of numbers describing the intensity of the input signal at each spatial frequency (Daniels et al. 1995).

Fig. (1-8a) displays an example of a white noise target with uniform PSD. The power spectrum of the image is shown in Fig. (1-9) and is nearly uniform over all spatial frequencies. The MTF of a system is determined by viewing a target with known PSD and calculating the PSD of the resulting image. The MTF is calculated as a continuous function of spatial frequency (ξ) by Eq. (1-9).

$$MTF_{system}(\xi) = \sqrt{\frac{PSD_{image}(\xi)}{PSD_{target}(\xi)}} \qquad 1\text{-}9$$

The image in Fig. (1-8b) represents the result of a system having the theoretical MTF from Fig. (1-9). It is clear that much of the high frequency components of the target have been obscured by the imaging system.

The major drawback of testing thermal imagers with random transparency targets is the cost. For imagers in the 8-14 μm range, the target must be constructed of ZnSe or Ge with various levels of metal deposits to block IR radiation from passing. The deposits must be small enough to act as individual sized pixels, randomly placed on the target, and random in their transmittance. For most practical testing purposes, the linear shift variance of traditional MTF measurements can be neglected.

(a) Original Target

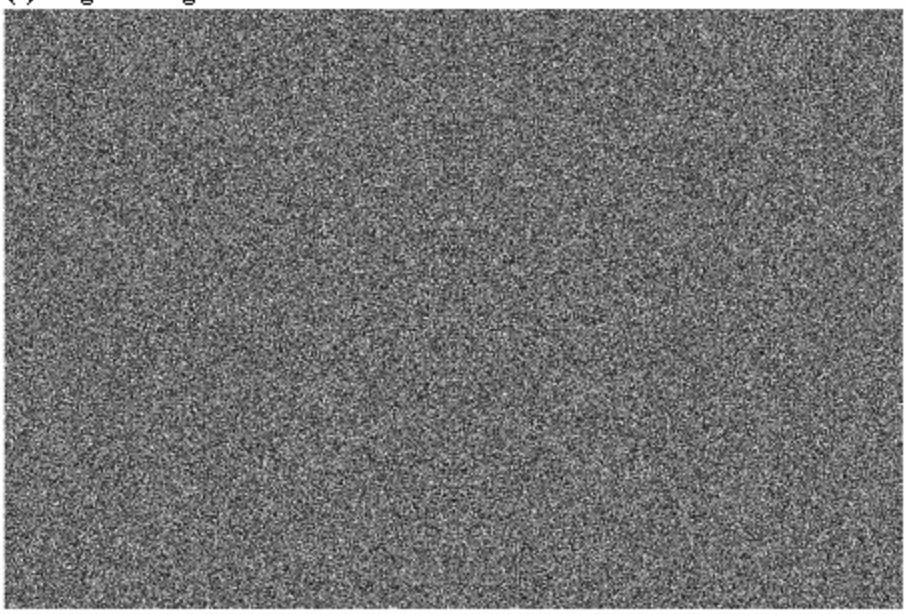

(b) Obtained Image

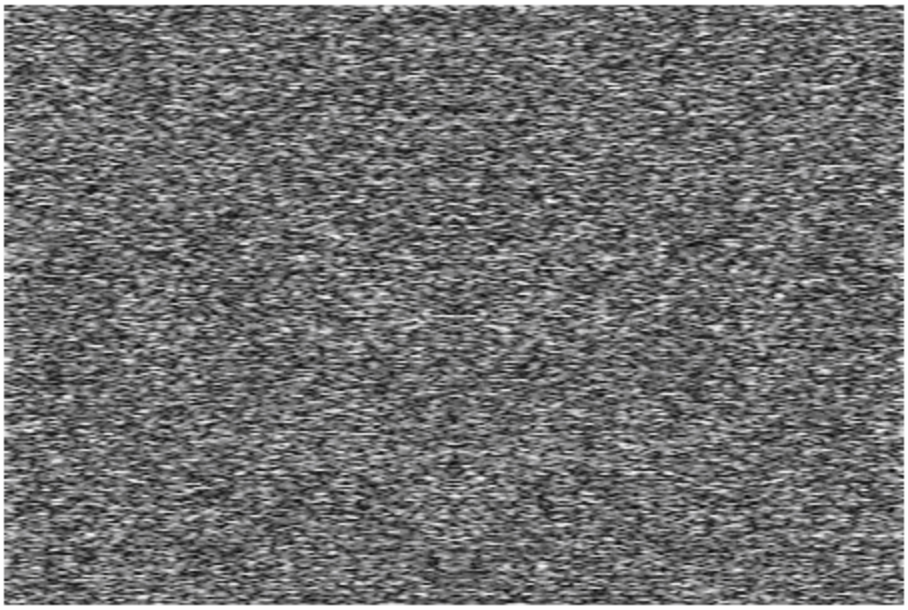

Figure 1-8 – 720 x 480 random noise target with uniform white noise PSD (a) and the image obtained through an optical system with a simulated MTF (b)

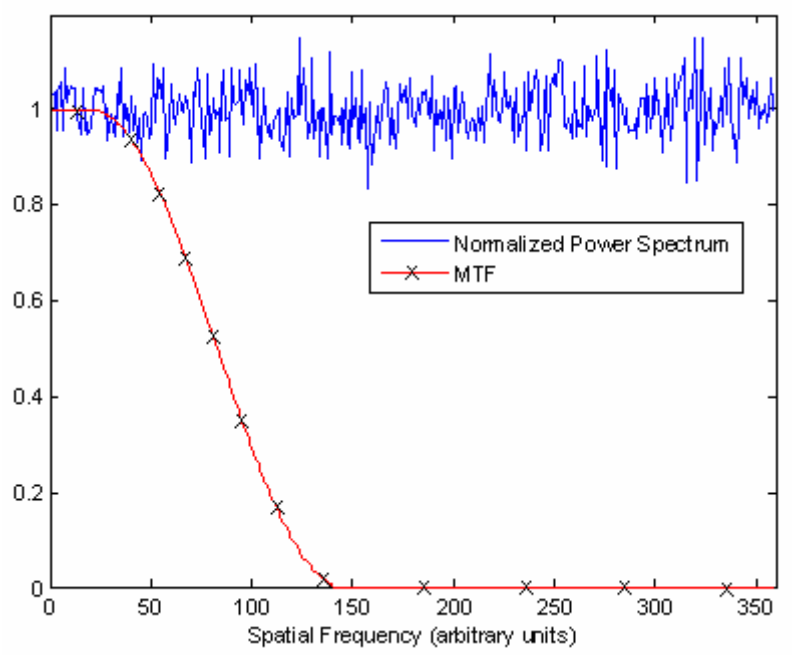

Figure 1-9 -Normalized PSD of white noise target and MTF of imaging system

Another measure of spatial contrast is the contrast transfer function (CTF). This test measures the transfer of Michelson contrast, $C_{Michelson}$, or the ratio of the difference between minimum pixel output signal, $S_{MIN,}$ and maximum pixel output signal, S_{MAX}, to their sum shown in Eq. (1-10).

$$C_{Michelson} = \frac{(S_{MAX} - S_{MIN})}{(S_{MAX} + S_{MIN})} \qquad 1\text{-}10$$

The CTF of an optical system or individual component is then simply the measured output contrast of an image divided by the input contrast shown in Eq. (1-11).

$$CTF_{Component} = \frac{C_{Michelson,in}}{C_{Michelson,out}} \qquad 1\text{-}11$$

The contrast transfer function is similar to the MTF, except it is defined as the ability of the system to transfer a square wave input signal instead of a sine wave. The CTF

can be measured easily for TIC because it measures the contrast between alternating light and dark line patterns rather than sinusoidal modulation. Targets are constructed as a hot background plate with cold fluid tubes placed in front. An example of a CTF target as seen by a TIC is shown in Fig. (1-10). The CTF measures the intensity of detected irradiation for both hot and cold target lines. The hot lines will produce a higher intensity signal in detector elements and the maximum and minimum pixel intensities are recorded. The CTF is recorded as a function of the spatial frequency, ξ, of the alternating target bars. The spatial frequency of the target is calculated in units of cycles/mrad by Eq. (1-12)

$$\xi = \frac{1}{1000} \times \left(\frac{D}{d} \right) \qquad 1\text{-}12$$

where D is the distance from the target to the camera and d is the width of one cycle, both the hot and cold bar (Holst 2000).

Figure 1-10 – Thermal bar target used for CTF measurements as viewed by a TIC with crosshair pointer

The MTF and CTF can be related mathematically through the square and sine waves by Eq. (1-13).

$$MTF = \frac{\pi}{4} CTF \qquad 1\text{-}13$$

The MTF and the CTF can be measured at any point in the signal transfer process and are the convolution of the MTF/CTF of each component in the system including lenses, sensors, amplifiers, display screen, etc. Currently most measurements are made from a voltage output like the video-out signal, however, and do not take into account additional signal processing or the effect of the display screen. The ability of the display screen to project an image is usually tested with a human observer.

1.3.2 Measuring an Image Signal

1.3.2.1 Trained Observer Testing

Current test methods for commercial (non-emergency response) infrared cameras are generally conducted in one of two ways. Firstly, TIC are subjected to tests in which trained observers describe the quality of a displayed image. The observers view spatial targets with adjustable temperature differences and the limits of identification are recorded. Examples of spatial targets and the TIC images obtained are shown in Fig. (1-11a) and (1-11b), respectively. This method is used to determine the minimum resolvable temperature difference (MRTD) shown in Fig. (1-11c), or can be adapted for the general recognition of targets such as people or vehicles. The results for a number of observers, or a number of observations by one observer, are then averaged to obtain a general description of camera performance. These tests are valuable because they describe the performance of the entire imaging system to a human observer. However, these tests are by definition subjective; they are subject to the influence of mood, age, vision, and a large number of other human variables.

While many of these effects can be eliminated through repeated testing and averaging of multiple observers, the limitations of subjective testing are apparent (Holst 1998).

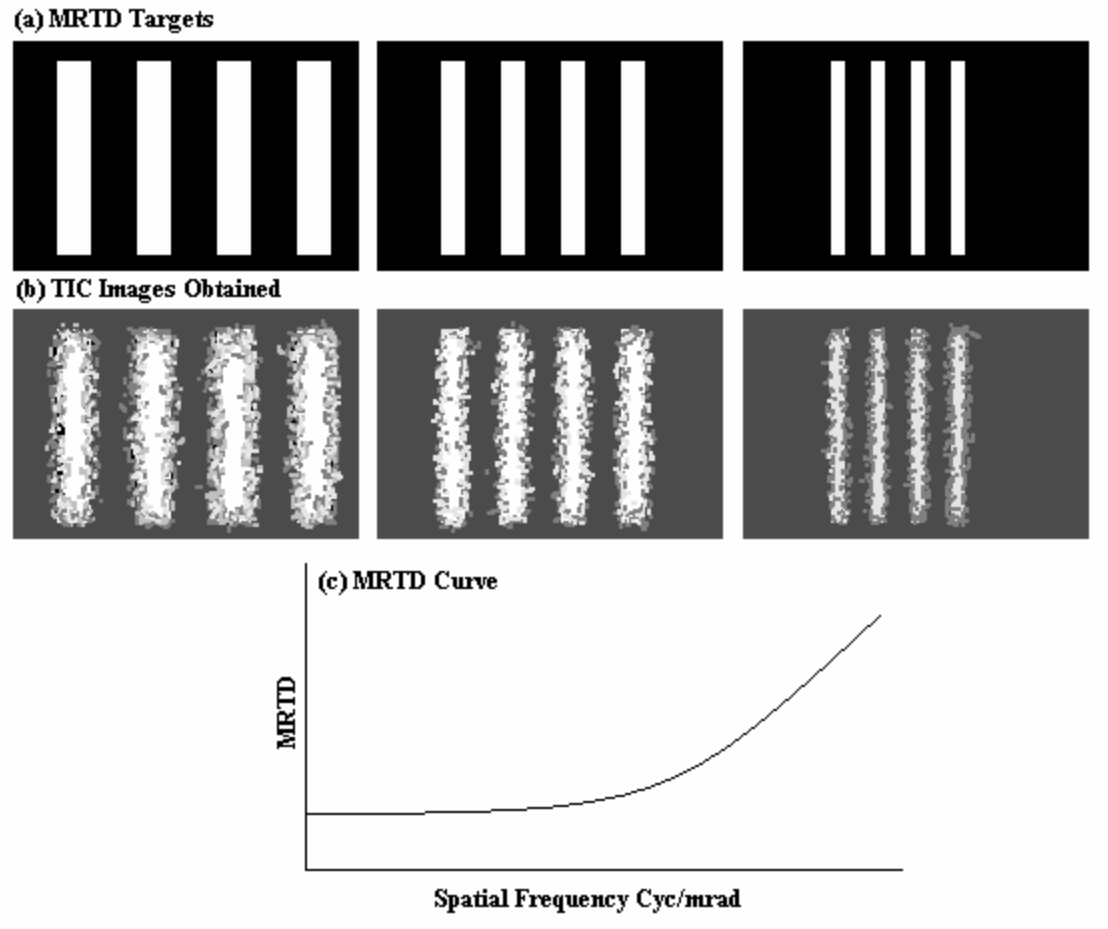

Figure 1-11– MRTD targets of various spatial frequency (a), images obtained of those targets from a TIC with some blur (b), and an MRTD obtained through multiple test cycles (c) (Based upon figures introduced by Driggers et al)

1.3.2.2 Testing the Composite Output Signal

The output image signal can be easily measured through the BNC connection. In this way, individual pixel intensities can be recorded and compared to determine the performance of the imager. Tests of this nature are effective at objectively comparing mathematical values recorded from the imagers from flexible and tailored test

conditions. The repeatability of this data is highly dependent upon the measurement, recording, and analysis system used. The performance of all components or their combination must be carefully characterized. The benefit of these measurements is that testing can be performed in fire and other hazardous conditions, and the data is easily comparable using various computer analysis programs. Limitations associated with this method include incomplete characterization of internal signal amplification, digitization, filtering, interpolation, and display screen projection luminance. The measurements are also subject to distortions from digital recording and transfer. As a result, users may be misled regarding the actual visible performance of the imager.

Thermal imaging cameras for firefighting applications are complete visualization systems. They include an infrared detector, integration and processing hardware, an output signal, and an image display screen. The final product of the camera is what the user can see on the screen, not the quality of the digital signal. In order to describe the actual system function to the user, the display screen output must be measured.

1.3.2.3 **Standard LCD performance metrics**

There are numerous standard tests for measuring flat panel display screens. These tests are used to measure contrast, linearity, uniformity, reflectivity, and luminance. These tests involve applying a specific and known input to an LCD and measuring the ability of the screen to portray that same input as output.

Determination of the electro-optical transfer function (EOTF) is one of the most basic tests for a display screen. The voltage command level of the signal sent to each display pixel will determine the amount of luminance generated by that pixel. The EOTF defines the relationship between the voltage command level and the displayed luminance by Eq. (1-14).

$$EOTF = \frac{L}{V} \tag{1-14}$$

where L is the luminance and V is the voltage input to a pixel.

Generally, this relationship is designed to follow a logarithmic relationship in order to make luminance appear linear to a human observer. The human eye is capable of much greater resolution at lower luminance, and thus the display output can be tailored to this effect. This relationship is often referred to as a gamma function, because γ is the logarithmic coefficient that relates the digital input and the display luminance. The general equation for this relationship is described in Eq. (1-15),

$$L = a_L V^{\gamma} + L_b \tag{1-15}$$

where L is luminance, a_L and γ are empirical constants, V is the digital input level, and L_b is the luminance of a pixel with zero input, where luminance is measured in cd/m^2.

The Video Electronics Standards Association (VESA) display metrology committee has defined a standard method of measuring the EOTF for flat panel display screens. The test requires measurement of the luminance of the display over a range of input levels. The screen is filled with a single grey level and the luminance is measured,

this measurement is then repeated for a number of grey levels ranging from 0-255 (for an 8 bit display) (Video Electronics Standards Association Display Metrology Committee 2001).

Standard display tests require a specific input to the screens, i.e. alternating pure black and pure white pixels. These specific inputs are not easily done for infrared cameras due to the integration of the system. A thermal target must be made to replicate the ideal signals used for standard display tests. In order to measure γ for TIC displays with reasonable accuracy, the detector pixels must span a range of targets with well characterized temperature and emittance. Only by viewing a full range of input intensity can the level of output be correlated to the luminance of the display screen. The design such a target will be discussed in detail in chapter 4.

1.3.2.4 **Aspects of a Quality Test Metric**

Although various test methods exist for other types of imaging systems, there are no standard test metrics for thermal imaging cameras used for first responders. Users have no basis for comparison of cameras. The National Institute of Standards and Technology (NIST) is currently working to produce a set of standard tests that will identify the quality of a TIC's performance.

A quality test metric for TIC should address three key issues of performance. The ability of the sensor array to produce a coherent image of the thermal scene is of utmost importance. This involves testing the ability of the camera to produce a low

noise, high contrast image of various spatial targets. Directly testing the camera for CTF/MTF and thermal sensitivity is fundamental to determining the performance of the camera.

The second key issue is the ability of the imager to perform well under realistic use conditions. These conditions should replicate fire scenarios and include the presence of variables such as smoke, heat, flames, and water. Determining the ability of the imager to perform in a real emergency is a key element to testing TIC for first responder applications that is not present in many other standard testing situations.

The next issue of concern is the ability of the camera to relate the signal to the user. It is important to define a metric that can objectively describe the performance of a TIC from the infrared sensor array to the display screen. Such a test will require luminance measurements of the display screen.

Most flat panel display measurements are not easily adapted for displays that are integrated into thermal imaging systems. Most tests require that specific digital command levels and patterns are displayed and analyzed. Display screen testing often requires input such as full screen black, white, or grey, alternating white and black pixel lines, and other complex shapes and patterns. The input of specific levels and patterns can prove very difficult when thermal scenes must be supplied as input to the system. TIC are complex, integrated systems; producing a representative input signal to the display screen would be difficult in many cases. Creation of a

controlled target image on the infrared detector array is important for display screen testing.

Ideally, a test would be developed that can relate display screen performance, at a suitably wide range of target conditions, to the easily measurable composite output signal which can be obtained under realistic emergency test conditions. This information would allow current objective test methods to reflect the actual performance of TIC through mathematical relationships to display performance.

In order to define such a test, one must understand the internal processing of the thermal image. The image signal undergoes a number of conversions and transitions throughout the data transfer process in the TIC. First, the sensor array converts target radiance into an electrical signal. This signal is then amplified, filtered, and scaled to produce an image. The image is converted into an NTSC composite signal to be sent to the camera output port. The signal is also digitized and sent to an LCD screen. The screen then displays the signal on its pixel array as a luminance image. The data transfer process is described in Fig. (1-12). The figure also includes two methods of measuring the output signals. While there is a relationship between the signals at each of these points, complex algorithms are used to modify the signal and are unique to each camera manufacturer and model. Describing the quality of the signal at one point in the data line does not necessarily provide an adequate estimate of quality at

another point.

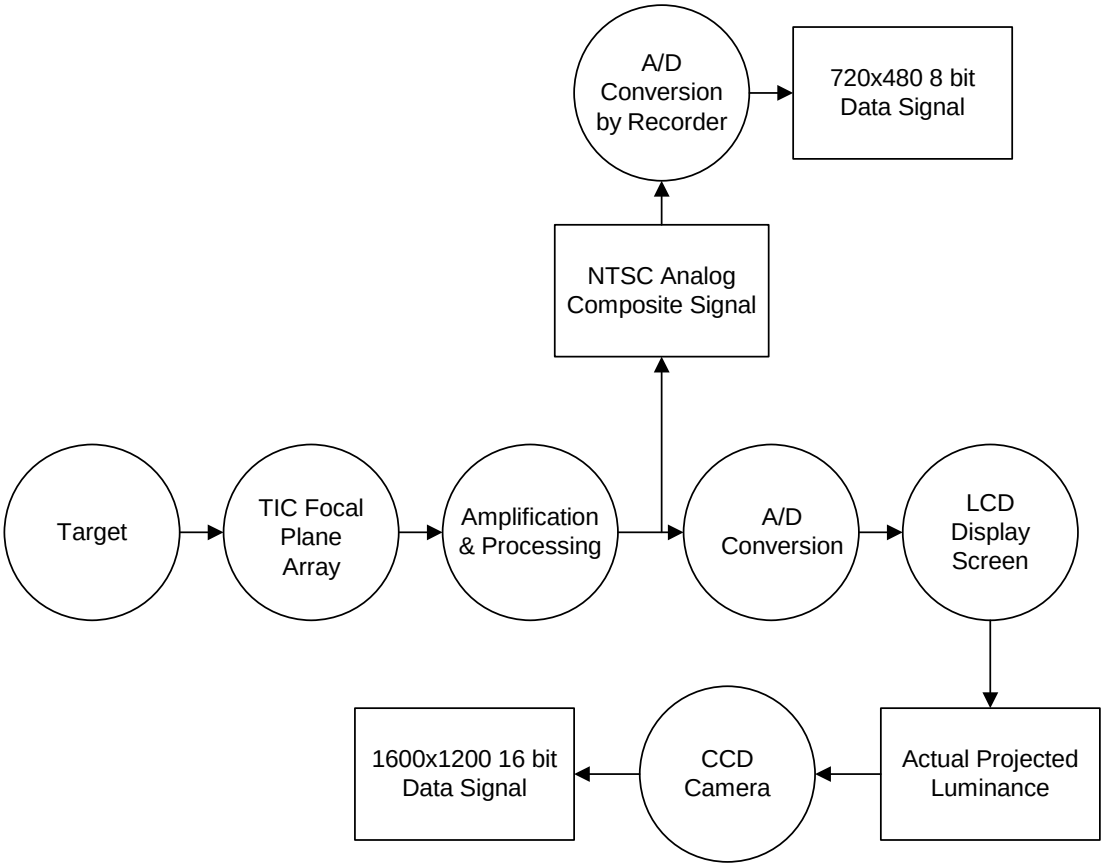

Figure 1-12- Basic data transfer process for TIC with LCD screen and recording devices. The particular signal modification system for specific TIC may deviate from this model.

A complete test of the imaging system would measure the quality of the sensor under realistic conditions and relate that data to actual visual output performance. The display screen performance should be calibrated to the video output signal and the output signal should be used to record noise and spatial resolution measurements in extreme use conditions.

1.4 Objectives

The purpose of the current study is to advance the development of standard performance metrics for TIC for first responder applications. The basic physics involved in the transport of radiation from a thermal source to the detector FPA will be discussed in Ch.2. This discussion will focus upon radiation transmission through typical combustion atmospheres. The following chapters will focus upon the actual performance of TIC. This research will focus on two aspects of the performance.

First, the ability of the imager to function in realistic conditions will be examined. Full scale fire testing will be performed to determine the ability of the imager to detect a target viewed through hot, smoky atmospheres. This will examine the both the detector response and the signal processing response to high temperatures and soot. The test itself will also be analyzed to determine if full scale fire testing provides adequate data to an investigator about the performance of TIC. This information can be found in chapter 3.

Second, the effect of the LCD display screen on final image performance will be determined. Parallel work on this project records only the video-output signal, and it is imperative to determine how this signal is related to the final image seen by the user. This study will examine the EOTF of the video-output for several TIC and determine if the effect of additional internal signal modification and the display screen significantly alter the signal. Information on this process can be found in chapter 4.

The significant conclusions from these studies will be summarized and recommendations for continued efforts into developing a standardized test metric will be discussed in chapter 5.

2 Radiation Transfer and Combustion Atmospheres

TIC measure thermal radiation emitted by objects at various temperatures after it has passed through a potentially obscuring path length. The radiance emitted from all objects in the imager FOV is focused onto the focal plane array (FPA) of the camera and a thermal image is created. The final thermal image is the result of the temperature and emissive properties of objects in the scene, the transmissive properties of the atmosphere between the object and the FPA, the camera optics, and the electrical response of the detector to irradiance. The most difficult thing to resolve from these various dependencies is the emissivity of the objects and the transmissivity of the atmosphere. These two topics and their impacts on TIC imaging and measurements will be discussed in this chapter. The emissivity of surfaces and the ability to assess that parameter for various surfaces will be presented in the first section and then a following section will present the impact of atmospheric composition and discuss how radiative properties of the combustion gases influence the ability to interpret thermal scenes through TIC measurements.

2.1 Surface Emission

2.1.1 Emissivity of surfaces

The radiative properties of a surface include the emissivity, ε, absorptivity, α, transmissivity, τ, and reflectivity, ρ. These properties are functions of wavelength and are all defined by ratios of actual radiative flux to the maximum possible flux for that surface. For emissivity, the maximum possible flux is blackbody flux,

determined by integrating Planck's Function for intensity, Eq. (1-1), with respect to direction. The maximum possible absorbed, reflected, or transmitted flux is considered to be the total incident flux at the surface.

In general, both objects and gas boundaries can be considered mathematically identical as surfaces with defined radiative properties. For the purposes of this discussion, however, the properties of opaque solid surfaces will be considered first, and contributing gases as transfer media will be discussed in the next section of this report. The distinction between the two is made largely for organizational clarity.

All objects above absolute zero emit and absorb thermal radiation. TIC detect the emitted radiation and use it to construct a thermal scene. The emitted radiation is a function of both the temperature and emissive properties of the object. A perfect blackbody emitter has emissivity of one in all directions and at all frequencies. No actual surface emits as a perfect blackbody. The emissivity of real surfaces is a function of the temperature of the surface, and the angle and the frequencies of emission. .

The spectral directional emissivity, $\varepsilon'_\lambda(\phi,\theta,\lambda)$, is a function of both the direction and wavelength of the emission. It is calculated by determining the intensity of radiation emitted by a surface shown in Eq. (2-1),

$$\varepsilon'_\lambda(\phi,\theta,\lambda) = \frac{I_{\lambda e}(\lambda,\theta,\phi)\cos\theta\sin\theta\Delta\theta\Delta\phi}{I_{b\lambda}(\lambda,T)\cos\theta\sin\theta\Delta\theta\Delta\phi} \qquad 2\text{-}1$$

where θ is the angle perpendicular to the emitting surface, ϕ is the azimuthal angle, $I_{\lambda e}$ is the determined intensity, and $I_{b\lambda}$ is the theoretical blackbody emitted intensity calculated from Planck's function (1-1).

The two angles can be combined to define the solid angle, $\Delta\Omega$, for a small area element ΔA by Eq. (2-2).

$$\Delta\Omega = \sin\theta\Delta\theta\Delta\phi \tag{2-2}$$

This can also be expressed in differential form in Eq. (2-3).

$$d\Omega = \sin\theta d\theta d\phi \tag{2-3}$$

The total directional emissivity can be determined by the ratio of the integral over all wavelengths of the actual intensity and of the blackbody intensity shown in Eq. (2-4).

$$\varepsilon'(\phi,\theta) = \frac{\int_0^\infty I_{\lambda e}(\lambda,\theta,\phi)\cos\theta\Delta\Omega d\lambda}{\int_0^\infty I_{b\lambda}(\lambda,T)\cos\theta\Delta\Omega d\lambda} \tag{2-4}$$

The spectral directional emissivity can be integrated over a hemispherical solid angle to determine the spectral hemispherical emissivity as in Eq. (2-5).

$$\varepsilon_\lambda(\lambda) = \frac{1}{\pi}\int_{2\pi}\varepsilon'_\lambda(\phi,\theta,\lambda)\cos\theta d\Omega \tag{2-5}$$

The final total hemispherical emissivity can be determined by combining both integration processes and can be simply written in the form of Eq. (2-6).

$$\varepsilon = \frac{1}{\pi}\int_{2\pi}\varepsilon'(\phi,\theta)\cos\theta d\Omega \tag{2-6}$$

Real surfaces can be very complex, exhibiting a different emissivity in all directions and at all wavelengths. The properties of many surfaces can be simplified, however.

Many surfaces act as diffuse emitters. This means that the emissivity is independent of the direction. In addition, other surfaces are often considered to be gray emitters. This implies that the emissivity is not a function of wavelength (Brewster 1992).

The emissive properties of real materials are often described depending on whether the material is metallic or nonmetallic. The emissivity of nonmetals tends to be high, while metals are mostly reflective with low emissivity. Both materials tend to have diffuse emission at angles near perpendicular, but act quite differently at glancing angles. Nonmetals tend to decrease in emissivity smoothly and uniformly past the diffuse angles before reaching zero at an angle of $\pi/2$. Metals, on the other hand, tend to increase in emissivity as the angle from normal increases, and then sharply decrease to zero at $\pi/2$. This trend is shown in Fig. (2-2).

The spectral emissivities of these materials also follow different trends. The emissivity of metals tends to decrease as wavelength increases, while the emissivity of nonmetals increases with wavelength. The general trends are shown in Fig. (2-3).

According to Kirchoff's Law, the emissivity and absorptivity of an isothermal surface will be equal in magnitude. Radiant flux striking an opaque (nontransmitting) surface will either be absorbed or reflected. This implies that the reflectivity of a material can be determined simply by Eq. (2-7).

$$\rho'_\lambda = 1 - \varepsilon'_\lambda \qquad 2\text{-}7$$

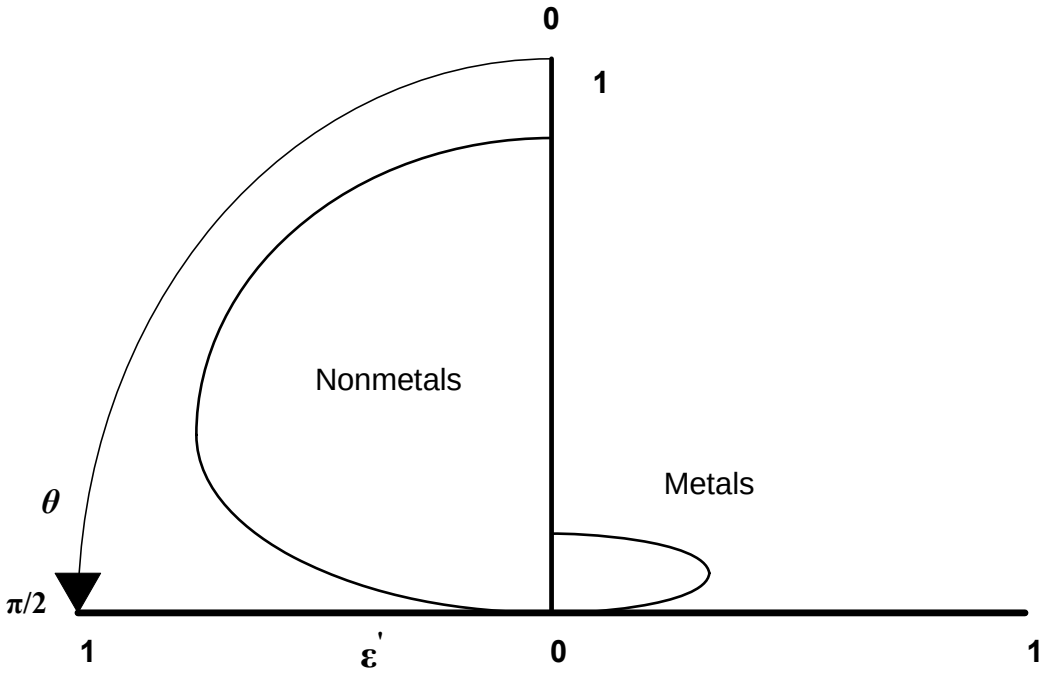

Figure 2-1 – Directional emissivity as a function of angle for metals and nonmetals (Based on figures introduced by Brewster)

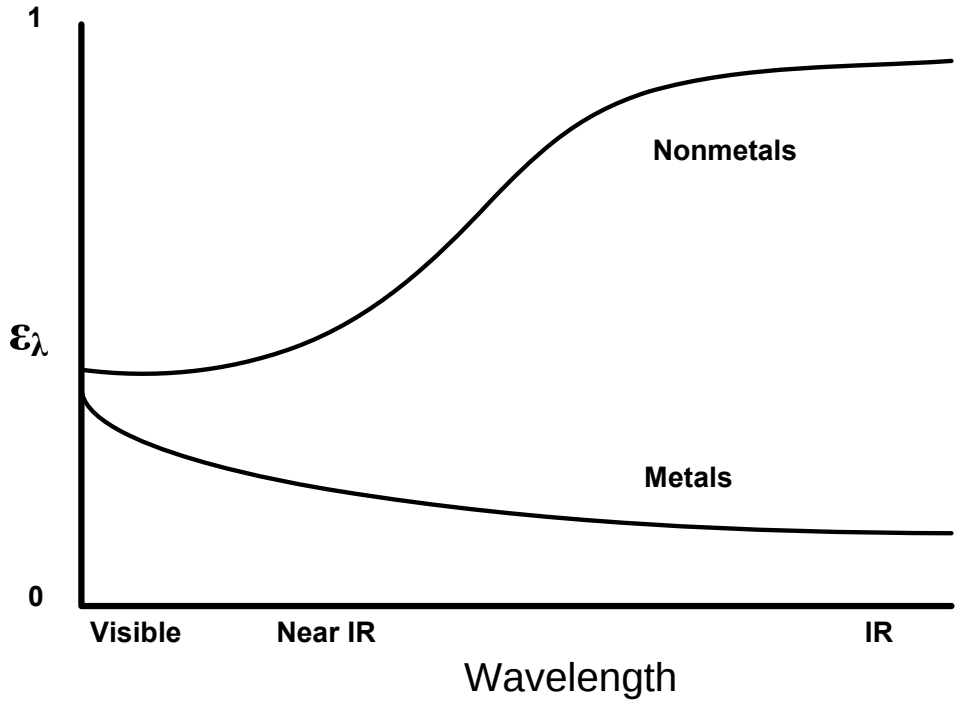

Figure 2-2 – Spectral emissivity as a function of wavelength for metals and non metals in the visible, near IR, and IR regions (Based on figures introduced by Brewster)

For materials in the FOV with low emissivity, such as metals, reflections of thermal radiation from other sources will become visible. Often, these reflections will be specular, implying that an image of the reflected source will be visible. Common glass that is perfectly transmissive in the visible is highly reflective in the IR region of the spectrum. These reflections will create a false image of the thermal scene and may even result in users seeing themselves in a pane of glass. It is important for users of TIC to recognize this principle to better understand the thermal scene and make decisions based upon it. Other common materials viewed by TIC for first responders include wood, plastic, carpet and upholstery, stone, and human skin. The total hemispherical emissivities of these surfaces at various temperatures are summarized in Table (2-1) (Brewster 1992).

Table 2-1 – Total hemispherical emissivity of common materials

Material	Emissivity
Wood	0.8-0.9
Plastic	0.91
Polished Steel	0.1
Cotton Cloth	0.77
Concrete	0.94
Skin	0.95

2.1.2 Thermal targets for Thermal Imaging Calibration

A thermal target is a complex array of emissive components that create a specific thermal signature. The thermal target is designed to perform a specific task, and can range from a uniform surface, alternating hot and cold lines, or even a human or vehicle on a complex background. A target is defined by its temperature and

emissive properties in contrast to those of a background. A discussion of thermal signature and target detection can be found in section 1.2.2 of this report.

Controlling the size, shape, temperature, and surface properties of a thermal target are key aspects in the design. The size and shape are determined by the desired type of performance test. The emissivity should be known and maximized to increase the thermal signal sent to the device under test (DUT). A flat, black paint of known emissivity is often used because it creates a diffuse and gray surface. This allows the radiance to be easily modeled without concerns about direction or spectral variation.

2.2 Transmission of IR Radiation in Combustion Gases

The atmosphere through which radiation travels will have a significant effect on the energy emitted from a surface as it travels to the detector. Atmospheres will transmit, reflect, absorb, scatter, and even emit radiation. Such events occur as gas molecules and particulates, such as soot, react to the incident radiative energy. Absorption and emission of radiation is due to changes in the energy levels of gas molecules.

2.2.1 Energy state transitions in gaseous molecules

The total energy level of a gas molecule is the sum of its translational, rotational, electronic, and vibrational energy states. Translational energy transitions are trivial in concept and total energy, and thus will not be discussed here. The other energy states, however, are quantized, or have discrete transitional values. The energy level of a photon in a radiative wave is defined by Eq. (2-8),

$$\Delta E = h\nu \qquad 2\text{-}8$$

where E is the energy in the photon, h is Planck's constant equal to 6.626 x 10^{-34} J·s, and υ is the frequency of the wave.

When an emitted photon strikes a molecule with energy equal to one of the possible discrete values, it is absorbed and the energy level of the molecule is increased. Emission from gas molecules occurs when an excited molecule drops from one energy state to another. The photon emitted carries the energy lost from this translation at a wave frequency determined by Eq. (2-8). The energy gained or lost from each transition is determined by the basic physical properties of that energy state.

The relative magnitude of the various energy transitions is $\Delta E_{elec} > \Delta E_{vib} > \Delta E_{rot} > \Delta E_{trans}$. Absorption and emission related to electronic transitions occur in the visible part of the frequency spectrum, vibrational in the IR, and rotational in the far IR and microwave regions. Thus the primary energy shifts relevant to IR radiation and thermal imaging are molecular vibrational transitions. A typical energy transition diagram for a diatomic molecule is shown in Fig. (2-3).

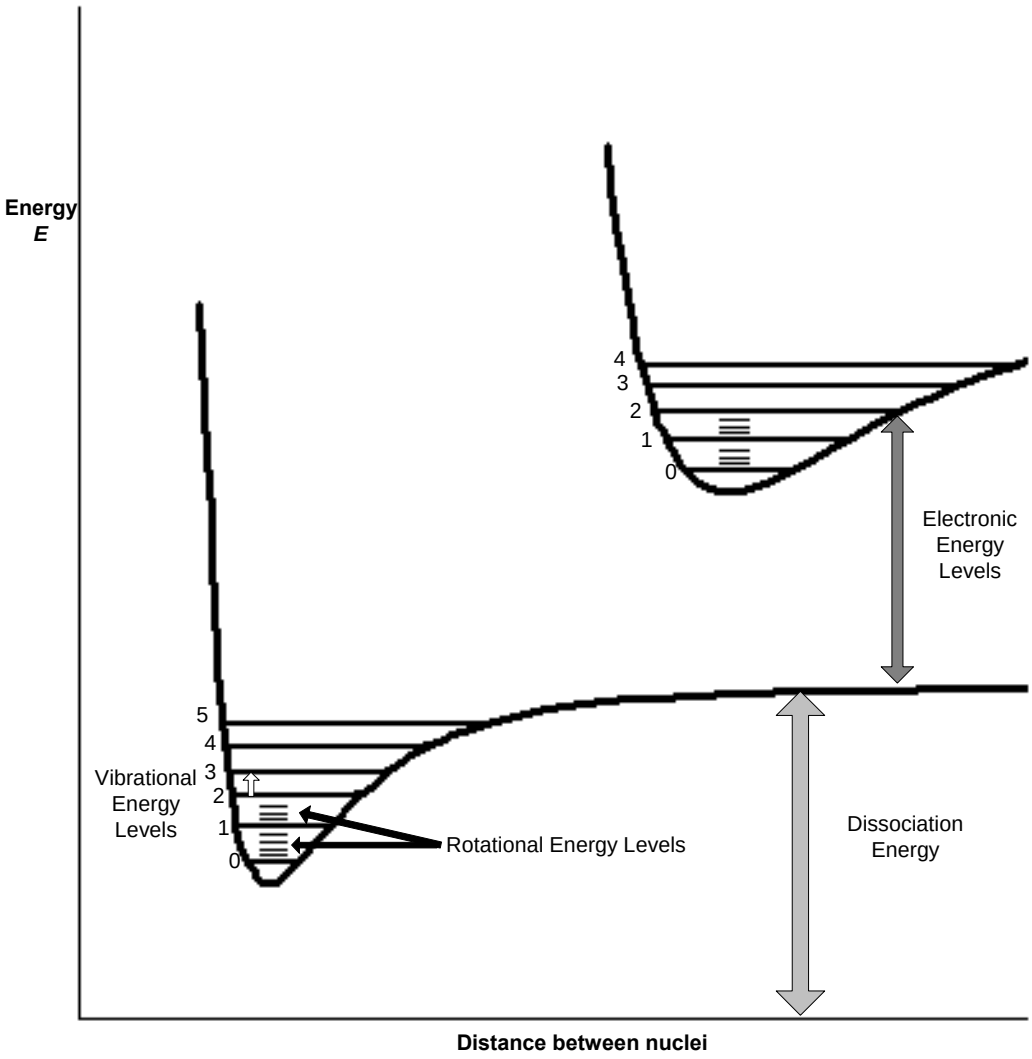

Figure 2-3 – Electronic, vibrational, and rotational energy level transitions for a diatomic molecule with Lennard-Jones potential energy curves

Molecular vibrations between two molecules are often modeled as harmonic oscillations similar to two masses connected by a spring. This model combines Hooke's law for energy in springs with the Shrödinger wave equation to describe the quantum rotational energy levels by Eq. (2-9),

$$E_{vib} = h\nu_0\left(\upsilon + \frac{1}{2}\right) \tag{2-9}$$

where υ is the quantum number(υ = 0,1,2,3…) and ν_0 is the oscillator frequency. The frequencies associated with emission and absorption due to vibrational transitions can be described by Eq. (2-10),

$$\nu = \frac{E_2 - E_1}{h} = \nu_0\left(\upsilon_2 - \upsilon_1\right) \tag{2-10}$$

where the subscripts $_1$ and $_2$ denote initial and final states, respectively.

Although the rotational transitions are not highly energetic, when combined with vibrational modes they can affect the spectral absorption bands. Molecule pairs are often modeled as rigid rotators. A rotational constant, *B*, is defined for the system and from quantum theory the energy levels associated with these transitions are described by Eq. (2-11),

$$E_{rot} = Bhc_0 j\left(j+1\right) \tag{2-11}$$

where *j* is the quantum number (*j*=0,1,2,3…), *h* is Planck's constant, and c_0 is the speed of light in a vacuum.

The frequency of emission or absorption due to a change in rotational energy can then be described by Eq. (2-12)

$$\nu = \frac{E_2 - E_1}{h} = Bc_0\left[j_2\left(j_2+1\right) - j_1\left(j_1+1\right)\right] = 2Bc_0 j_2 \tag{2-12}$$

because the selection rules for rotation require that $\Delta j = \pm 1$.

Although the energy transitions due to pure rotational frequencies are quite small, they often occur in conjunction with vibrational transitions. This results in additional absorption bands surrounding the fundamental vibrational bands. The rotational and vibrational energy states can be combined to provide a relatively complete description of energy transitions of this form. This representation is known as the rigid rotator, harmonic oscillator model and the energy state is described by Eq. (2-13).

$$E = E_{rot} + E_{vib} \tag{2-13}$$

The quantum nature of gaseous energy levels results in discrete absorption and emission lines associated with various gases. This equation can also be applied to determine these frequencies. The probability of a photon having the exact frequency required for pure spectral absorption is very slim, however. The absorption of photons with frequencies close to the discrete spectral lines is facilitated by several physical processes including collision broadening, Doppler broadening, and natural broadening.

Collision broadening is perhaps the most significant of these processes in regular atmospheres. When a gas molecule collides with another molecule energy is transferred between the two objects. This process allows for photons with energy $v+dv$ to be absorbed by a molecule. The collision acts to supply or remove the energy dv required to match the quantum energy level for absorption.

The process of collision broadening is conceptually similar to adding a damping mechanism to the simple harmonic oscillator model. The effect of collision broadening is controlled by the temperature and pressure of the gas itself.

Doppler broadening relies on the motion of the molecule to change the relative frequency of a photon by *dv*. Natural broadening relies on the Heisenberg uncertainty principle to predict the momentum of the molecule. In common conditions and atmospheres, however, the effects of these types of broadening are insignificant compared to collision broadening.

The spectral response of many gases has been explored through the results of dispersion, electromagnetic, and quantum theories. These results help determine the optical constants *n*, the refractive index, and *k*, the absorption index, as functions of wavelength for various species. These topics can be further explored in classic radiation textbooks (Brewster 1992).

2.2.2 Radiative Transfer

The main concern of this section is the transfer of IR radiation through a contributing medium. As a beam of radiation passes through a reacting gas medium of path length *s*, its intensity is attenuated by the absorption and emission caused by the energy level transitions as well as scattering. The incident intensity upon the gas, $I_{\lambda 0}$, is a result of the emitting target surface described in the previous section. The change in intensity only due to absorption along the path length is shown in Eq. (2-14),

$$\left(dI_\lambda\right)_{absorption} = -\kappa_\lambda I_\lambda ds \qquad 2\text{-}14$$

where κ_λ is the linear absorption coefficient determined from the absorption index, k, of a gas by Eq. (2-15).

$$\kappa_\lambda = \frac{4\pi k}{\lambda} \qquad 2\text{-}15$$

The optical thickness of a medium over path length s is determined by integration over the distance through Eq. (2-16).

$$t_\lambda = \int_0^s \kappa_\lambda ds \qquad 2\text{-}16$$

The optical thickness is used to determine the radiative intensity at any point along the path length shown in Eq. (2-17).

$$I_\lambda(s) = I_{\lambda 0} e^{-t_\lambda} \qquad 2\text{-}17$$

The spectral absorptivity of the gas layer of total thickness s can be determined by Eq. (2-18).

$$\alpha_\lambda = \frac{I_{\lambda 0} - I_\lambda(s)}{I_{\lambda 0}} = 1 - e^{t_\lambda} \qquad 2\text{-}18$$

A reacting gas layer does not only attenuate radiation through absorption, it also contributes intensity through emission. The emission is modeled in the same way as the absorption above. According to Kirchoff's Law, an isothermal gas layer will have the same emission coefficient as the linear absorption coefficient. The change in intensity along the path length due to emission is shown in Eq. (2-19)

$$\left(dI_\lambda\right)_{emission} = \kappa_\lambda I_{b\lambda} ds \qquad 2\text{-}19$$

where $I_{b\lambda}$ is the intensity of blackbody radiation at the gas temperature.

The single ray intensity is also both attenuated and augmented from scattering. Incident radiation is scattered out of the direction of travel and radiation from other directions is scattered into the direction of interest. Attenuation due to scattering is modeled in the same way as absorption where $\sigma_{s\lambda}$ is the scattering coefficient.

$$\left(dI_\lambda\right)_{scattering} = -\sigma_{s\lambda} I_\lambda ds \tag{2-20}$$

Intensifying radiative intensity from scattering is a more complex analysis because radiation from all solid angles can be scattered into the direction of interest. If the probability that radiation from any direction, $\vec{\mathbf{s}}_i$, is sent into a particular direction, $\vec{\mathbf{s}}$, is $\Phi_\lambda(\vec{\mathbf{s}}_i, \vec{\mathbf{s}})$ then the energy flux scattered into direction $\vec{\mathbf{s}}$ is determined by integration over all solid angles in Eq. (2-21).

$$\left(dI_\lambda\right)_{scattering}(s)d\Omega d\lambda = ds\frac{\sigma_{s\lambda}}{4\pi}\int_{4\pi} I_\lambda(\vec{\mathbf{s}}_i)\Phi_\lambda(\vec{\mathbf{s}}_i, \vec{\mathbf{s}})d\Omega_i \tag{2-21}$$

Combining the effects of absorption, emission, out-scattering, and in-scattering gives the final equation of transfer along a single path (2-22).

$$\underbrace{\frac{\partial I_\lambda}{\partial s}}_{\substack{Spatial\\ Derivative}} = \underbrace{\kappa_\lambda I_{b\lambda}}_{Emission} - \underbrace{\kappa_\lambda I_\lambda}_{Absorption} - \underbrace{\sigma_{s\lambda} I_\lambda}_{Out\ -\ scattering} + \underbrace{\frac{\sigma_{s\lambda}}{4\pi}\int_{4\pi} I_\lambda(\vec{\mathbf{s}}_i)\Phi_\lambda(\vec{\mathbf{s}}_i, \vec{\mathbf{s}})d\Omega_i}_{In\ -\ scattering} \tag{2-22}$$

Further discussion on the equation of radiative heat transfer in contributing gaseous atmospheres can be found in Radiative Heat Transfer by Modest (Modest 1993).

2.2.3 Transmissivity of Gases Relevant to Combustion Environments

Common combustion atmospheres often contain significant contributions of CO2, H2O, CO, and smoke. Fig. (2-5) shows the transmissivity of common combustion products in the infrared range over a one meter path length.

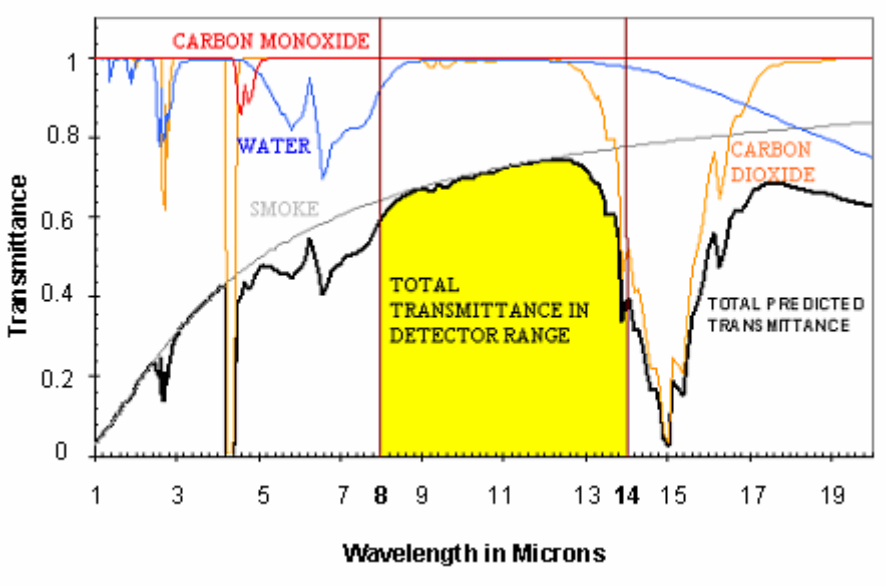

Figure 2-4 - Atmospheric transmittance for common fire conditions (Grosshandler 1993)

The emission of these products, highlighted in the 8-14 μm range, is shown in Fig. (2-6) and is moderately low even at the high temperatures found in burning environments.

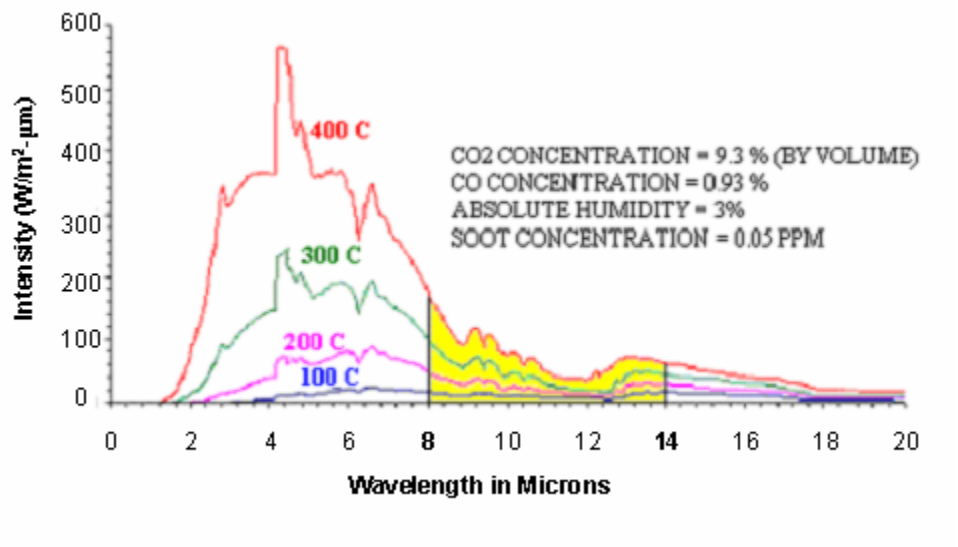

Figure 2-5 - Intensity of emitted radiation from combustion products at various temperatures (Grosshandler 1993)

Due to the high transmittance and low emission, TIC operating in this spectral range are capable of producing an accurate depiction of the thermal scene even in the presence of combustion products in the atmosphere.

Often, an important aspect of the thermal scene will be the identification of a human target. Fig. (2-7) shows the human contribution to the total radiance in a combustion atmosphere. The total radiance includes the sum of the radiance from the human body attenuated by absorption in the atmosphere and the emission of the atmosphere itself. Even at high gas temperatures of 400°C the human target will contribute a significant amount to the received signal.

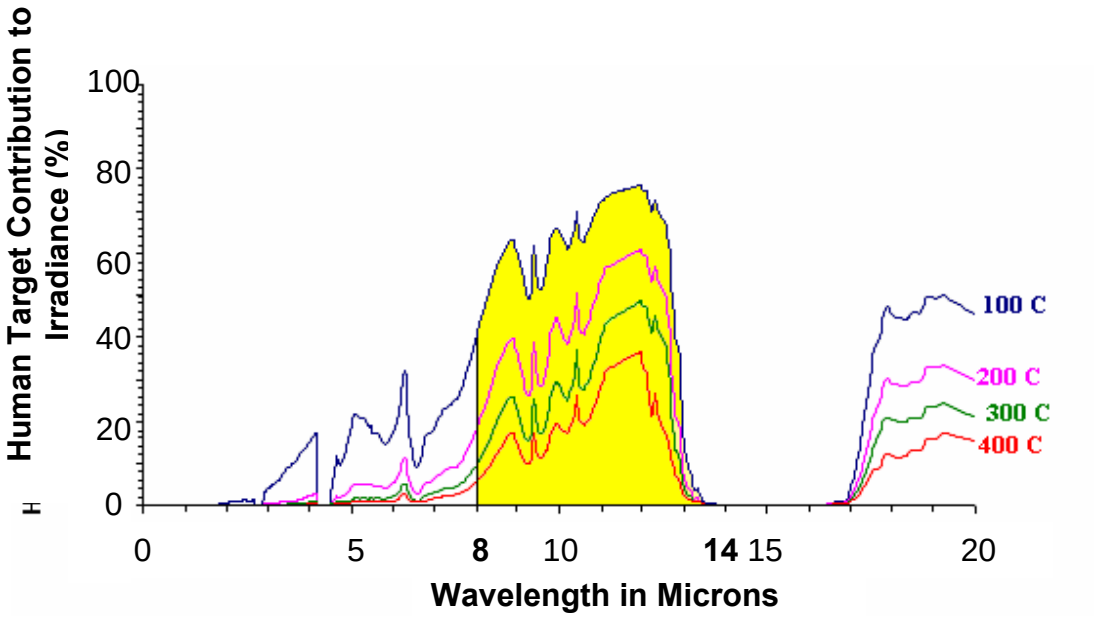

Figure 2-6 - Contribution of a human body at 30°C to total detected irradiance at various atmospheric temperatures (Grosshandler 1993)

Absorption bands of various combustion gases result in a reduction of the perceived gray body irradiance at specific frequencies. The use of the 8-14 μm range greatly reduces the effects of these absorption bands. In addition, although the peak of gray body radiation is shifted toward shorter wavelengths at higher temperatures, it should be noted that the total integrated radiative intensity is greater even in the 8-14 μm band for higher temperature surfaces.

2.2.4 Transmission through Soot and Its Impact on Thermal Imaging

Particulate matter is often of great concern in the radiative properties of combustion atmospheres. Particles suspended in the air contribute absorption and scattering effects to the transmission of radiation. The scattering of waves due to particulates result in diffraction, refraction, and reflection. The modes of particle attenuation are

shown in Fig. (2-8). If *w*, the distance between the particles, is much greater than the wavelength of interest the system can be modeled as single spheres.

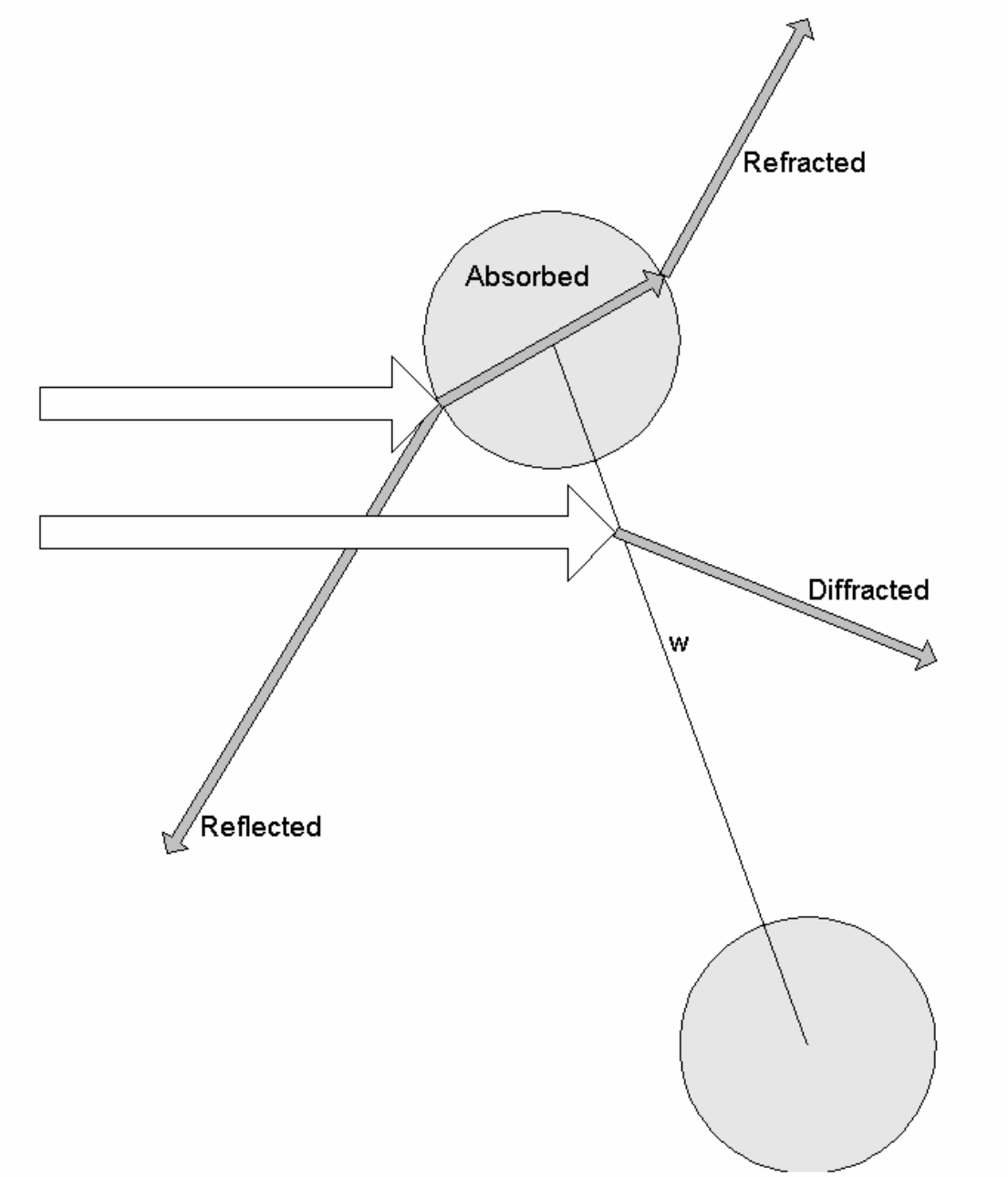

Figure 2-7 – Attenuation of incident radiation from particles due to reflection, diffraction, refraction, and absorption

Particles are frequently modeled as spheres reacting to incident radiation. The most common theory used to represent particles is the Rayleigh scattering model. This model is valid as long as the size of the particles is small compared to the wavelength of the radiation. This is the model used for gas molecules but it is also valid for small, submicron particles characteristic of soot. The validity is assessed by the size parameter, p_s, where a is the diameter of the particle.

$$p_s = \frac{2\pi a_D}{\lambda} \qquad 2\text{-}23$$

Soot is a particulate produced in fires. The size of soot particles is often on the order of 0.1 μm, so for infrared radiation in the 8-14 μm range, the size parameter is 0.045-0.079, well within the Rayleigh scattering regime. The scattering of radiation for particles of this size is proportional to $1/\lambda^4$. The absorption is proportional to $1/\lambda$. This implies that the amount of radiation scattered is significantly less than the radiation absorbed by soot particles.

For spherical soot particles in the Rayleigh regime, the linear absorption coefficient approximately depends only upon the volume fraction of particles in the atmosphere, and not on the distribution of particle sizes. The absorption coefficient can be determined by Eq.(2-24),

$$\kappa_\lambda = \frac{C_s f_v}{\lambda^{a_s}} \qquad 2\text{-}24$$

where C_s and a_s are empirical constants and f_v is the volume fraction of the soot (Modest 1993). Results by Millikan show that the exponent a is nearly directly proportional to the hydrogen to carbon ratio in the soot (Millikan 1961).

Augmentation is often of greater significance than attenuation from soot in thermal imaging applications. This is because soot acts as a strong emitter and is generally at a higher temperature than the targets of interest. The presence of highly concentrated, hot soot in the FOV will often result in a "white out" scenario, greatly reducing visibility and contrast.

The emissive and absorptive effects of soot cannot be avoided by careful spectral range selection the way that gas absorption bands can, however. The spectra of soot particles are broadband in nature and thus emissions occur at all spectral values. As presented in the full scale fire results in chapter 3, the reduction in target signal intensity due to soot in the FOV can not be avoided for current imager technology.

2.3 Imaging Optics

The imager lens contributes several components to the final irradiation received by the detector pixels. First, the lens attenuates the radiance due to imperfect transmission. The tranmissivity of Ge and ZnSe was shown in Fig. (1-2). The transmissivity for ZnSe is about 0.6 and for Ge 0.45 in the spectral range of interest.

This represents the ratio of radiation in the range of interest that passes through the lens to reach the detector.

The lens focuses and magnifies the intensity of the radiance. Pencils of rays from a large thermal scene enter the lens and are focused upon the small detector array. TIC for first responder applications often have a wide FOV and thus the magnification of rays is significant. The magnification factor is a geometric property of each unique optical system. Basic optical properties and design can be found in any rudimentary optics text.

A more complex optical property of the lens that becomes important is the spectral refractive index. The refractive index of the lens determines the angle to which incident radiation is bent and thus the location that energy is focused upon the detector array. The refractive index of materials, however, is spectral in nature. The refractive index of Ge is shown in Fig. (2-9) highlighted in the spectral range of interest for TIC (Infrared Handbook 1993).

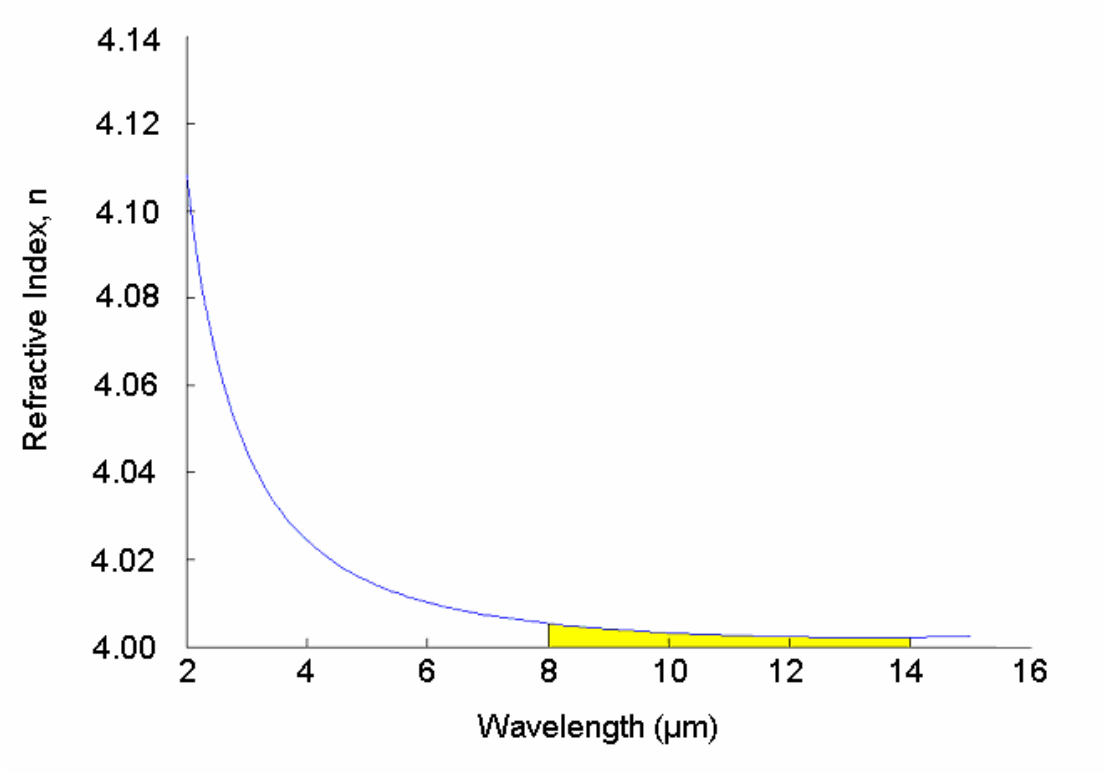

Figure 2-8 - Refractive Index of Ge as a function of wavelength, there is a very flat response in the operational region mitigating the effect of chromatic aberations

A dynamic refractive index can result in severe chromatic aberrations in the resulting image. This is due to the non-uniform bending of radiation of different wavelengths. Thus, much like a prism, the spectrum is focused at different locations on the pixel array. The index of Ge is very flat over the 8-14 μm range, and for this reason most TIC manufacturers choose Ge lenses instead of ZnSe, which has a much more dynamic refractive index in the range of interest. ZnSe is an appropriate material for long wave IR transmission windows, but is not often used as a lens material.

2.4 Conclusion

The radiative intensity of a thermal scene is subject to considerable alteration as it leaves the surfaces of interest and travels to the detector array. The final irradiance on the detector from the environment is a function of the emitting surfaces, the separating atmosphere, and the optics. The detector then converts this signal into an electrical signal, from which it is finally converted into a useful image for the user.

Ultimately, the ability of the imagers to convert the perceived irradiance into an image should be determined by a quality performance metric. The metrics examined will include the ability of the imager to detect a target signature in the presence of optical obscurants and high temperatures, and the ability of the imager to project that image onto a display screen for the user.

3 Fire Condition Performance Testing

An important aspect in the development of performance metrics for TIC is the ability of the imagers to function in realistic use conditions. In this regard, it is invaluable to consider the performance of the TIC for first responder applications in hot, smoky environments. Many full scale fire tests have been performed at NIST and the results of a few will be presented here as a basis for further understanding the complete process of developing performance metrics. These experiments were aimed at testing the spatial resolution of the imagers in hot combustion atmospheres through CTF testing. Various fuels and materials were burned and the imagers focused upon alternating hot/cold bar targets through the hot combustion gases.

3.1 Spatial Frequency Contrast Resolution in Burning Atmospheres

The purpose of these experiments was to test the ability of the imager to see through the hot upper smoke layer from multiple fire sources. The ability of the sensors and the internal gain functions were tested in various realistic fire situations.

3.1.1 Test Facility

The facility built for these experiments consisted of a long corridor with an adjacent room at one end. The room was constructed of fire resistant Marinite[2] and the corridor was constructed of regular sheet rock. CTF targets were placed on the wall

[2] Certain commercial entities, equipment, or materials may be identified in this document in order to describe an experimental procedure or concept adequately. Such identification is not intended to imply recommendation or endorsement by the National Institute of Standards and Technology, nor is it intended to imply that the entities, materials, or equipment are necessarily the best available for the purpose.

at the end of the hallway near the room. TIC were placed in four locations in the hallway to view the target from both near and far as well as high and low position. A scaled schematic of the burn facility is shown in Fig. (3-1).

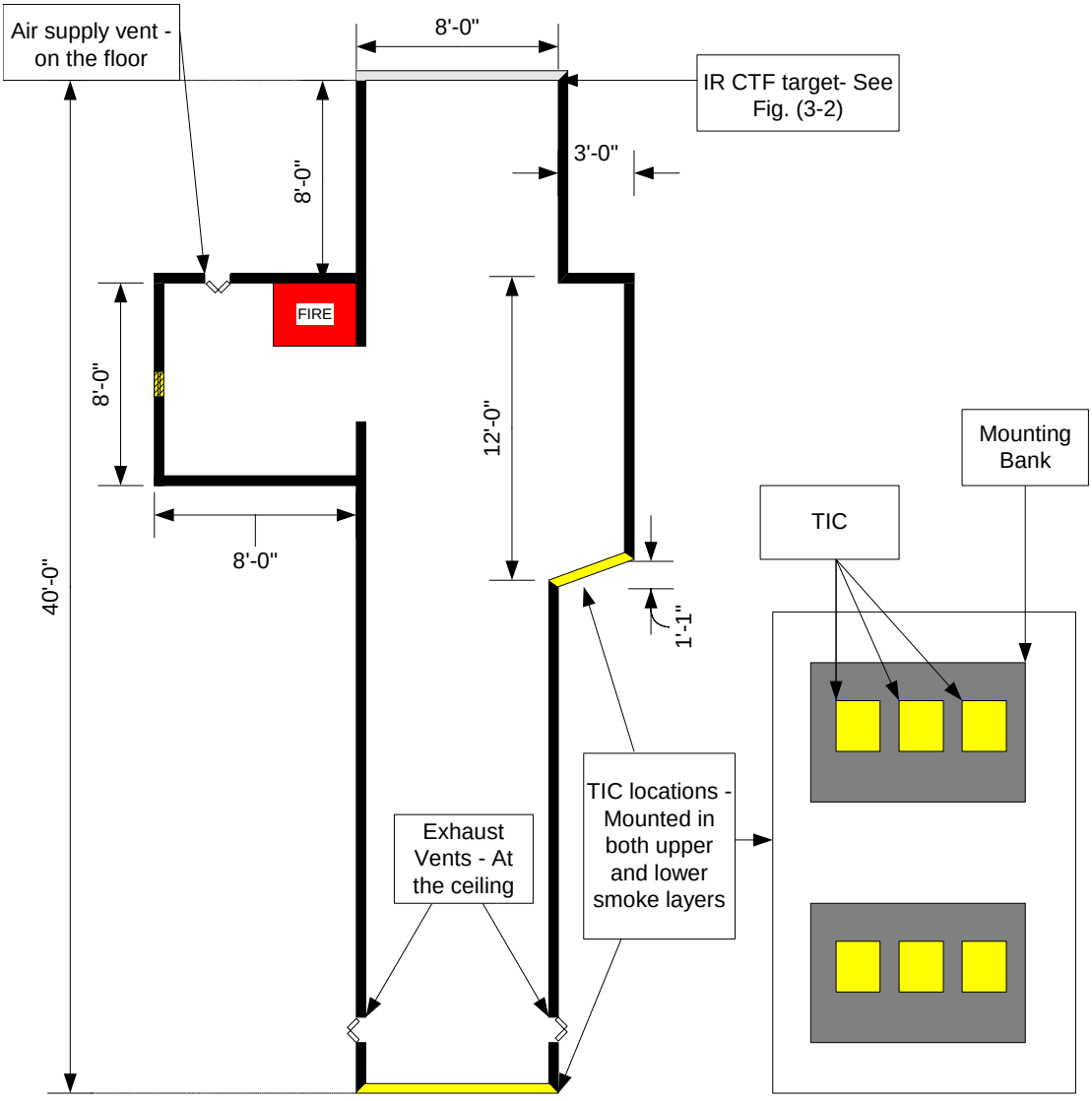

Figure 3-1 – Full scale fire facility design

The fires were burned in an adjacent room to remove hot flames from the FOV to avoid saturation of the cameras. The purpose of the experiments was to measure the effects of smoke on viewing targets, not the effects of saturation and glare due to flames. The fires were burned upon a large electronic scale. The scale was used to measure the mass loss rate of the fuel. This information was combined with the energy density of the fuel to determine the heat release rate (HRR) of the fire.

The air supply and ventilation rates in the system were controlled to maintain the neutral plane of the hot upper layer. Due mostly to temperature driven buoyancy effects, hot combustion gases and smoke particles rise in a fire. The buildup of these products over time results in a hot upper layer full of smoke particles and combustion gases, and a cooler lower layer. Often the line between these two regions is very distinct and abrupt (Drysdale 1998). The air supply to the fire room and ventilation rate in the hall was controlled to maintain the height of this line at 1.2 m. Two CTF targets were stacked vertically to allow for contrast measurements to be taken in both the hot upper layer and cool lower layer.

The targets consisted of a hot plate background with cold water bars placed in front. The background was a solar panel with water channels attached to an electric hot water heater supplying water at 50°C. The cold bars were copper pipes attached to the main building water supply at 23°C. The targets consisted of three different spatial frequencies having four inch, three inch, and two inch bars against the

background. Two targets were built so that one could be placed in the upper smoke layer and the other at floor level. The targets are shown in Fig. (3-2).

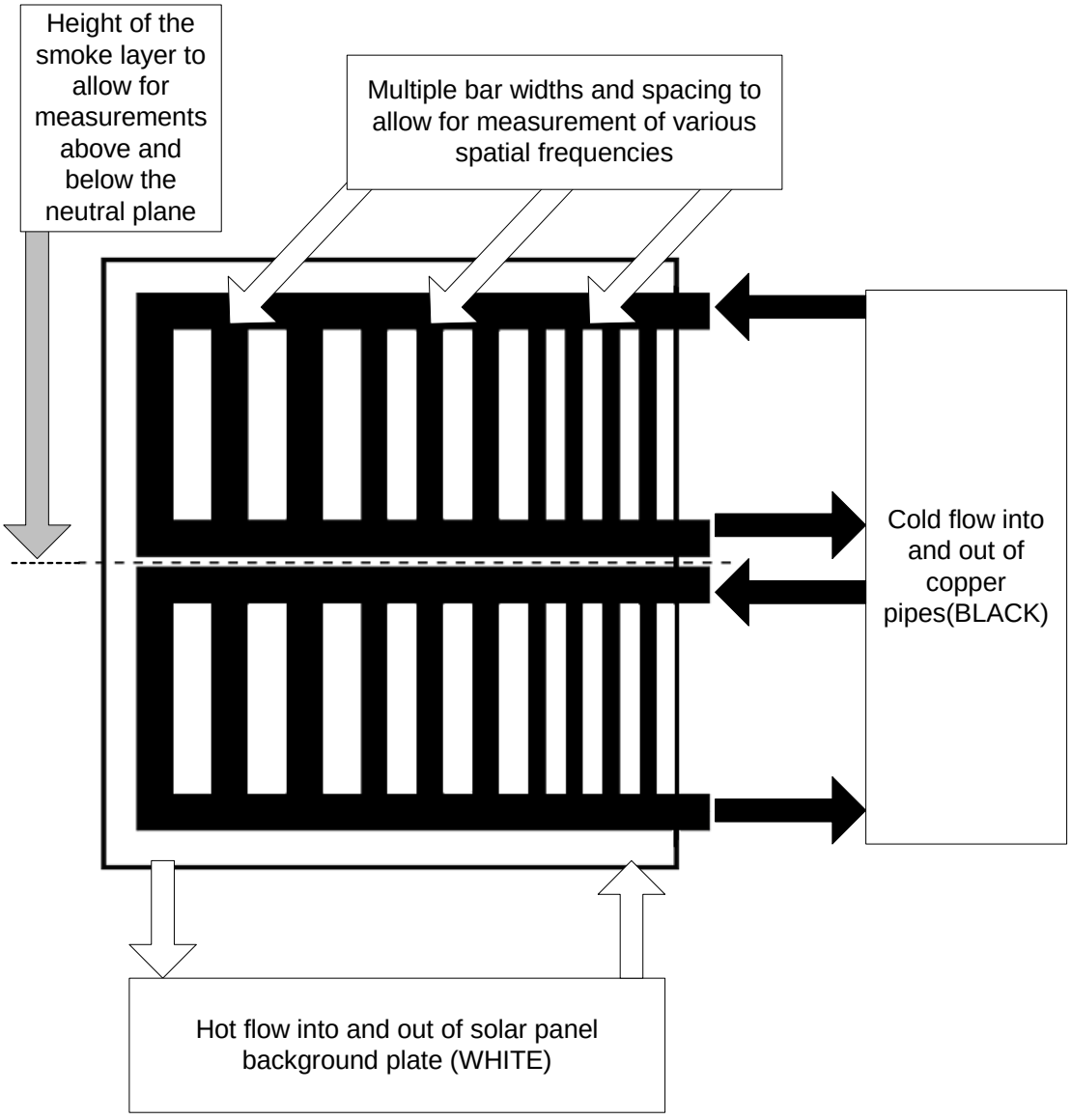

Figure 3-2 - CTF targets with three different spatial frequencies in the smoke layer and below the smoke layer used in full scale fire experiments

The TIC were mounted on rigid supports that could be rotated through each of the four locations during a single fire test. The supports also provided a weak nitrogen purge on the lens of each camera to prevent buildup of soot during testing. The video

output signal from the imagers was recorded through a 60 Ω coaxial cable with a Sony mini-DV digital tape recorder. The video from all the imagers was synchronized using an electronic match consisting of a hot wire running through a packet of regular matches with a thermocouple inside. At the start of each test the match was ignited in the FOV of the imagers providing a visible occurrence to synchronize the tape. Each burn lasted for about thirty minutes and the positions of the TIC were moved to each of the four camera locations at five minute intervals.

3.1.2 Data Analysis

The CTF of the imagers was analyzed from the digital tape by a LABVIEW program. The program selects a specific area of the FOV containing a target of contrast at known spatial frequency. Each frame contains six regions to be selected, one for each of the three spatial frequencies at both target heights. The minimum and maximum intensity is determined for each row and then averaged for all rows and the CTF calculated for each frame in the video. The data presented here is the CTF calculated from the time average of the minimum and maximum pixel intensities. Ordinarily, CTF measurements are normalized to the contrast at zero spatial frequency. This provides information solely about the contrast reduction due to increasing frequency. In this case, however, we are concerned with both the spatial resolution and the absolute contrast, so the CTF is normalized to the maximum possible contrast in 8 bit recording. The error is determined by calculating the temporal standard deviation of the pixel intensities and combining as the sum of squares with the deviation from multiple tests. The maximum and minimum CTF is then calculated from these

deviations in pixel intensities and is shown as the error bars on the data plots. This variation in repeated testing is considered to be the uncertainty in these measurements. The procedure is described in Table (3-1).

Table 3-1 – CTF Data Analysis Procedure

Step	Input	Processing	Output
1	Complete burn video	Cutting 2 minute segments in each imager location	4 fire video clips
2	Single position video clip	Select region of interest; i.e. single spatial frequency segment	Trimmed video segment
3	Trimmed video segment	Convert RGB to grayscale with 0.299 red, 0.587 green, 0.114 blue standard ratio	Gray video data
4	Gray video	Determine maximum and minimum pixel in each row, average, and calculate CTF for each frame	Chart of max and min pixels and CTF vs. time for each video
5	Data chart	Determine time averaged maximum and minimum pixels, calculate mean CTF	Mean CTF
6	Data chart	Determine standard deviation of maximum and minimum pixels, calculate best and worse case CTF values	Standard deviation of CTF, value of error bars
7	Mean CTF and temporal deviation from each test	Average CTF from each test, combine sum of squares of temporal deviation with test to test deviation	Complete data for single spatial frequency
8	-	Repeat for all spatial frequencies observed	Plot of CTF vs. frequency with error bars

Although data was obtained for many various TIC, the data presented here only represents the four TIC that were also subjected to display screen testing described in the following chapter. These four TIC are selected because they employ the flat

panel LCD technology designed to be tested in the next chapter of this report. The other TIC utilize various other display technologies such as cathode ray tube (CRT) or headmounted displays.

It should be noted that viewing the 2" target from the close position results in the same spatial frequency as viewing the 4" target from the far position. This results in contrast resolution measurements at five different spatial frequencies. The identical frequency points provide insight into the effect of the optical path length on the contrast resolution. Because the further position of the 4" target requires a longer path length through absorbing gases and particulate matter, it should have a lower CTF as shown in the sample results in Fig. (3-3).

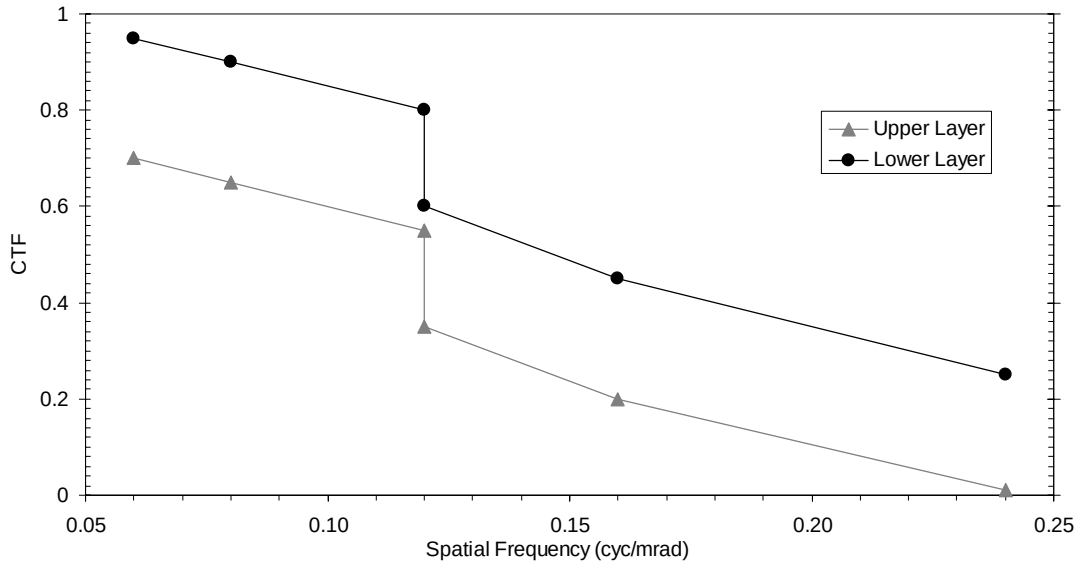

Figure 3-3 – Example of a CTF curve obtained from a generic full scale fire experiment highlighting the effect of the upper layer and the optical path length on CTF

One serious of tests burned methanol, CH_3OH, pool fires of different sizes. Methanol was used in these tests because it gives off very little smoke, creating an upper layer that would consist primarily of hot combustion gases. These tests determined the effect of hot gases on the resolution of the imagers. As discussed in chapter 2, the hot gases should not excessively absorb the signal from the targets nor contribute a large signal from emission. There is only one 350 kW fire included in the data because the walls of the enclosure began to burn during the other test producing smoke and increasing the HRR, making the results invalid. The results of 50 kW methanol fires on imager contrast resolution are shown in Fig. (3-4) for various TIC and in Fig. (3-5) for 350 kW methanol fires. No data was obtained for imager A during these tests.

An increase in the HRR of the fire reduced the spatial contrast resolution of all three imagers. This result is expected because internal gain functions in the imagers are controlled by the effective temperature range in the FOV. The hot gases should not absorb or emit radiation in the desired spectral range along the line of sight to the target, but rather they act to heat the walls and other surfaces in the FOV. The required range of temperature detection is increased as the size of the fire grows, and thus the thermal resolution is decreased reducing the apparent contrast within the target.

Imager C was the only TIC forced to shift into EI mode by the high temperature gases. This mode represents a drastic change in the thermal range of the detector

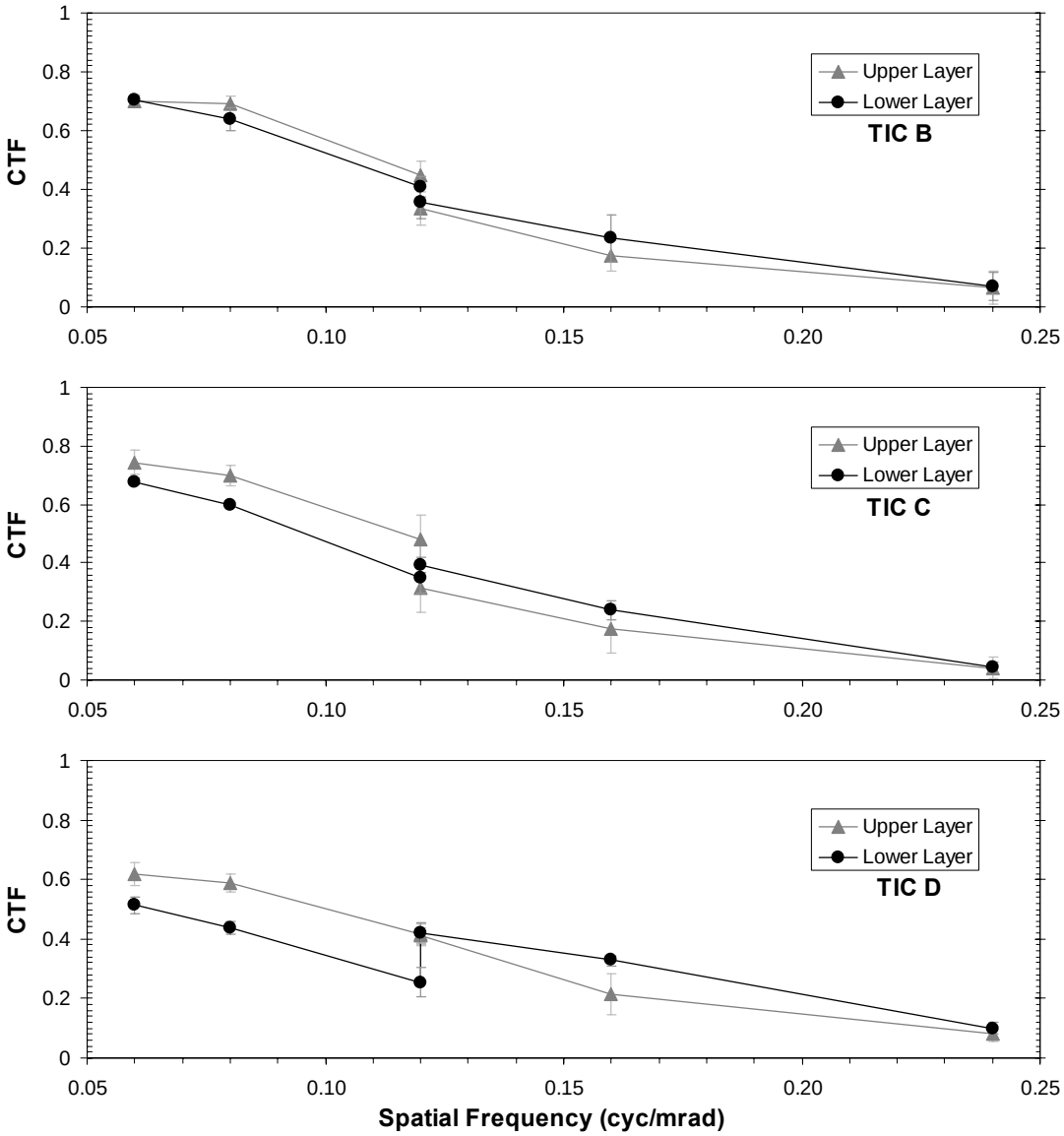

Figure 3-4 - The effect of spatial resolution, path length, and imager height on CTF for four TIC during 50 kW methanol fire

through a decrease in the thermal sensitivity. In this case, the transition into EI mode improved the CTF of the imager.

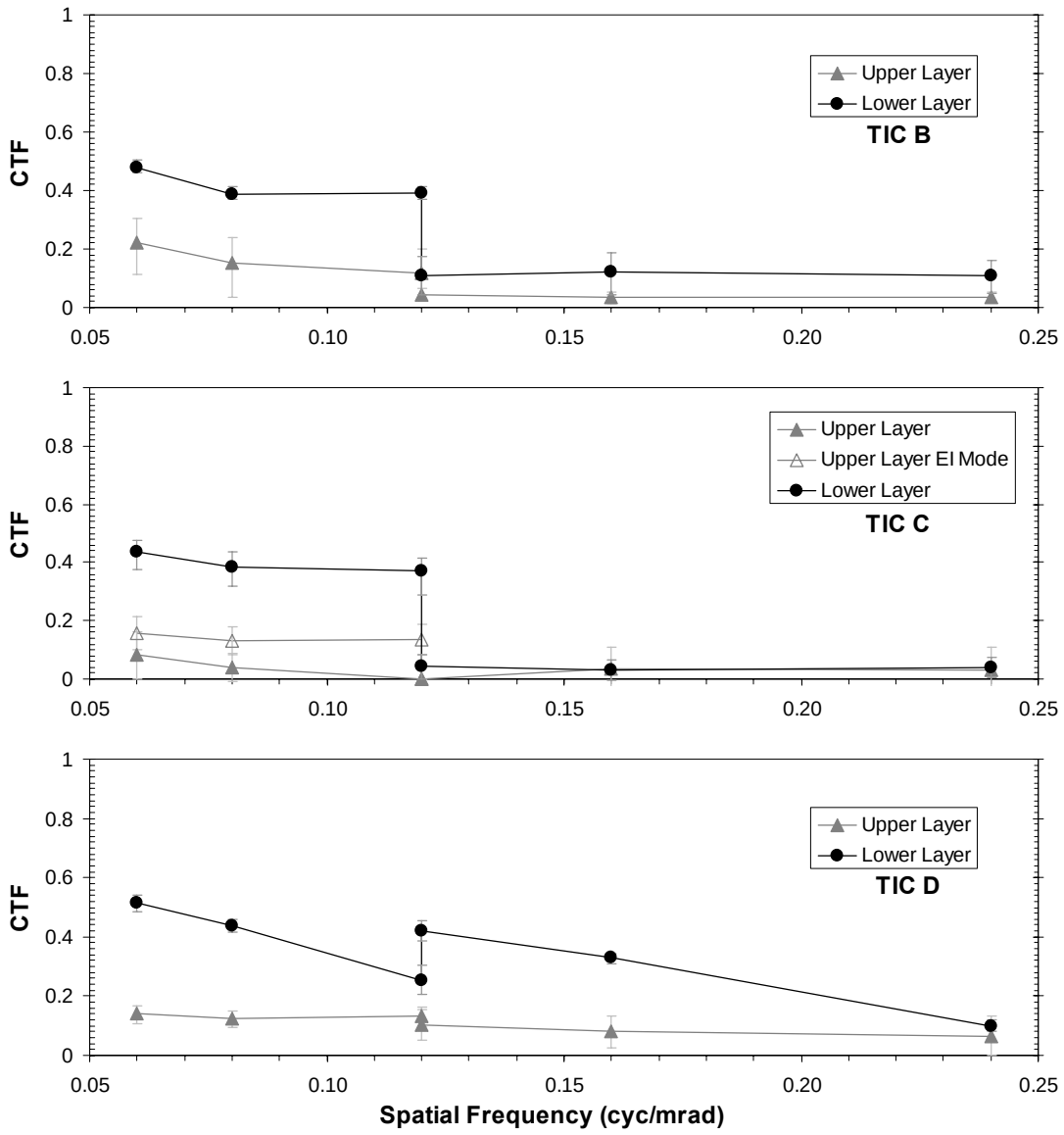

Figure 3-5 - The effect of spatial resolution, path length, and imager height on CTF for four TIC during 350 kW methanol fire including a shift by TIC C into EI mode

One unusual result from the 50 kW tests is that all three imagers showed better resolution in the upper layer at low spatial frequencies (20' distance). This could be due to geometric abnormalities in the flow of hot gases near the exit of the fire room, the burn rate of the fires, or unusual gain functions within the imagers. The effect of the upper layer on CTF was fairly minimal for TIC B, slightly greater for TIC C, and

even greater for TIC D. The CTF of TIC D at the repeated spatial frequency of 0.12 cyc/mrad drastically improved with the increase in path length in the far position. This is probably due to the overall reduction of wall temperatures in the FOV, but this cannot be known for certain.

Unlike the 50 kW fire, the contrast resolution of all three imagers was reduced when viewing through the hot upper layer during the 350 kW fire. At very high temperatures, the emission from the combustion gases can become significant due to small emission bands in CO_2 and H_2O shown in Fig. (2-5). This can be seen in the significant drop in CTF due to path length even in the lower layer. In the upper layer, Imager B can only resolve the target in the close position, imager C only in EI mode, and imager D is almost completely incapable of viewing the target in the upper layer during this test.

The next series of tests were designed to assess the effect of a moderately smoky atmosphere on the CTF of the imagers. Three 32 kW propylene, C_3H_6, fires were burned. Propylene was used because it generates a moderate amount of smoke. Smoke, unlike gases, will act as a broadband absorber and emitter. The smoke will generally be hotter than the target and will thus cause an increase in the overall signal received by the TIC detectors. This effect should tend to "whiteout" the dark target bars and reduce the overall CTF of the imagers. The results of this series of experiments can be seen in Fig. (3-6) for various imagers.

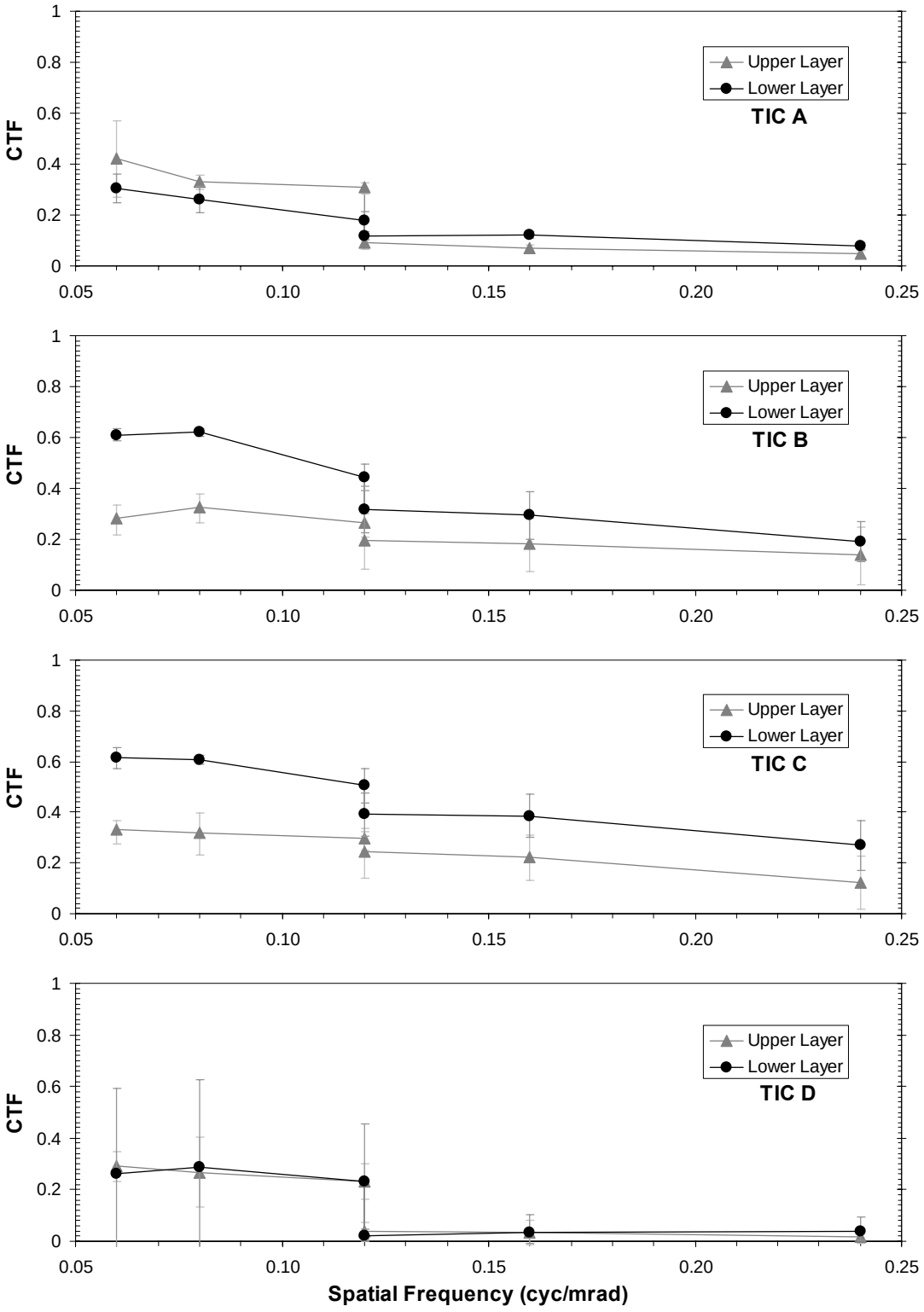

Figure 3-6 - The effect of spatial resolution, path length, and imager height on CTF for four TIC during 32 kW propylene fire

The propylene provided a visible smoke layer to be controlled by the ventilation rate. The effect of height on CTF due to smoke layer for a small propylene fire in comparison with the relatively smoke-free methanol fires is clear. Imagers B and C showed the most expected and the best overall results. Resolution was significantly better in the lower layer and an increase in path length also reduced the contrast.

Imager A exhibited the same unusual response in the close position as did all imagers in the methanol tests. The CTF is actually better in the upper layer. This may be due an unusual gain function due to temperatures in the FOV, inconsistencies in the burn rate over time, or from some other unknown effect. Overall, however, the CTF performance of imager A in the presence of smoke is significantly lower than for imager B or C.

Imager D showed the worst overall CTF results for moderately smoky environments. For short path lengths the height of the camera did not appear to significantly affect CTF performance, but at longer distances the effect of absorption and emission in the upper smoke layer became apparent.

The final tests discussed here focused upon the burning of toluene, C_7H_8. Toluene has high carbon content and is a particularly smoky and sooty fuel. These tests are intended to measure the CTF performance of the imagers under worst case smoke conditions. The results of the toluene fire tests are shown in Fig. (3-7).

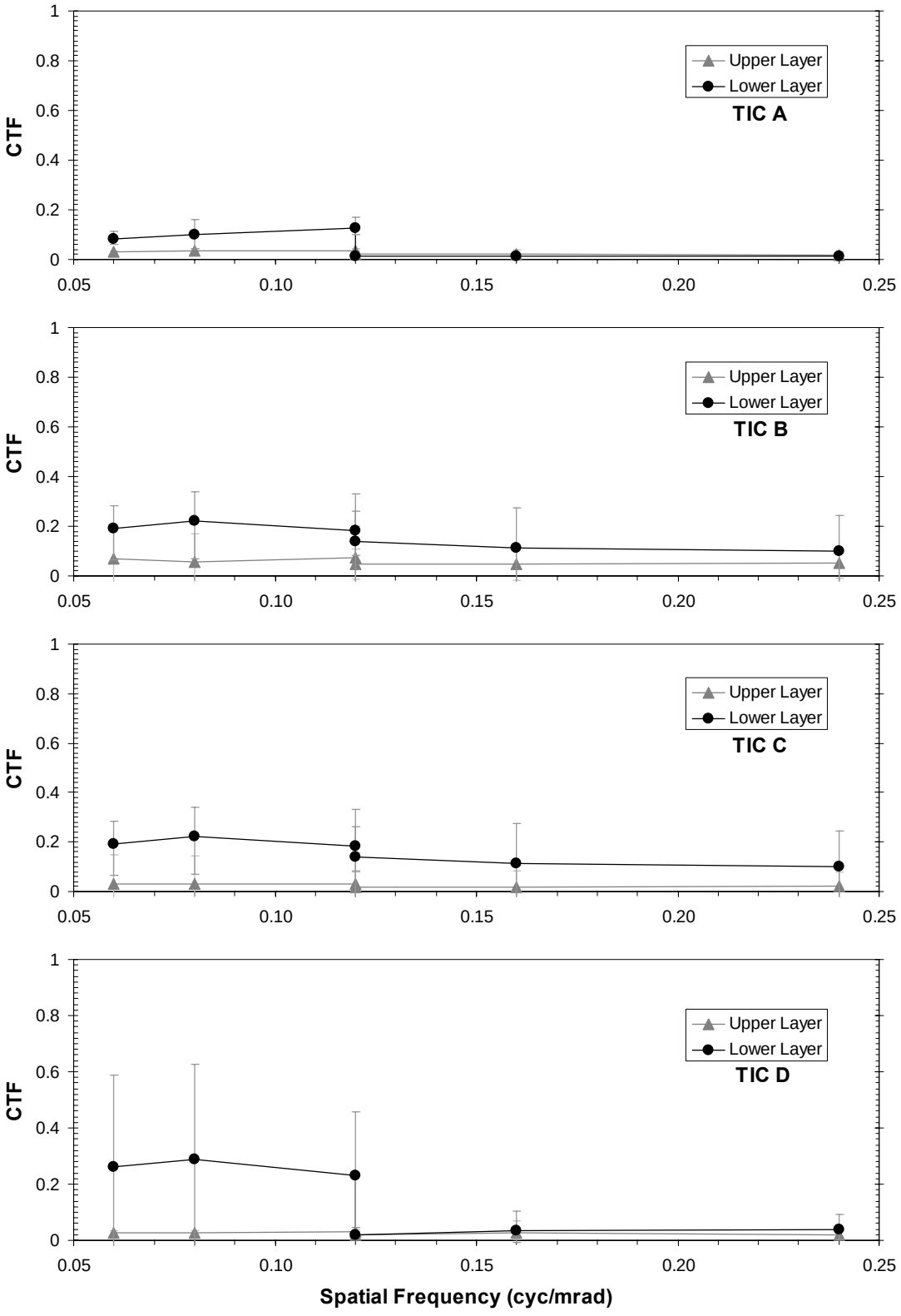

Figure 3-7 - The effect of spatial resolution, path length, and imager height on CTF for four TIC during 200 kW toluene fire

As shown in all four graphs, the IR visibility in a toluene fire is poor even in the lower layer. The visibility of in the upper layer is almost completely vanished for any spatial frequency reaching its highest level at about 0.08 in imager B. In the lower layer, most imagers are able to barely resolve the target with a contrast of about 0.10 and reaching the highest level at 0.2 for imager C.

The amount of variability in this type of fire is evidenced by the large amount of uncertainty in the measurements. The smoke concentration in a toluene fire is extremely unpredictable and difficult to control. Imagers A, C, and D all show an increase in resolution at the higher target frequencies in the lower layer and close position. While imager B shows a relatively flat response in this region. This effect is probably due to the fact the low frequency target was closest to the doorway of the fire room where smoke entered the corridor.

Other full scale tests were conducted to measure the CTF performance of the imagers for other fire types. These fires included burning wooden cribs, carpet samples, and couch cushions. While these types of fires are more comparable to those encountered by actual first responders, they are also extremely difficult to control, characterize, and reproduce. The data obtained during these tests was highly variable, and drawing meaningful conclusions proved difficult. In general, however, these types of fires were very smoky and produced similar results to the toluene tests described above.

The tests performed in these experiments determined the CTF performance data for several TIC in actual combustion and high temperature conditions. While this is not the only valid measure of TIC performance, it is a significant aspect of TIC quality. All of the imagers in this test proved that relative smoke concentration in the line of sight has a significant effect upon the resolution of the imager. This was most apparent in the effect of viewing the target within the hot, upper smoke layer or below it. The effect of path length was also significant as distance in smoky environments proved to reduce the overall contrast of the target image.

High temperature gases and surfaces in the FOV also proved to reduce the overall contrast resolution of the imagers. While this effect was far less significant than for broadband smoke emission, the dynamic temperature ranges and gain functions of the imagers were affected and altered the CTF of the imagers.

While all no imager performed especially well in the highly smoky toluene environment, imagers B and C clearly performed best in the moderately smoky propylene environment. This is valuable information to a user who intends to use a TIC for smoky environments. Full scale fire testing is the most direct method for testing TIC under realistic first responder use conditions. These tests are very expensive to design and implement and result in significant uncertainty in results due to poor reproducibility. For a standardized performance test to evaluate realistic use conditions, it may be necessary to explore alternatives to full scale testing.

4 Bench Scale TIC Display Screen Measurements

4.1 Goals

The primary goal of this work is to develop a method for measuring the visual display performance of a TIC as a function of its video output. This method will then be used to facilitate additional performance testing by characterizing a transfer function between the recorded output signal and the onscreen display luminance for commercial TIC. Many TIC performance metrics require measurement of the analog output signal. This procedure will be used to determine if that signal is linearly related to the display output and if the transfer of that signal is consistent from imager to imager.

4.2 Development of Test Procedure

Essentially the goal of this test is to determine an EOTF for each TIC (See section 1.3.2.3). Standard EOTF testing measures the relationship between the input to the display and the output luminance and requires measuring the screen luminance at several discrete gray levels. Testing for a TIC will necessitate two distinct differences from the standard test. First, the direct input to the screen cannot be measured; instead the imager output signal must be measured. Second, the display screen cannot be filled with each desired grey level.

TIC do not allow for the direct input to each display pixel to be measured without imager modification. In order to overcome this limitation, a well specified measurement and recording method can be used to digitize the composite output signal. The values measured under this system can then be related to the display luminance. Although the actual signal may be significantly modified before being sent to the display, these modifications will be accounted for within the measured EOTF. It is important to note that the values obtained for the EOTF will be entirely dependent upon the measurement and recording equipment used; therefore they must be carefully specified and routinely calibrated. It is also important to note that any future output measurements should be made with the same recording equipment for the obtained EOTF to be consistent.

Second and more significant, full screen gray levels cannot be displayed on TIC screens. At first thought, one might assume that viewing a blackbody at various temperatures would provide each of the required gray levels. However, automated functions inherent in TIC image processing algorithms interfere with full screen grey levels, such that they do not follow a predictable path. This effect can be exploited through a thermal gradient target. When viewed by a TIC, this target will provide an image signal ramping from high to low gray levels which can be analyzed for luminance.

The best method for displaying a range of temperatures over the field of view is to apply two temperature boundary conditions to each end of a conductive rod. The rod

will then develop a temperature gradient from one temperature to the other along its length. All temperatures between the two fixed temperatures will occur on the rod. Radiative and convective losses along the length of the bar will result in minor non-linearities in the temperature gradient, but so long as conduction is the dominant mode of heat transfer, a nearly linear temperature profile should be obtained. This will allow for estimates of temperature viewed by each detector pixel and the gray level obtained from the output and on the screen.

In this experiment, the temperature boundaries on the rod will be enforced with convective heat transfer from water flows. The rod will be inserted into both a hot and cold flow and conduction will carry energy across the rod. The rod will emit thermal radiation as a function of its temperature, and the camera will produce a thermal image of the rod. In addition, the background will be filled with a uniform ambient temperature source in order to minimize the effect of the background on the gain functions of the imager. The background will also have low reflectivity to reduce the effect of reflections upon the perceived image. A conceptual image of the rod is shown in Fig. (4-1) with a gray background and alternating cold rods included to make CTF and EOTF measurements simultaneously.

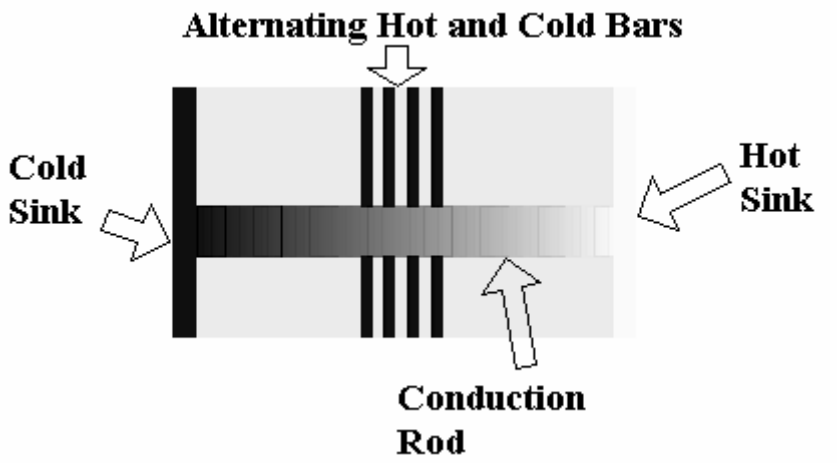

Figure 4-1 – Conceptual target with conducting rod bridging hot and cold temperature sinks, a uniform ambient temperature gray background, and alternating cold bars for simultaneously measuring CTF and EOTF on a display screen

It was determined that the simplest method for controlling temperature and creating hot and cold sinks was to flow water over the ends of the conduction rod. A model of this design is shown in Fig. (4-2) and the final target design is shown with water connection lines and thermocouples mounted in place in Fig. (4-3).

A MATLAB model was created to simulate heat transfer in the conducting rod to determine an ideal design. The program uses the correlation determined by Zukauskas, Eq. (4-1),

$$Nu = C_N \, \mathrm{Re}^u \, \mathrm{Pr}^v \left(\frac{\mathrm{Pr}}{\mathrm{Pr_s}} \right)^{\frac{1}{4}} \qquad 4\text{-}1$$

to estimate the heat transfer coefficient of water flowing over a cylinder (Kreith Gordon and Bohn 1993).

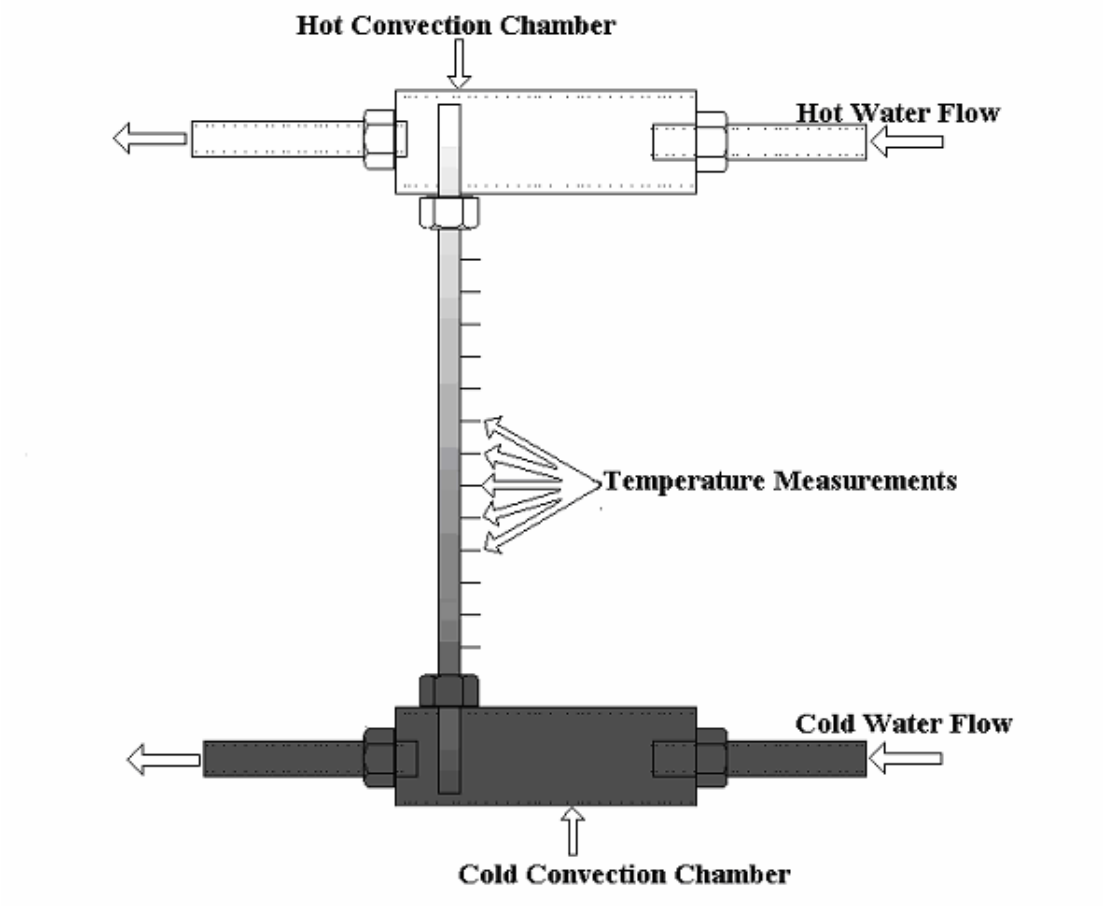

Figure 4-2 – Water flow temperature controlled gradient target for determination of EOTF. Darker color implies lower temperature as viewed by a TIC

The length of the rod exposed to the environment experiences axial conduction as well as radial losses from natural convection and radiation. Natural convection is estimated by the correlation in Eq. (4-2),

$$Nu_D = 0.53\left(Gr_D \,\mathrm{Pr}\right)^{\frac{1}{4}} \qquad 4\text{-}2$$

an empirical fit to data obtained by Eckert and Soehnghen (Kreith Gordon and Bohn 1993). The model assumed that $dT/dr << dt/dx$, or that radial temperature gradients are not significant.

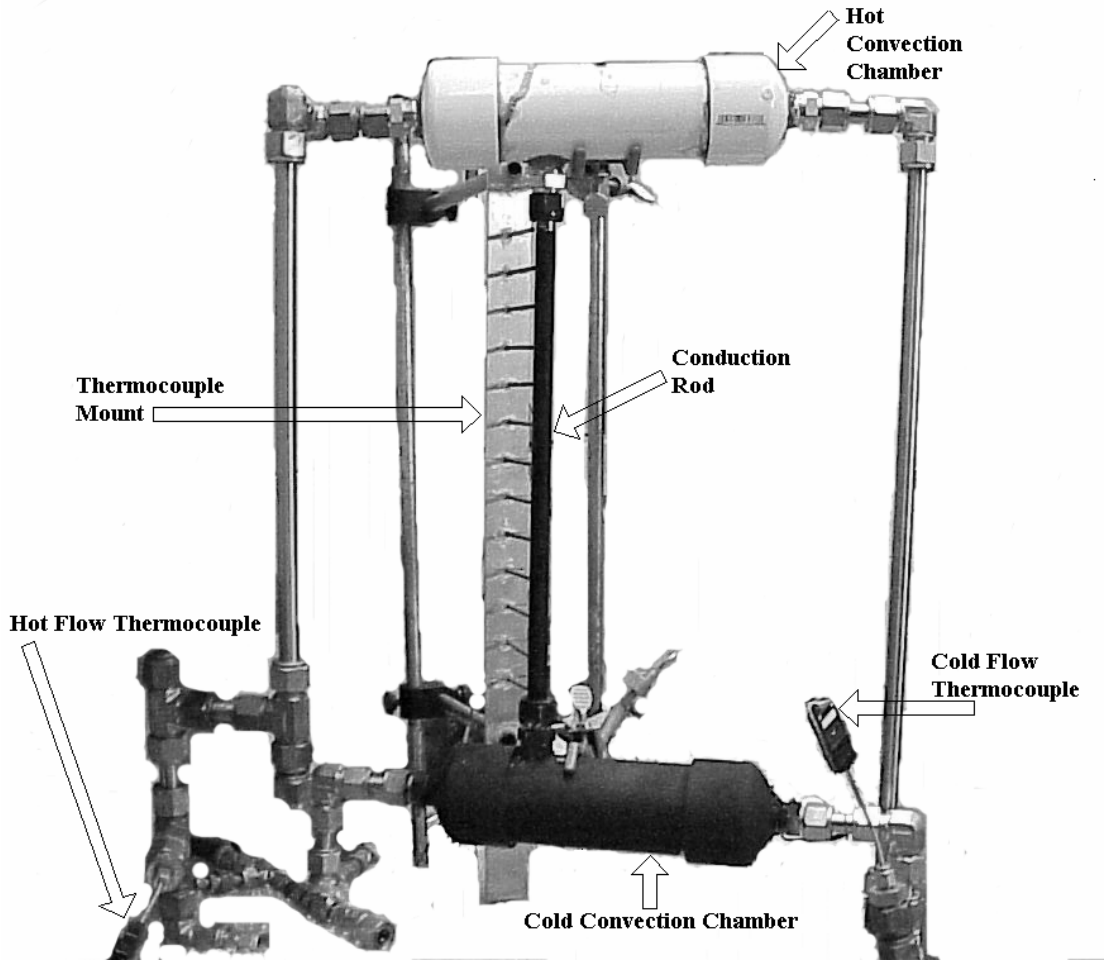

Figure 4-3 – EOTF target with water connection lines and thermocouples mounted in position on the conduction rod and in the water flows

This allows the model to numerically integrate slices of the cylinder as elements, rather than angular or radial sections. Figure (4-4) shows that varying the thermal conductivity affects the linearity of the temperature profile. The ideal profile is calculated by Eq. (4-3),

$$T_i = T_H - \frac{T_H - T_L}{0.3048}\left[x_i - x_{i-1}\right] \qquad 4\text{-}3$$

where the profile is perfectly linear in the exposed region between T_H and T_L, the hot and cold temperatures, respectively. The offset deviation, O, is calculated by Eq. (4-4),

$$O = \sqrt{\sum_{m=1}^{N}\left(T_m - T_{i,m}\right)} \qquad 4\text{-}4$$

where $T_{i,m}$ is the ideal temperature, T_m is the temperature of the actual rod, and N is the number of points.

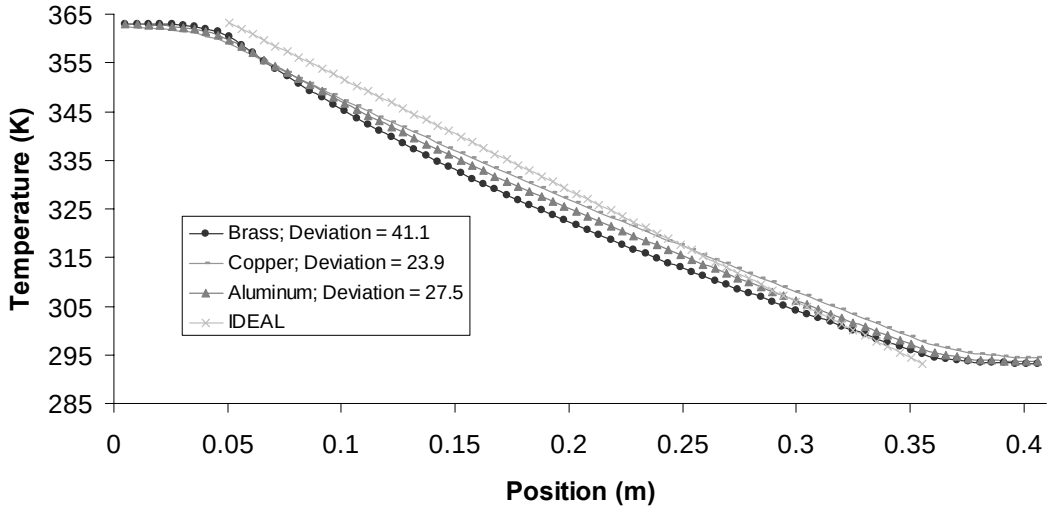

Figure 4-4 – Simulated temperature gradient for three different metals with 0.0508 m exposed to 363.15 K and 293.15 K water flows on opposite sides and an ideal profile between those temperatures

Decreasing the conductivity causes the temperature profile to become less linear as radiative and convective losses are no longer dominated by conduction in the rod. A highly conductive material will increase the ratio of conduction to convective and radiative losses, thus creating a more linear temperature gradient. This is a preferred

situation because a linear temperature gradient will provide the greatest spatial resolution for all temperatures in the target. The tradeoff of a highly conductive medium is the increase in the heat flux through the medium, thus increasing the amount of energy that must be provided to the hot flow and removed from the cold flow.

Continued simulation determined that the flow velocity and length of rod exposed to flow were not significant contributors to the temperature gradient on the rod. The high thermal capacity of water and the high transfer coefficients of forced convection the flow velocity is not a significant factor to the thermal gradient. And while exposing more material to flow will slightly decrease the approach temperatures at the ends of the rods, the slight gain is offset by the physical limitation on this parameter due to the amount of energy required to heat and pump a water flow of several inches diameter.

There are several factors to consider when choosing a final design for such a target. In order to reach a balance between heat flux and linearity, brass alloy number 360 was selected as the conductive medium for the target in this experiment. The target used for this experiment is a 1.27 cm (0.5") diameter brass rod 45.7 cm in length. A 7.62 cm section of the rod on each side is then subjected to hot and cold temperature water flows in PVC chambers. The basic target design is shown in Fig (4-2). The brass rod is painted black with spectrally characterized Medtherm paint having a reported emissivity of 0.94. The spectral emissivity was previously measured at NIST through reflectivity measurements and is shown in Fig. (4-5).

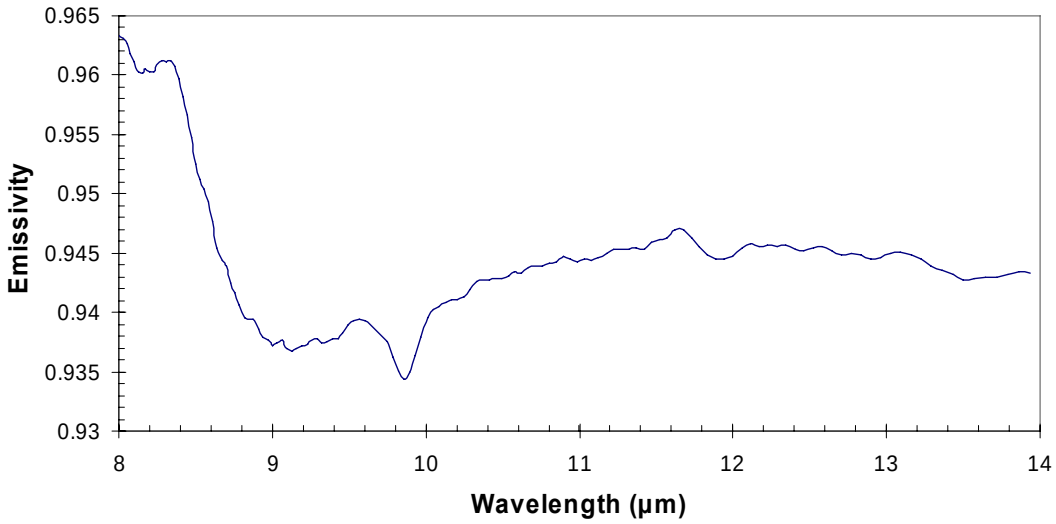

Figure 4-5 – Spectral emissivity of Medtherm paint in the 8-14 μm range determined at NIST through reflectivity measurements

The water flows were hot and cold tap water at temperatures of 40° C and 15° C, respectively. The temperature was measured along the backside of the exposed rod at 2.5 cm intervals with type J thermocouples connected to the rod via thermally conductive paste. The actual temperature profile is shown in Fig. (4-6).

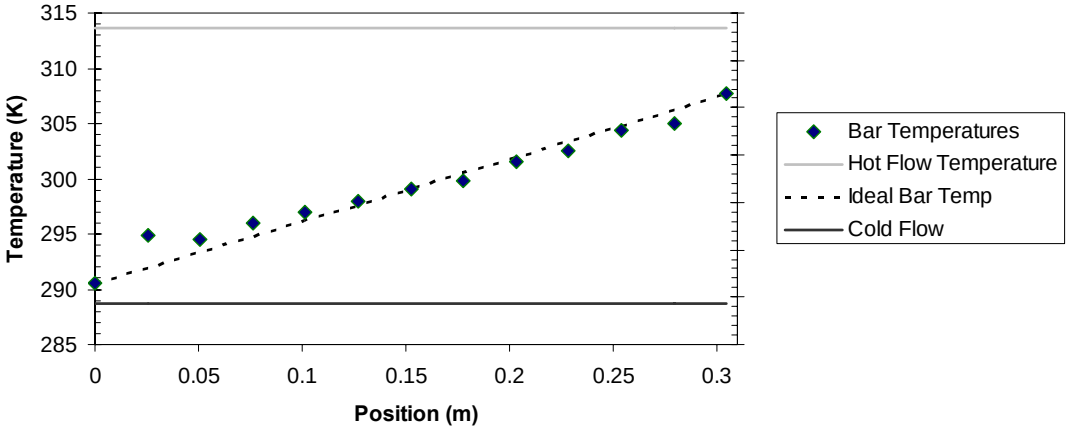

Figure 4-6 – Measured temperature profile along the length of the brass conduction rod, the temperatures of the hot and cold water convection flows and an ideal linear fit between the measured approach temperatures, thermocouple measurements subject to 5% error

There are several issues involved in the width of the target bar. The 1.27 cm bar at a distance of one meter fills 12.7 mrad of the FOV, or 9-10 pixels of width in the video output signal. At the outer boundaries of the bar, edge effects will result in a sharply sloping image signal. In addition, the bar is round which means that the outer edges of the bar are viewed at glancing angles. Due to the directional dependence of emissivity, the outer edges will reflect radiation from the ambient environment rather than emit in the direction of the detector at the intensity consistent with the temperature. To eliminate the spatial and emissive effects of the bar edges five pixels in the center of the bar are selected for video output and luminance measurements.

Once the target had been designed and built, the display screen measurement system was defined. The screen was to be viewed by a well characterized 1600x1200 SBIG ST-2000XM CCD camera array. The camera recorded images in 16 bit format through an IEEE1394 connection to a laptop computer with MaximDL CCD controller software. The linearity of the CCD was evaluated with a luminance source and a photometer, and the resulting data is displayed in Fig. (4-7).

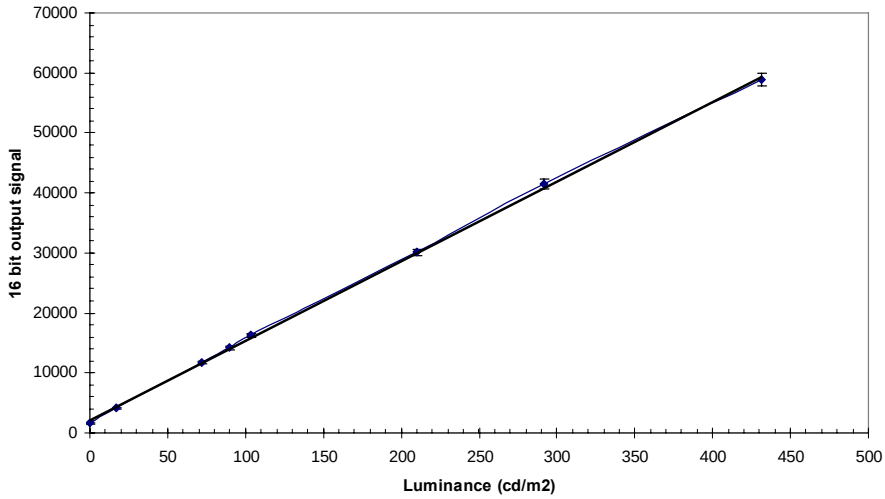

Figure 4-7 -16 bit CCD camera output signal as a function of luminance in cd/m^2 for a 0.5 second exposure.

For this evaluation, the full array is exposed to an integrating sphere luminance source of controlled intensity. The reported value is the mean pixel intensity and the error bars represent the standard deviation of the intensity for each measurement recorded in 16 bit digital format. The output, Z_{out}, is determined to be a function of luminance, L, by the line shown in Eq. (4-5).

$$Z_{out} = 132.67L + 2147.6 \tag{4-5}$$

This fit has a correlation coefficient of $r = 0.9997$ calculated by Eq. (4-6),

$$r_{xy} = \frac{n\sum x_i y_i - \sum x_i \sum y_i}{\sqrt{n\sum x_i^2 - \left(\sum x_i\right)^2}\sqrt{n\sum y_i^2 - \left(\sum y_i\right)^2}} \tag{4-6}$$

where N is the number of points in the data set, x are the known data points and y are the fit data lines. The value of r^2 can be interpreted as the proportion of the variance in y attributable to the variance in x (Microsoft Excel 2002).

A CCD camera is used because of its linear response to luminance, thus making this characterization simple and applicable to further measurements. If the CCD response is acceptably linear, the CCD images of display screens can be correlated to the relative display screen luminance. It is important to note that the CCD array only measured relative luminance[3] for these tests, as we were interested in how the relative luminance varied over a linear range of the CCD. Furthermore, measurements made by the CCD array will include contributions from stray light in the CCD camera lens.

Due to the contributions of glare and stray light, accurate luminance measurements must be made under very sensitive conditions. This makes it very difficult to measure the display screen performance in full-scale applications such as in a burning structure. However, once the display performance has been determined in a controlled laboratory measurements of the composite output signal that are less sensitive to environmental conditions can be mathematically related to actual display performance via the EOTF.

In order to obtain repeatable values, it is important to first determine the slope of the CCD response to luminance. This slope can be controlled by limiting the light falling on the array through the f/# and exposure time. The slope represents the number of CCD counts per cd/m^2; all CCD count measurements should be divided

[3] *all luminance measurements in this paper are assigned an expanded uncertainty of U = 10% with a coverage factor of k=2.*

by this number so that the values can be repeated for any desired data acquisition session.

As seen in Fig. (4-7) and Eq. (4-5) the CCD response contains an offset at zero input due to electronic noise in the detector pixels. Before taking display measurements it is important to obtain an exposure of the CCD without the display screen turned on. This image should be subtracted from any subsequent images taken of the display. This will eliminate both the black noise and any signal obtained due to stray light entering the system.

When the TIC views the target, simultaneous measurements are taken of the composite output signal and the display screen luminance and the relationship between the two signals is determined for various TIC. TIC screens were recorded by the CCD array with a 0.5 second exposure time and an f/# of 0.4 into 16 bit .tif images. The f/# and the exposure time are related to the slope of the CCD response to luminance. Therefore, the same optical settings should be used in experiments as for calibration.

The video output signal was recorded simultaneously through a 70 Ω coaxial cable and a Sony mini-DV digital tape recorder. The images from the composite output signal video were transferred to computer and stored in 8 bit .tif format. The time code was used to synchronize the CCD image to the video output and 15 frames

were averaged to coincide with the 0.5 second exposure of the CCD and to remove any temporal noise.

The images were then compared using a MATLAB program. A line was drawn down the center of the gradient target and 5 horizontal pixels were averaged to obtain the pixel intensity at each vertical position. The pixel intensity along the length of the target in the CCD image was fit using a 15^{th} order polynomial least squares fit. The CCD intensity is then solved at positions coinciding with each pixel in the recorded video image. The pixel intensities in each row of the video image are averaged and rounded to the nearest integer and the data is stored as a direct relationship at each corresponding pixel location and value in the CCD image. The data analysis process is described in Table (4-1).

This experiment was carried out for 4 different models having TIC with LCD display screen technology. The CCD camera and the thermal imager were both mounted on an optical bench.

Table 4-1 – EOTF Data Processing Method

Step	Input	Processing Step	Output
1	Analog video output	Recording with mini DV and 70 Ohm coaxial cable	30 fps 8 bit digital tape
2	CCD camera output	Record with MAXIM DL software	16 bit gray image
3	16 bit display image and background image	Subtract background image from display image	16 bit background corrected display image
4	Digital tape	Transfer to computer hard drive	30 fps 8 bit .mpg file
5	.mpg file	Convert frames to individual images	8 bit .tif images
6	.tif images	Align timecode to CCD image and average video frames	One 8 bit .tif image
7	8 bit and 16 bit .tif images	Draw a line along gradients and average 5 pixels wide	Grayscale profiles
8	16 bit grayscale profile; Pixel number in 8 bit profile	Obtain polynomial for 16 bit profile; solve at location of each 8 bit pixel row	Grayscale profile from 16 bit image aligned with pixels from 8 bit image
9	Pixel aligned 16 bit profile; 8 bit profile	Find gray levels (0-255) in 8 bit profile, average 16 bit levels at each matching location	Data plot of digital output level vs. relative luminance
10	Data plot	Divide relative luminance by slope of CCD line	Standardized and repeatable data plot
11	Multiple data plots	Average measured luminance from many experiments	Final data plot

4.3 Results

The measured display performance of the TIC is shown in Fig. (4-8). Each time that a digital output level is measured along the length of the rod, a luminance value is assigned to it. The error bars represent the standard deviation of the luminance values assigned to that digital output level from many identical experiments. A luminance value of zero implies that no luminance value was measured for that digital output level.

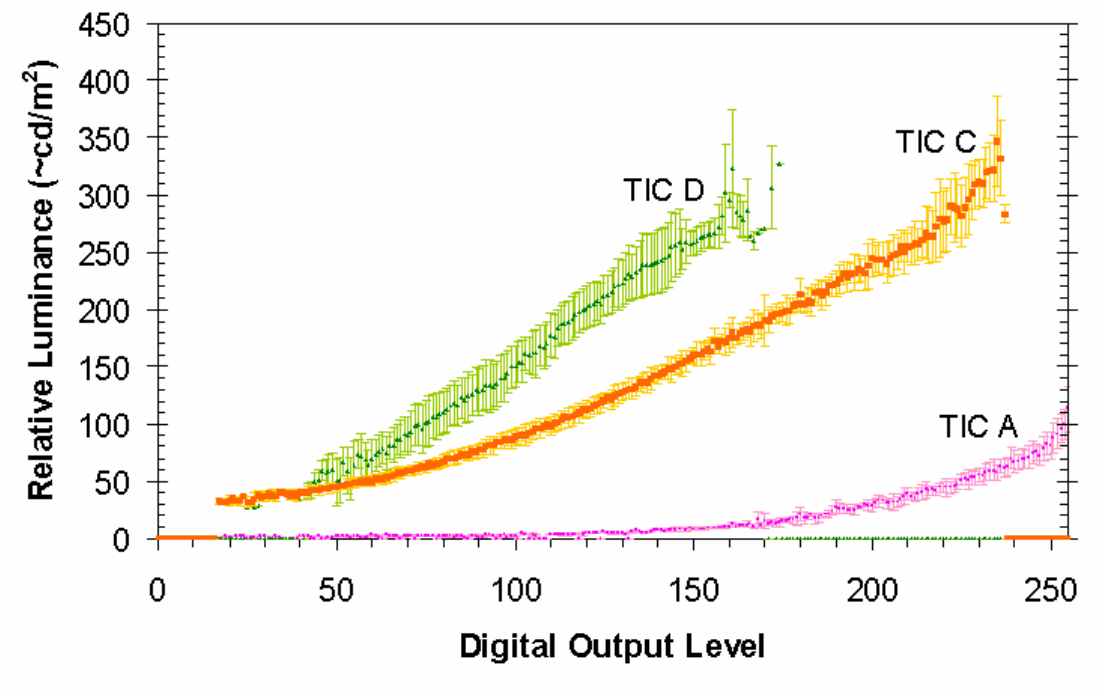

Figure 4-8- Relative luminance as a function of 8 bit recorded output signal for 3 different TIC, output levels where data not obtained shown as zero luminance, error bars are one standard deviation of all luminance measurements

It is clear that the three imagers subjected to this test do not exhibit similar display screen characteristics. There is no universal correlation between the recorded digital

output level and the actual display screen luminance. Therefore, any test measuring only the video-output signal will not accurately describe the quality of the imagers relative to each other, highlighting the necessity of these display screen measurements.

To further advance the results and to better simulate human perception of the display screen, the test was modified by applying an IR filter to the CCD camera to remove any signal obtained from near visible radiation emitted from the LCD screen. Originally, the filter was loosely attached to the end of the lens. This resulted in a reduction in the measured luminance of each screen as a result of removing the IR contribution to the measurement, but the poor mounting system of the filter resulted in a great deal of deviation in the data shown in Fig. (4-9). It was clear that a more repeatable positioning system for the CCD camera and the IR filter would be necessary to obtain reproducible data.

A new positioning system was built and the experiment repeated. The mounting system allowed for four dimensions of motion for the CCD array. The camera could be translated in the X, Y, and Z dimensions, and could also be rotated about the Y-axis. This rotation allowed the line of sight to be aligned perpendicular to the LCD surface, improving the accuracy of the measurement. In addition, a positioning system for the IR filter allowed it to be placed reproducibly in front of the CCD lens, further reducing errors. A photograph of the positioning system in shown in Fig. (4-10).

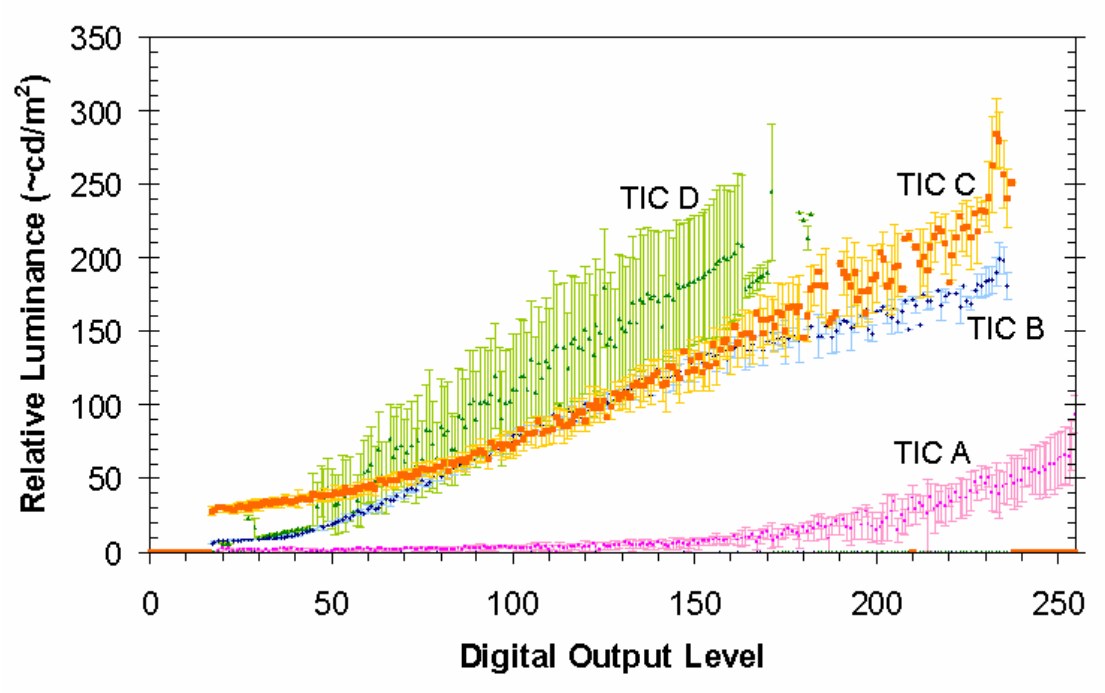

Figure 4-9- Relative luminance as a function of 8 bit recorded output signal for 4 different TIC with IR filter

The final mounting system allowed for a much more repeatable measurement of luminance for each TIC as shown in Fig. (4-11). The vast difference in visual performance of each imager indicates that determining performance solely from the video output may significantly mislead users about the actual quality of TIC. The data taken confirms the necessity for display screen measurements as a part of a complete TIC system performance analysis.

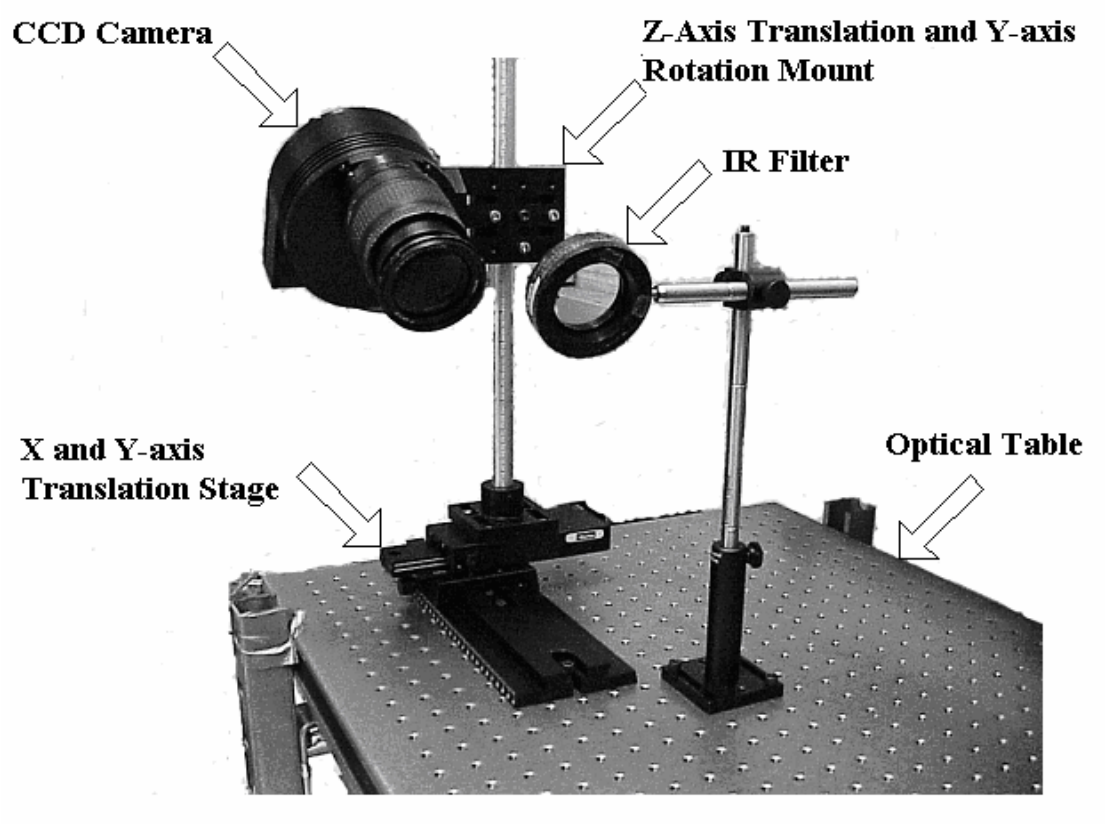

Figure 4-10 – CCD camera positioning system shown with camera and IR filter

The video output signal has previously been used to determine the CTF of TIC. The CTF was also measured for the LCD display screens to examine the effects of veiling glare on the CCD measurement system.

Veiling glare is a consequence of measuring adjacent light and dark patterns. Light from the bright segments of the target may be scattered in the lens, IR filter, or even in the atmosphere, and recorded as a signal on the dark segments of the image (Boynton and Kelley 2002). This distortion produces a reduction in the observed contrast due only to the measurement system optics.

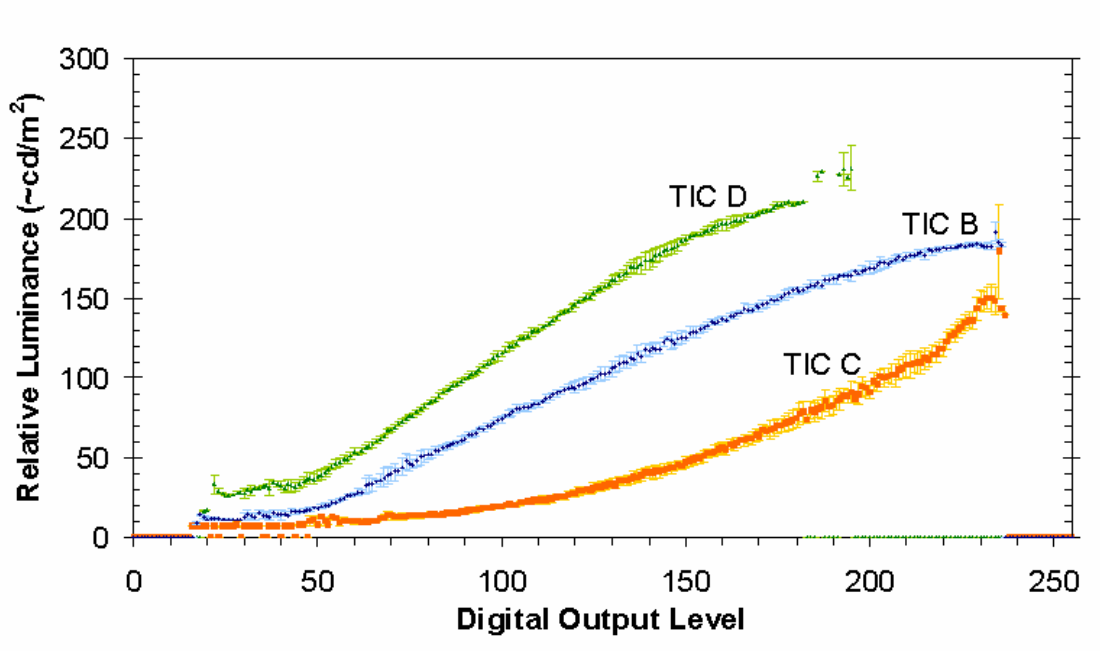

Figure 4-11 - Relative luminance as a function of 8 bit recorded output signal for 3 different TIC with IR filter and multi-axis positioning system

The CTF was measured simultaneously with the EOTF by placing bar targets in the hot water flow loop and placing the bars in front of the cold water chamber. Both the bars and the chamber were painted with black Medtherm paint. When the CTF is measured by the video output signal of the camera and transformed using the EOTF data obtained above, the contrast is significantly higher than is actually measured by the CCD array. This is due to a false increase in the dark measurement due to veiling glare. Fig. (4-12) shows the recorded images and the luminance images of the three targets taken with three different TIC.

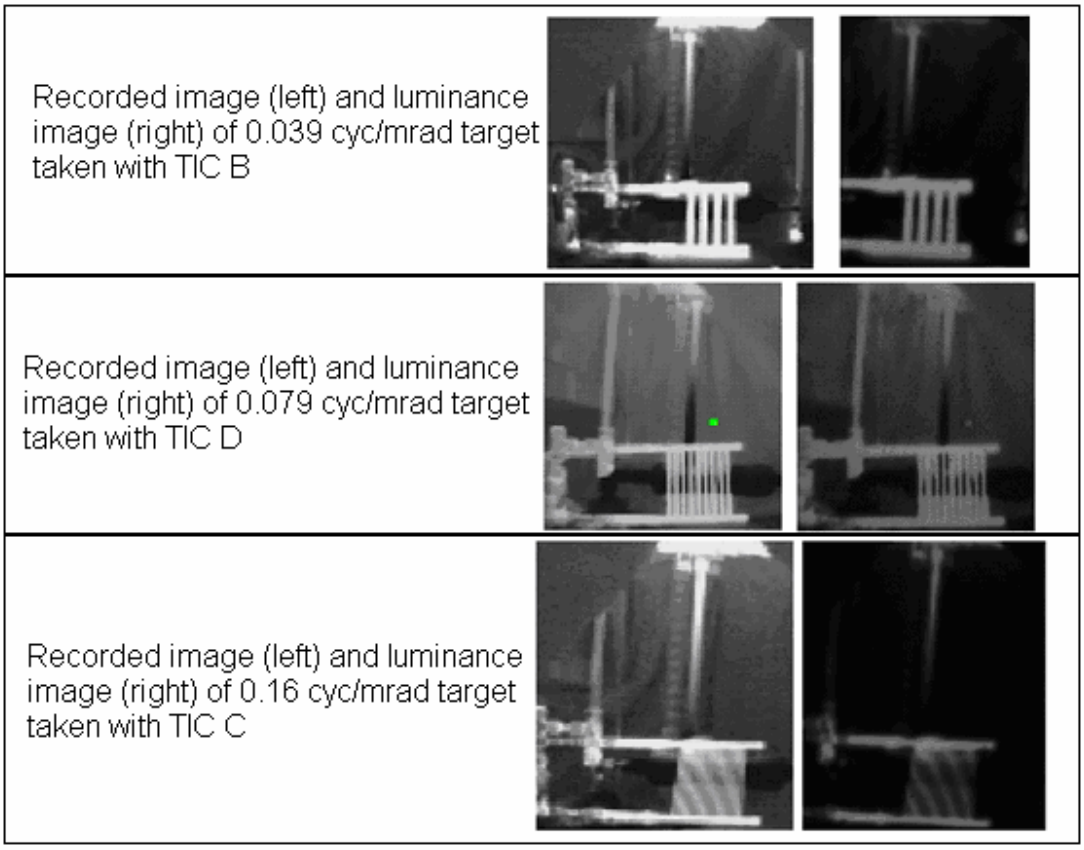

Figure 4-12 – Recorded images (left) and CCD array measured luminance images (right) of 3 different spatial frequency CTF targets and EOTF gradient target taken with 3 different TIC

The shape of the EOTF function, however, may improve the apparent contrast of the image. The CTF data points in Fig. (4-13) were obtained from the digital output recording, calculation based on EOTF correlation from the gradient target, and direct luminance measurement.

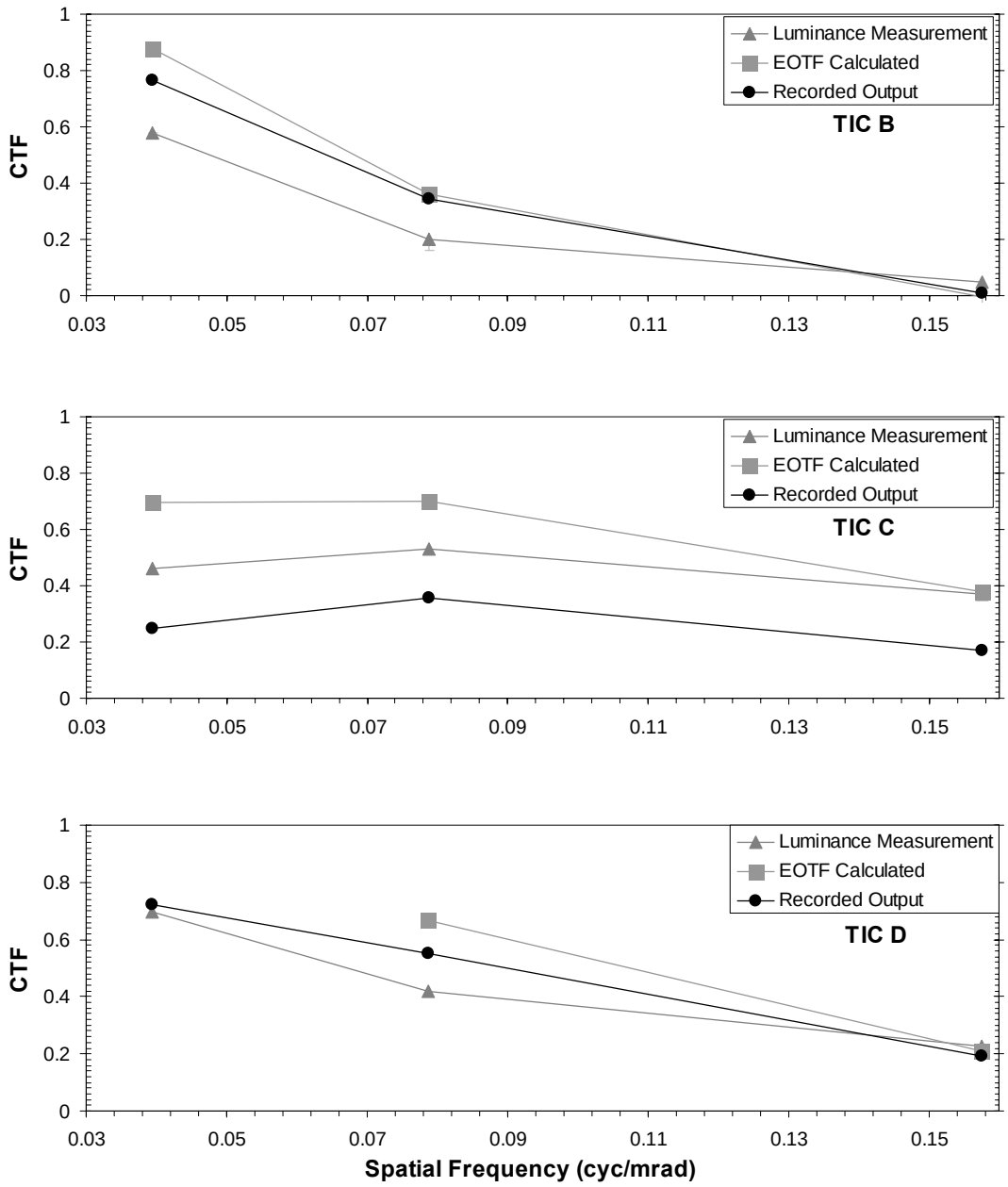

Figure 4-13 – CTF measurements obtained through image recording software, direct luminance measurement by the CCD array, and EOTF calculation for 3 TIC at 3 spatial frequencies *TIC D CTF not calculated at 0.039 cyc/mrad because digital output levels not matched with luminance from the EOTF target

Due to the curve of the EOTF and the weighting of CTF to dark images, the calculated CTF is almost always higher than the recorded image. Even with the

veiling glare, the measured luminance CTF of imagers B and C is still better than the video output signal. The EOTF of display screens is intentionally designed to have this effect.

Fig. (4-12) shows an unusual resolution pattern on the high frequency target. This pattern is due to the spatial variance of the target as viewed by the discrete pixel array. The alignment of the pixels with the variations in the target can greatly affect the ability of the camera to view contrast. Fig. (4-14) shows the same target viewed by the same TIC with a slight adjustment of the imager. The alternating bars are much better aligned with pixel columns and thus the image is much clearer.

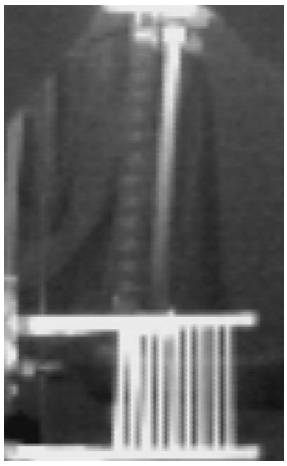

Figure 4-14 - High frequency target resolution demonstrates the effect of spatial variance on image

Unless a spatially invariant target can be measured, it is important to perform several measurements of CTF for pixilated imaging systems. This will help to reduce errors from spatial variations and alignment issues. Spatial variations will exist with any sinusoidal or square wave target pattern, and can only be eliminated with random

white noise test patterns described in chapter 1. Of course, the cost of these targets will often limit their use in realistic testing situations.

The result of this investigation into display screen performance has aided in the recommendation of a standard test for handheld TIC. The recommendations outline the important aspects of display screen testing learning through this procedure. It was sent to the National Fire Protection Association (NFPA) and is still under review. The recommendation can be found in the appendix.

5 Conclusions and Future Recommendations

5.1 Concluding Summary

5.1.1 Full Scale Fire Measurements

Users are concerned that existing laboratory metrics may not accurately portray the realistic performance of an imager. First responders use TIC in a wide array of harsh and grueling situations where the performance of the imager is integral to safety. Full scale fire and smoke testing is the most direct method for assessing TIC in realistic use conditions. The real world performance of the sensor, optics, and electronics can be identified by customizing tests to meet the exact needs of the users.

There are many factors contributing to the performance of an imager, so it is important that the test be as similar to the intended uses as possible. Full scale tests can be tailored to meet the exact needs of users. The performance of the imager can be determined for various burning fuels, smoke types, heat sources, or other obscuring media. The ability of the sensor to function in a multitude of temperatures or burn rates can also be examined. The ability of the camera to perform under various fuels or temperatures can be the result of spectral filtering due to lens coatings or spectrally selective absorbers on the sensor pixels or even electronic gain effects.

These tests can provide information about the internal gain or saturation methods of imagers. Many of the imagers include an electronic iris to increase the thermal range

by decreasing sensitivity when the temperature range of the image is too great. Full scale fire testing is often necessary to examine this function and force the transition from normal to EI mode.

In addition to a host of atmospheric conditions, full scale testing can also be used to identify an intended target. TIC are used to identify humans, fire sources, electronic hot spots, and various other targets. By controlling the size, temperatures, and emissivity of targets, tests can be customized to match the intended use of the imager.

The difficulty of full scale testing is in the unpredictability of full scale atmospheric control. Fire, for example, is by nature wild and often unpredictable, and seemingly trivial occurrences can greatly change the combustion rates of controlled fires. This fact was more evident for wood and carpet or cushion fires than for fires of pure fuels. These fire types, however, are the most often encountered in first responder situations. For this reason full scale fire testing can often provide highly unrepeatable and unreliable data to the potential user. Due to the high variability and the high cost of full scale fire testing, other alternatives should be considered.

5.1.2 Bench Scale Display Measurements

All existing TIC performance metrics developed at NIST for this project record the image quality of the output signal. The need for display screen testing is clear. Each TIC tested in this experiment exhibited an entirely different relationship between the measured output signal and the displayed image. This means that testing the composite output signal alone is not adequate for describing the performance of

handheld TIC devices. A complete test of the system must include all components, including any measurement devices. The effect of additional signal modification and the visual performance of the display screen to the final product quality should not be ignored.

The purpose of this experiment was to determine the general luminance response of TIC and determine if multiple TIC would exhibit dissimilar characteristics. Although this test does not provide correlations between output signal and calibrated display luminance, the relative luminance values can be compared between imagers and an assessment of quality can be determined. It is important to remember that in order to make CCD analysis repeatable and comparable, the background image must be subtracted and the slope of the CCD response to luminance must be determined. This allows for the testing procedure to be repeated in any laboratory and image quality to be compared. The ease of testing display screens with a CCD array makes it an attractive option over a pixel by pixel analysis of luminance.

The data obtained in this experiment determined the relative luminance of display screens in reference to the video output signal. With continued testing the correlation between the video output and the display screen performance can be fully defined for various TIC devices. This will allow the use of the video output signal for other standardized performance measurements such as full scale tests or other bench level metrics.

5.2 Recommendations for Further Research

Although the tests performed and analyzed here are preliminary the value of continued research is apparent. The work presented here is only a foundation and has helped to open several new discussions and issues for the ongoing development at NIST of a final performance standard for handheld TIC used by emergency responders.

5.2.1 Full Scale Fire Measurements

One alternative to full scale fire testing being investigated is the use of optical density filters to simulate fire conditions. For example, wire meshes of various grid sizes can be heated to hot gas temperatures and used to simulate actual smoke. The visual effects of various filters can be used to represent standard burn conditions. This could provide a standard, repeatable, and reproducible alternative to full scale fire testing. Continued research at NIST into simulation of realistic conditions in a repeatable, laboratory setting is ongoing.

5.2.2 Bench Scale Display Screen Measurements

One important issue that must be overcome to achieve better correlation is the measurement of actual display screen luminance in standardized units. The current proposed method uses a CCD array to measure relative light intensity across the entire screen. An array of luminance detectors cannot measure light in calibrated units because of interference and scattering effects such as veiling glare. In order to measure luminance in calibrated units, an isolated scanning photometer must be used to measure each LCD pixel independently. This type of testing is time consuming,

expensive, and can result in errors due to temporal effects. These errors can be the result of temperature changes in the target, sensor array, or LCD screen. In addition, battery life may influence the screen luminance. Prior to subjecting TIC to such a rigorous test it was important to determine the general luminance response by using a CCD array.

The issue of luminance brings rise to another concern in display testing; the consideration of human visual performance. It is difficult to assess the quality of an image to a user. For this reason most of the current testing including a display screen is performed with human observers. There are, however, defined psychrometric functions that can relate an image to its quality to a human observer. These models take into account human spectral and intensity responses. An excellent dissertation of contrast and the human response can be found in "Contrast Sensitivity of the Human Eye and its Effects on Image Quality" by Peter Barten (Barten 1999).

The use of the IR filter in this experiment was designed to lead the project closer to modeling human vision. By removing the short wave infrared signal from the CCD array, the obtained image better represents the screen as viewed by a human observer. Continued testing will include the use of a photopic filter. This is a filter designed to follow the spectral response of human vision to further improve the description of the display to a user. Future work may also involve the use of band pass filters to fully define the spectral output of the LCD display screens.

Another issue with the proposed display testing is in the range of gray levels which were tested. All the imagers viewed the same target with the same temperature boundary conditions. This target relied on the automated gain functions inherent in the imagers to drive the hot to white and the cold to black. The gain functions of the imagers performed very differently, and the full range of gray levels was not tested for all imagers. In order to develop a complete display screen correlation without extrapolation, the temperature boundary conditions must be tailored to each imager under test. This may require use of a fluid other than water that can reach temperatures below 0°C or above 100°C, or the use of thermoelectric coolers or heating devices. To define a complete function it is important that the camera signal be driven to both a full white and black.

This test has only been defined for TIC with LCD display screens. This technology is not a standard in the TIC industry, and the proposition for this test should not be considered an endorsement of such a standard. Other display types, such as (CRT), plasma, or even head mounted eye pieces, must be considered when developing a standard. Similar testing should be designed and implemented to accommodate these products.

An additional consideration is in the combination of display screen testing with realistic use conditions. Future tests may require measuring the performance of the imager through various optically obscuring media, such as smoke, dust, and fog, and extreme temperatures. This performance will mostly be a function of the total brightness of the screen, and thus the general response can be inferred from EOTF

testing. These tests may, however, aid in determination of the minimum performance criteria for such a standard.

Finally, it is imperative that the final standard testing matrix does not drive the industry. It is important that the tests are tailored to the needs of the users and forces the industry to provide products that better suit the needs of those users. Metrology should never set arbitrary standards for products. Once a performance matrix has been fully examined, the determination of minimum performance criteria together with the users will be imperative.

6 Appendices

A.1 Final Proposition for Standard Test

The information obtained from refining the display screen test procedure was used to develop the following proposition for a standard. These recommendations have been submitted to the National Fire Protection Association (NFPA) for review and deliberation.

A.1.1 Apparatus

A.1.1.1 Thermal Gradient Target

The target for this test is a linear temperature gradient. It is the purpose of the target to provide a continuous ramp of input signal to the thermal imaging camera. This target is designed such that the relationship between all recorded output levels and display luminance can be measured in one single test.

The target shall be a bar or rod comprised of a conducting medium with temperature boundary conditions imposed upon opposite ends. This design should generate a nearly linear temperature profile along the length of the target. The temperature can be controlled with electric heating elements and/or temperature controlled convective fluid flow. It is recommended to use a highly conductive material, such as brass, to increase temperature linearity but the conductivity will be limited by the available heat flux. The temperature boundaries shall be the lowest and highest temperatures required to drive the TIC to its lowest and highest outputs. These temperatures may not need to be extreme if the automatic gain functions of the TIC can be exploited.

The temperature of the target shall be measured at many points along its length using thermocouples or pyrometric equivalent. The temperature gradient dimension of the target shall be long enough that 50 recorded output pixels subtend the length of the target. The target shall also be wide enough that each temperature level is viewed by a width of at least 5 recorded output pixels. This size will depend upon the angular pixel subtense and the minimum focusing distance of the TIC.

The emissivity of the target should be well characterized so that radiance can be calculated. The emissivity should also be maximized to increase signal sent to the TIC.

A.1.1.2 Luminance Measurement

The display screen luminance shall be measured by an imaging CCD array or equivalent photometer. This device shall include a recording device such as computer software or equivalent.

The linearity of the measurement device shall be characterized by viewing at least five different luminance values in an integrating sphere. This characterization shall be performed with the same lens system, f/#, and exposure time as them TIC standard tests. The slope of the CCD response to luminance in counts per cd/m^2 shall be determined so the obtained data can be standardized. The measurement device should not introduce any non-linearities in the system under test.

A.1.1.3 Thermal Imaging Camera

The angle of the display screen must be determined so the measurement device can be mounted at the same angle to eliminate the effect of viewing angle from any measurements. Other measurements can be designed to evaluate the effect of viewing angle on display screen performance.

The purpose of this experiment is to equate the results of other performance measurements to the image on the display screen. The exact measurement equipment, including transmission devices and recording equipment, used for other measurements should be used in this experiment.

This measurement is intended for TIC utilizing LCD display technology. Measurement of other display technologies should refer to display screen measurement standards for that particular technology.

A.1.1.4 Positioning and Mounting Equipment

It is recommended that all imaging and target apparatus be mounted to an optical workbench to ensure angular accuracy and repeatability.

A mounting device shall be designed for the TIC in conjunction with the display screen angle determined in section 4.4.1.3. The imager shall be mounted at a minimum distance to ensure accurate focusing of the thermal target. This distance is often specified by the imager manufacturer. All of the imagers tested in this experiment require a minimum focusing distance of 1 meter.

The luminance measurement device shall be mounted on a piece of equipment allowing four degrees of freedom. The x-direction, towards or away from the imager, the y-direction, left or right of the imager, the z-direction, up and down, and rotation about the y-axis to align the device to the angle of the display screen. The luminance measurement device should be positioned at a minimum focusing distance of the optical system and so that the entire thermal target on the TIC display screen can be viewed by the luminance meter. There shall be alignment such that there is zero viewing angle between the display screen and the device.

The entire system should be placed underneath a non-reflective hood to reduce the influence of ambient and reflected light in both the infrared and visible regions of the spectrum.

A.1.2 Procedure and Data Analysis

The first step in the data acquisition procedure must be to obtain a background image with the luminance measurement device. This image will be subtracted from all future measurements to correct the display screen images for background light and dark noise in the CCD array. If the measurement device has a linear response to luminance, this subtraction will not affect the data, it will only remove undesired signal.

The data obtained for each test will be taken simultaneously. It will include temperature measurements on the target, the output from the TIC, and the output from the luminance measurement device.

The images recorded from the TIC output must first be averaged over the time interval of the luminance measurement exposure. Most imagers have a frame rate of 30Hz and this will mean that several frames will be recorded while the luminance meter is exposed. The average of these frames will not only align the frames with the exposure, but also will help to filter out random temporal noise from the frames.

A problem may arise when trying to compare the results of the luminance and the averaged video output frames. The images recorded by the luminance measurement device will often not have the same number of pixels viewing the target as the TIC recording. Luminance measurements of pixels viewing the same temperature level shall be averaged to create a one dimensional profile and a function shall be fit to define the luminance gradient. The curve shall be fit by polynomial or equivalent fitting process. The function shall then be solved at points coinciding with each pixel in the gradient direction in the TIC output image.

Pixels in the TIC output image viewing the same temperature level shall then be averaged along the length of the target. These values can now be matched directly with the luminance values determined by the gradient function determined above. The data is then reported as a number of discrete points describing the relative output luminance as a

function of the recorded signal. The relative luminance values should be divided by the slope of the luminance meter response line to standardize the reported values. The acquisition of luminance data shall be repeated at least three times or until standard deviations of less than 10% are obtained.

Standard LCD display screens are often designed to follow a curve in which the luminance is controlled by the input by a logarithmic function in the form of $L = aV^{\gamma} + L_b$ where L is the luminance, a and γ are empirical constants, and L_b is the luminance of the screen at zero input. The data obtained by this experiment can often be fit to a curve of this type. If adequate fits are not obtained, several regions of the output signal may be divided and fit to separate functions, or other fitting methods may be used.

Reference List

(1993). *The Infrared Handbook*, 4th Ed., The Infrared Information Analysis Center.

(2002). *Microsoft Excel* Microsoft Corporation, 1985-2000.

(2006). "Optical Materials: Zinc Selenide." International Crystal Laboratories.

ASTM E1543-00(2006). "Standard Test Method for Noise Equivalent Temperature Difference of Thermal Imaging Systems." ASTM International.

Barten, P. G. J.(1999). "Contrast Sensitivity of the Human Eye and Its Effects on Image Quality." SPIE - The International Society ofr Optical Engineering, Bellingham, WA.

Boreman, G. D. (2001). *Modulation Transfer Function in Optical and Electro-Optical Systems*., SPIE - The International Society for Optical Engineers, Bellingham, WA.

Boynton, P. A., and Kelley, E. F. (2002). "NIST Stray Light Elimination Tube Prototype." *Rep. No. NISTIR 6861*.

Brewster, M. Q. (1992). *Thermal Radiative Transfer And Properties*., John Wiley & Sons, Inc., New York.

Daniels, A., Boreman, G. D., Ducharme, A. D., and Sapir, E. (1995). "Random Transparency Targets for Modulation Transfer-Function Measurement in the Visible and Infrared Regions." *Optical Engineering*, 34(3), 860-868.

Driggers, R. G., Webb, C., Pruchnic, S. J., Halford, C. E., and Burroughs, E. E. (1999). "Laboratory measurement of sampled infrared imaging system performance." *Optical Engineering*, 38(5), 852-861.

Drysdale, D. (1998). *An Introduction to Fire Dynamics*, 2nd Ed., John Wiley and Sons, Chichester.

Grosshandler, W. L. (1993). *NIST Technical Note 1402*., National Institute of Standards and Technology.

Hanson, C. M.(1997). "Hybrid Pyroelectric -Ferroelectric Bolometer Arrays." In: *Uncooled Infrared Imaging Arrays and Systems*, P. W. Kruse, and D. D. Skatrud, eds., Academic Press, San Diego.

Holst, G. C. (1998). *Testing and Evaluation of Infrared Imaging Systems*., SPIE Optical Engineering Press and JCD Publishing, Winter Park, FL.

Holst, G. C. (2000). *Common Sense Approach to Thermal Imaging*., SPIE Press and JCD Publishing, Winter Park, FL.

Kreith Gordon, F., and Bohn, M. S. (1993). *Principles of Heat Transfer*, Fifth Ed., West Publishing Company, St. Paul, MN.

Kruse, P. W.(1997). "Principles of Uncooled Infrared Focal Plane Arrays." In: *Uncooled Infrared Imaging Arrays and Systems*, P. W. Kruse, and D. D. Skatrud, eds., Academic Press, San Diego.

Millikan, R. C. (1961). "Optical Properties of Soot." *Journal of the Optical Society of America*, 51, 698-699.

Modest, M. F. (1993). *Radiative Heat Transfer*., McGraw-Hill Inc., New York.

Muralt, P. (2001). "Micromachined infrared detectors based on pyroelectric thin films." *Reports on Progress in Physics*, 64(10), 1339-1388.

National Television Systems Committee(2006).

Polla, D. L., and Choi, J. R.(1997). "Monolithic Pyroelectric Bolometer Arrays." In: *Uncooled Infrared Imaging Arrays and Systems*, P. W. Kruse, and D. D. Skatrud, eds., Academic Press, San Diego.

Tsai, C. F., and Young, M. S. (2003). "Pyroelectric infrared sensor-based thermometer for monitoring indoor objects." *Review of Scientific Instruments*, 74(12), 5267-5273.

Video Electronics Standards Association Display Metrology Committee(2001). "Flat Panel Display Measurements Standard Version 2.0.".